Doctoral Thesis

An Improved Trajectory of Bipedal Robot Walking along a Step with Dual Length Linear Inverted Pendulum Method (DLLIPM)

Fariz Bin Ali

Division of Electrical and Computer Engineering
Graduate School of Engineering
Yokohama National University

Supervisor Professor Atsuo KAWAMURA

March, 2013

An Improved Trajectory of Bipedal Robot Walking along a Step with Dual Length Linear Inverted Pendulum Method (DLLIPM)

by

Fariz Bin Ali

Dissertation submitted to the
Graduate School of Engineering of the Yokohama National University
in partial fulfillment of the requirements for the degree of

Doctor of Philosophy

in

Electrical and Computer Engineering

Supervisor Professor Atsuo Kawamura

Department of Electrical and Computer Engineering
Yokohama National University

Yokohama, Japan
March, 2013

Advisory Committee:
Atsuo Kawamura, Chair
Yasutaka Fujimoto
Tsutomu Oyama
Takao Tsuji
Tetsuro Yabuta
Tomoyuki Shimono, Observer
Naoki Motoi, Observer

Printed in Japan

Abstract

Biped robot should be robust and able to move or explore freely in human environments. Therefore, many researchers have explored the biped robot research in certain environments such as on uneven surface, slope and stairs. Reseach for biped robot walking on slope and stairs have been started since 90s. However, it is not reported that the mentioned research are done for walking along stair. Therefore, in this dissertation the research related to biped robot walking along a step is chosen for further investigation.

The main parts in this dessertation are chapter 4 and 5 where we proposed a new method to obtain walking parameters for 2 (2-D) and 3-dimensional (3-D) of biped walking along a step. First, the derivations are shown for 2-D cases which are sagittal and lateral. Then, the method is extended for the 3-D case. As mentioned earlier, it is realized that many researchers concentrated on walking directions of climbed up or down of stairs only. In conventional methods, center of mass (CoM) moved up or down during walking in this situation because the height of pendulum is kept at the same length at the left and right legs. Thus, extra effort is required in order to bring the CoM up to the higher ground. In order to improve this situation, different height of pendulum is applied at the left and right legs and named as dual length linear inverted pendulum method (DLLIPM). However, when different height of pendulum is applied, it is quite difficult to obtain symmetrical and smooth pendulum motions. Furthermore, synchronization between sagittal and lateral planes are not confirmed. Therefore, DLLIPM with Newton-Raphson algorithm is proposed to solve these problems.

In our proposed method, the walking pattern for sagittal and lateral planes are designed systematically and synchronization between them is ensured. As for confirmation, the proposed method is verified by the simulation and experimental results. It is realized from the results that the maximum impact forces are reduced with our proposed method.

Acknowledgements

This dissertation would not have been possible without the assistance, help and guidance from several individuals who directly or indirectly contributed in the preparation and completion of my Ph.D. study.

First and foremost, my utmost gratitude to Professor Kawamura, who has guided me for years in my research. His sincerity and encouragement will always be remembered. Professor Atsuo Kawamura has been my inspiration as I overcome all the obstacles in the completion of this research work.

Secondly, I would like to express my sincere gratitude to Dr. Naoki Motoi for helping me and giving valuable ideas and advice during my study, especially during my initial stages of finding suitable research topic. Appreciation is also given to all panel Professors, Yasutaka Fujimoto, Tsutomu Oyama, Takao Tsuji, Tetsuro Yabuta, and Tomoyuki Shimono for giving comments, ideas and recommendations to improve my research topic.

Next, my gratitude goes to several teammates who helped me a lot such as, Dr. Barkan who has guided me during my first and second year of Ph.D. study, Mr. Kirill who helped me a lot in doing experiments by using MARI-3. Also to my good companions, Aliza, Saifulza, Zaki, Herman, Fatehy, Naimul and Dr. Fahmi who always been around for discussions and as good listeners when I have problems.

Not to forget to the scholarship and allowance providers, Universiti Teknikal Malaysia Melaka (UTeM) and Global COE (Centers of Excellence) Program. Without the funding, it is impossible for the author to complete his study in Yokohama National University.

The next person that I would like to express my gratitude is Sohana Sabir Ahmad who helped me alot in proffreading my journal paper. She helped me during my paper submission to Journal of Robotics and Mechatronics.

Last, but not least, I would like to thank my lovely wife, Juwita and my beloved children, Fathnin and Fateh for their understanding and love during the past few years. Their support and encouragement was in the end what made this dissertation possible. Also to my parents, Rashidah and Ali @ Ibrahim, for their prayers that contributed to my success.

Fariz Bin Ali
November, 2012

I dedicate this dissertation to my family members;

to Mak, Ayah, Ita, Fathnin, Fateh, Yong, Yeop, Nyah and Jeli...

"la tahzan innallaha maana."

Muhammad S.A.W. (571 - 632)

Contents

List of Figures

List of Tables

Chapter 1

Introduction

1.1 Background and Motivation

There are several types of mobility for ground robots such as by wheels [1], legs or hybrid locomotion that combined wheels and legs [2]. Moreover, there are various kinds of the legged robots such as hexapod [3], quadruped [4] and biped [5]-[22]. The less number of the legs, the more difficult it is, in order to ensure the dynamics stability of the robots. Since the biped has advantages to explore the human environment, therefore in this thesis, the biped platform is used.

Most of human environment is unmade for a biped robot. Therefore, researchers have worked hard to realize stable biped walking in human environment with several proposed concepts such as zero moment point (ZMP) [7, 8], virtual supporting point (VSP) [9] and linear inverted pendulum mode (LIPM) [10, 11]. ZMP concept introduced an indicator to obtain stable biped walking. Whenever the ZMP point is inside the support polygon, the robot will be able to keep standing without fall down or tip over during walking. In VSP method, the supporting point can be placed at any virtual point within the stable region in order to realize biped walking on uneven floor. Finally, in LIPM method the motion of CoM of a biped robot during walking can be moved with the dynamics representation of linear inverted pendulum. In this thesis, a proposed method with modification of LIPM concept is used and will be explained further later.

There are also researchers who investigated biped robot motions in specific environment such as on slope surface [12] and stairs. Sato *et al.* [13] proposed the virtual slope method for walking trajectory planning on stairs. In this method, the CoM trajectory of the biped robot is generated based on the virtual slope surface. Fu *et al.* [14] proposed the walking pattern synthesis and sensory feedback control for humanoid stair climbing. This method consists of a feedforward stair-climbing gait and a feedback sensory controller. Hu *et al.* [15] proposed a scheme which is developed with regulable step length and walking speed. This method is tested for walking over stairs by using a compass-like biped robot. Powell *et al.* [16] proposed the control techniques for multiple locomotion behaviours from the examination of experimental human data for walking.

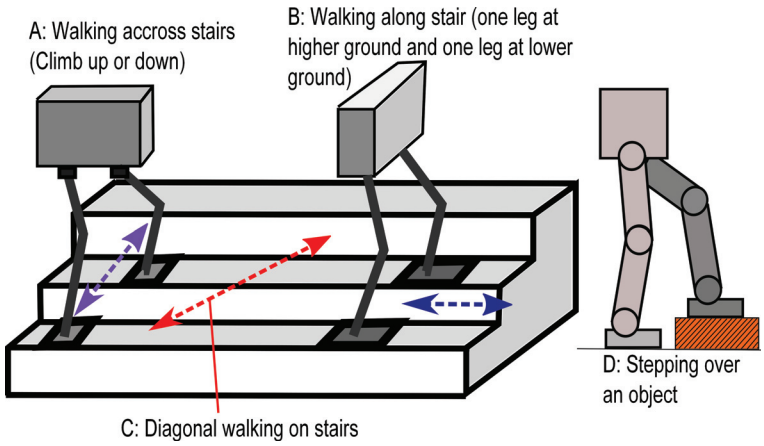

Figure 1.1: Definitions of walking on stairs or on a step.

The method is tested for walking on flat ground, upstairs and downstairs.

Some other researchers proposed several methods to detect the physical dimension of the stair. Park *et al.* [17] proposed a method to detect stair boundaries for a humanoid robot by using a 2D laser scanner is installed on the head of a humanoid robot called MAHRU-1. Chestnutt *et al.* [18] proposed a method to navigate biped robot around by using an on-board Hokuyo laser scanner which swivelled up and down while operating. In this method, the scan data is combined with other data from odometry and gyro sensor to construct a 3D environment. Guodong *et al.* [19] proposed the stereovision based system for humanoid navigation.

A bipedal robot should be able to perform various of walking directions on the stairs or slope such as walking accross, diagonal walking and walking along a stair as shown in Fig. 1.1. However, many of researchers only concentrate in the walking direction of across the stairs (Shown by A in Fig. 1), which means climbed up or down directions. Walking along the stair has not been investigated yet. For that reason, the main task of this thesis is to design walking parameters for biped walking along stair or a step.

Walking along a stair (Shown by B in Fig. 1) and stepping on an object (Shown by C in Fig. 1) can be solved with the same technique. In the conventional methods, the center of mass (CoM) is suggested to be brought up or down in order to maintain the same pendulum length at the right foot and left foot. In this thesis, a method known as dual length linear inverted pendulum method (DLLIPM) is developed based on some modifications from previous researh on LIPM [10]. In DLLIPM, CoM is always constant to the lower ground floor as shown in Fig. 1.2. As seen in Fig. 1.2, the LIPM requires extra effort in order to move the CoM up to the higher ground. Therefore, this situation is avoided in the DLLIPM by making the CoM always moves in horizontal motion. It is also expected that in the LIPM, higher force impact will be felt at the landing foot especially when the CoM is moving down from higher to the lower ground. However, when different height of CoM is assigned at right foot

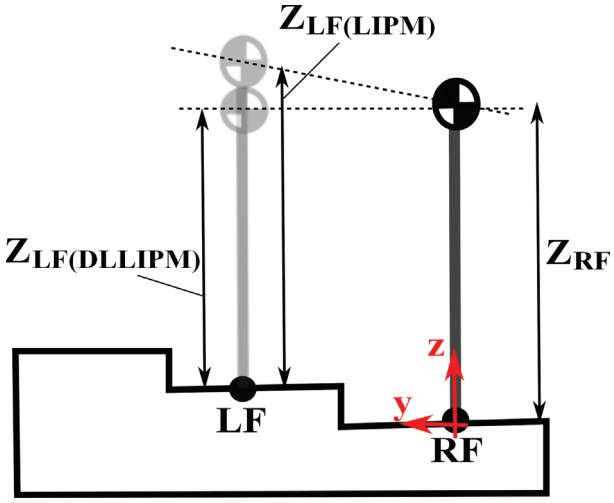

Figure 1.2: CoM trajectory in lateral plane for walking along stair by using LIPM and DLLIPM.

(RF) and left foot (LF) in DLLIPM, there is a possibility of unsmooth and non-symmetrical pendulum motions. Therefore, DLLIPM with Newton Raphson algorithm is proposed to find the appropriate parameters for the walking pattern. In this thesis, 3-dimensional (3D) pattern generation for walking along stair is investigated. Sagittal and lateral effects are analysed and ensured to be synchronized during the walking.

There are several merits expected from the proposed method. One of the merits is that the work the biped robot need to perform for the biped walking along a step is less compared to the conventional LIPM, as described by Fig. 1.2. Furthermore, since the CoM in the DLLIPM is maintained horizontally without up and down motion as in the LIPM, it is expected that maximum impact forces are less in the DLLIPM. Besides that, smooth motions and synchronization between lateral and sagittal is confirmed with the proposed method. However, in this thesis the step height is a known value. Detection of the floor height is beyond the scope of this paper.

In section 1.2, the biped robot platforms used in simulations and experiments are presented. In section 1.3, the concept of DLLIPM is explained. The proposed method of DLLIPM with Newton Raphson algorithm, simulations and experimental results are presented in section 4 and 5.

1.2 The Biped Robot Walking

The biped robot used in simulations and experiments in this thesis is known as MARI-3 [20]. MARI-3 has total of 13 degrees of freedom (DOF); 6 DOF in each leg and 1 DOF at the waist. The height and weight are 0.6 [m] and 33.64 [kg], correspondingly. In order to verify the proposed method, a 3-D dynamic simulator known as ROCOS (RObot COntrol Simulator) [21] and MARI-3 actual biped robot have been used. Fig. 1.3 shows the actual robot, its ROCOS

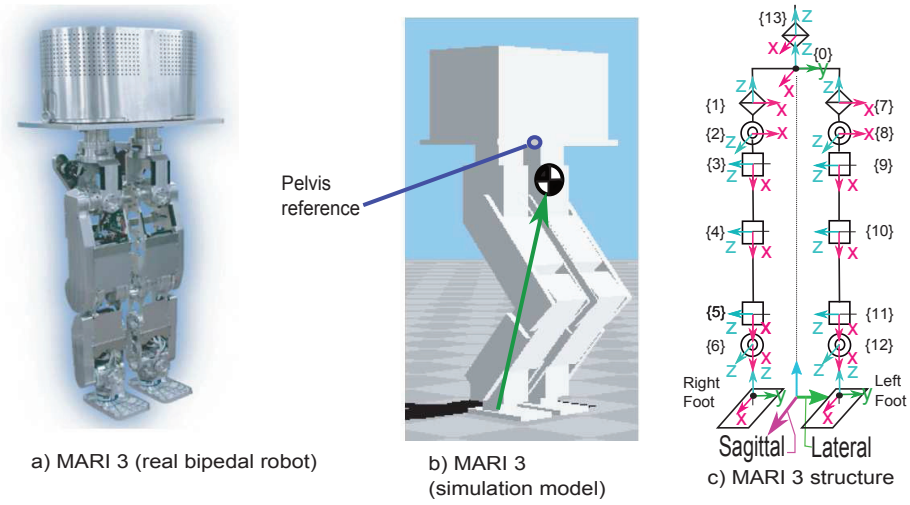

Figure 1.3: Biped robot MARI-3.

simulation model and the robot structure.

One of the advantages of DLLIPM with Newton Raphson algorithm is that it is a generalized method which is applicable to any type of bipedal robot platform. However, it is compulsory to calculate the CoM of the robot and it must be trackable during the walking. This is essential because all the derivations in this thesis is developed based on the dynamics of linear inverted pendulum which is assigned to the motion of the CoM. The calculation of the CoM can be done from the kinematics of the robot [22]. A picture of a general biped robot with its center of mass location is shown in Fig. 1.3 b).

Some researchers used pelvis as reference point for simplicity of calcultations. As seen in the Fig. 1.3 b), the reference point of the pelvis and the real CoM position is located at different place. If the motion reference trajectories are given based on the pelvis reference point, the robot may fall down in some situations because the exact CoM location is inaccurate. All calculations and derivations are developed based on the dynamics of the pendulum which is assigned to the CoM position. Therefore, it is compulsory to include the CoM position in kinematics and all the trajectories should be given based on the CoM position, instead of the pelvis position.

There are two different coordinate system references used in this thesis. For the trajectory planning, the center of landing foot is used as reference of coordinate system. Therefore, both RF and LF repeatedly used as the reference point, one after another. On the other hand, the reference of the coordinate system during simulations is always located at the center of RF at the initial position. This reference point is known as the world coordinate system.

The details of the kinematics of the biped robot and its applications for walking will be explained further in Chapter 3. In chapter 3 the proposed kinematics are applied for biped straight walking and diagonal walking.

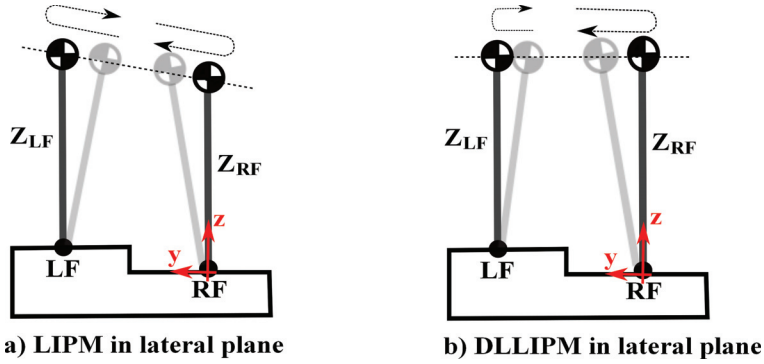

Figure 1.4: CoM motion of biped robot in lateral plane.

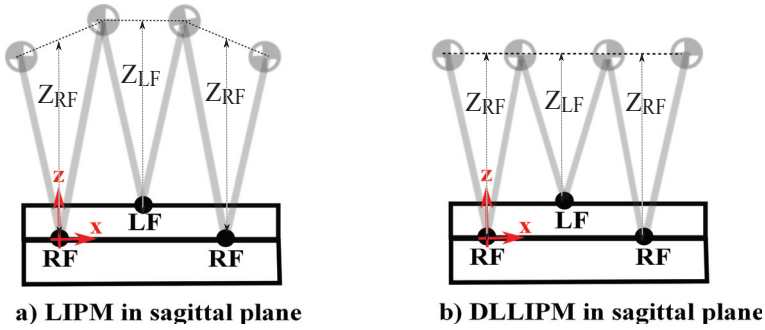

Figure 1.5: CoM motion of biped robot in sagittal plane.

1.3 Dual Length Linear Inverted Pendulum Method (DLLIPM)

DLLIPM is developed based on some modifications of LIPM which is proposed by Kajita et.al.[10]. DLLIPM can be used to solve biped walking along stair or stepping on an object if the object is blocking in front of one leg only. In both situations, the problems are solved by maintaining the CoM height always constant to the lower ground. In order to realize this, the DLLIPM is used where the length of pendulum at the RF and LF is different.

In LIPM, the CoM is brought up to the higher ground in order to let the height of pendulum the same at right and left foot. Both LIPM and DLLIPM concepts are shown in Fig. 1.4 and 1.5. In these figures, Z means the height of inverted pendulum. As for DLLIPM shown in Fig. 1.4 b) and 1.5 b), Z_{LF} is also known as Z_{SP} and Z_{RF} is known as Z_{LP}. '$_{SP}$' and '$_{LP}$' stand for short pendulum and long pendulum respectively.

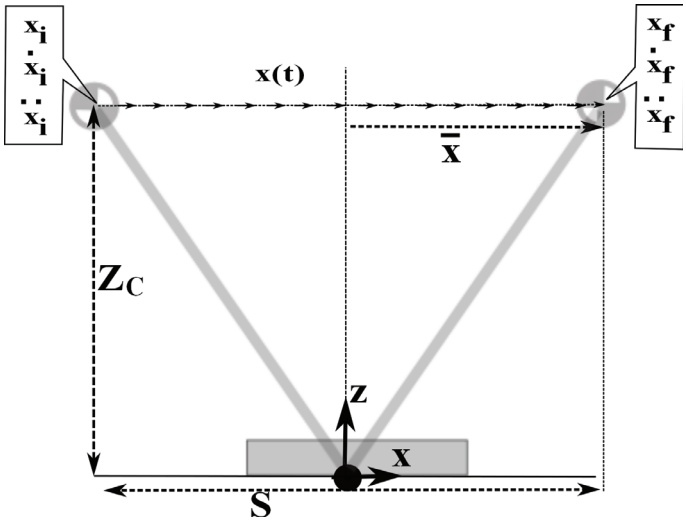

Figure 1.6: LIPM model for sagittal plane.

1.3.1 Linear Inverted Pendulum Mode

In this sub-section, the equations of position and velocity of a single linear inverted pendulum are derived [23]. The single linear inverted pendulum model for sagittal and lateral motions are shown in Fig. 1.6 and 1.7, respectively. In these figures, x_i, $\dot{x}_i$, $\ddot{x}_i$, y_i, $\dot{y}_i$ and $\ddot{y}_i$ are the position, velocity and acceleration at the beginning points. On the other hand, x_f, $\dot{x}_f$, $\ddot{x}_f$, y_f, $\dot{y}_f$ and $\ddot{y}_f$ are the position, velocity and acceleration at the ending points. $x(t)$ and $y(t)$ denote the constantaneous value of CoM trajectory in sagittal and lateral planes, correspondingly. Furthermore, S denotes the CoM stride motion between LF and RF. While Z_c denotes the height of pendulum, from the foot to the CoM position vertically. The motion equation of LIPM in sagittal is shown as in (1.1). The same equation is also applicable for the lateral plane.

$$\ddot{x} = \frac{g}{z_c} x \tag{1.1}$$

Position

In this sub-section, the derivations of equations which are related to position in single inverted pendulum model are shown. From analytical solution of (1.1), the equation of position is obtained as shown in (1.2).

$$x(t) = (\frac{x_i - T_c \dot{x}_i}{2}) e^{-\frac{t}{T_c}} + (\frac{x_i + T_c \dot{x}_i}{2}) e^{\frac{t}{T_c}} \tag{1.2}$$

where

$$T_c = \sqrt{\frac{z_c}{g}} \tag{1.3}$$

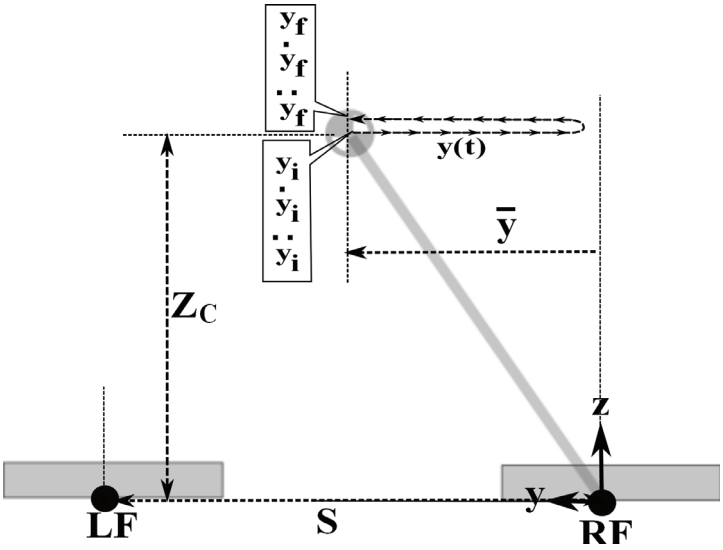

Figure 1.7: LIPM model for lateral plane.

The position equation as shown in (1.2) is applicable for sagittal and lateral planes.

Velocity

In this sub-section, the derivations of equations which are related to velocity in single inverted pendulum model are shown. Time derivative of (1.2), gives equation of velocity as shown in (1.4).

$$\dot{x}(t) = (\frac{\dot{x}_i - \frac{x_i}{T_c}}{2})e^{-\frac{t}{T_c}} + (\frac{\dot{x}_i + \frac{x_i}{T_c}}{2})e^{\frac{t}{T_c}} \tag{1.4}$$

The velocity equation as shown in (1.4) is applicable for sagittal and lateral planes.

1.3.2 Trajectory Planning Method of DLLIPM

DLLIPM trajectory planning consists of 11 steps as shown below. This trajectory planning is based on LIPM proposed by Kajita et. al.[23] with some changes.

Step 1) Decision of the length for short pendulum and long pendulum: Suppose that the biped robot walks on flat floor at certain CoM height. This CoM height at flat floor denotes the length of the long pendulum, Z_{LP}. The height of one stair or a step is a known value, h. The length of the short pendulum, Z_{SP} is given by (1.5). One leg will be on the lower ground, and one leg will be on the stair. The pendulum on the lower ground denotes by the longer pendulum and the pendulum on the stair denotes by shorter pendulum. The length of the Z_{LP} in sagittal plane is the same as in the lateral plane. Also the length of the Z_{SP} in sagittal and lateral planes are equal.

$$Z_{SP} = Z_{LP} - h \tag{1.5}$$

Step 2) Decision on odd and even number of foot landing points, n^{th}: It is needed to determine which foot lands on the higher ground or on the lower ground based on the forward moving direction of the biped robot. Also, it is required to determine which foot the robot starts to walk. For example, the robot is walking along a stair as shown in Fig. 1.4 b) and 1.5 b). The robot moves in such a way that the left foot is always landing on the higher ground, right foot always lands on the lower ground and the motion starts from the right foot. Therefore, the even and odd number of foot landing points in this case are given as in (1.6) and (1.7).

$$n = 0, 2, 4...(RF, LP) \tag{1.6}$$

$$n = 1, 3, 5...(LF, SP) \tag{1.7}$$

Step 3) Decision of the walking parameters such as walking cycle, strides, initial CoM positions and initial landing positions: In conventional LIPM method, these parameters should be decided before the robot starts to walk. Suppose that the walking cycle for short and long pendulum denote by Δt_{-SP} and Δt_{-LP}, correspondingly.

Step 4) Setting of foot landing points modifications in sagittal and lateral, P_x^* and P_y^*, initial time T and initial number n, of landing point: $T := 0$ and $n := 0$. Initially $P_x^* = 0$ and $P_y^* = 0$.

Step 5) Using LIPM equations to obtain CoM trajectory: For long pendulum, which means n as in (1.6) in this example, the CoM is moved from T to $T + \Delta t_{-LP}$ by using (1.8) for sagittal and (1.9) for lateral. Here the value of Z_c equal to Z_{LP}. For short pendulum, which means n as in (1.7), the CoM is moved from T to $T + \Delta t_{-SP}$ also by using (1.8) for sagittal and (1.9) for lateral. In this case, the value of Z_c equal to Z_{SP}.

$$\begin{aligned} x(t) &= (x_i^{(n)} - P_x^*)\cosh(\mathrm{t/T_c}) \\ &+ T_c \dot{x}_i^{(n)} \sinh(\mathrm{t/T_c}) + \mathrm{P_x^*} \end{aligned} \tag{1.8}$$

$$\begin{aligned} y(t) &= (y_i^{(n)} - P_y^*)\cosh(\mathrm{t/T_c}) \\ &+ T_c \dot{y}_i^{(n)} \sinh(\mathrm{t/T_c}) + \mathrm{P_y^*} \end{aligned} \tag{1.9}$$

where $T_c = \sqrt{\frac{Z_c}{g}}$. P_x^* and P_y^* are the foot landing points modifications for sagittal and lateral, respectively. These values are initially 0 for $n = 0$. After that, for $n \neq 0$, the calculations are done as shown in step 10.

Step 6) Increment of number of foot landing point and time:

$$n := n + 1 \tag{1.10}$$

If n is even number, T:=$T + \Delta t_{-LP}$.
If n is odd number, T:=$T + \Delta t_{-SP}$.

Step 7) Calculation of next foot landing points in sagittal and lateral planes, $P_x^{(n)}$ and $P_y^{(n)}$: The next foot landing point for sagittal and lateral planes are calculated by using (1.11) and (1.12), respectively.

$$P_x^{(n)} = P_x^{(n-1)} + s_x^{(n)} \tag{1.11}$$

$$P_y^{(n)} = P_y^{(n-1)} - (-1)^n s_y^{(n)} \tag{1.12}$$

where $s_x^{(n)}$ and $s_y^{(n)}$ mean the foot strides of n^{th} step in sagittal and lateral directions.

Step 8) Calculation of final position and final velocity of CoM for each single support phase: If n is even number, the final CoM position and the final velocity for sagittal plane are calculated as in (1.13) and (1.14), respectively. On the other hand, the final CoM position and the final velocity for lateral plane are calculated as in (1.15) and (1.16), respectively.

$$\bar{x}_{LP}^{(n)} = \left(\frac{\bar{x}_{LP}}{\bar{x}_{LP} + \bar{x}_{SP}}\right) s_x^{(n+1)} \tag{1.13}$$

$$\bar{v}_{x-LP}^{(n)} = \left(\frac{C+1}{T_c S}\right) \bar{x}_{LP}^{(n)} \tag{1.14}$$

$$\bar{y}_{LP}^{(n)} = (-1)^n \left(\frac{\bar{y}_{LP}}{\bar{y}_{LP} + \bar{y}_{SP}}\right) s_y^{(n+1)} \tag{1.15}$$

$$\bar{v}_{y-LP}^{(n)} = \left(\frac{C-1}{T_c S}\right) \bar{y}_{LP}^{(n)} \tag{1.16}$$

If n is odd number, the final CoM position and the final velocity for sagittal and lateral planes can be solved in the same way as (1.13)-(1.16) but with the respect to short pendulum.

Values of C and S in (1.14) and (1.16) are given in (1.17) and (1.18) (suppose that the instantaneous time at the end of each single support phase denotes by t_{end}).

$$C = \cosh\left(\frac{\mathrm{t_{end}}}{\mathrm{T_c}}\right) \tag{1.17}$$

$$S = \sinh\left(\frac{\mathrm{t_{end}}}{\mathrm{T_c}}\right) \tag{1.18}$$

Where the values of T_c in (1.14), (1.16), (1.17) and (1.18) are the same values used in step 5.

Step 9) Calculation of desired final position and desired final velocity of CoM in sagittal, x^d and $\dot{x}^d$, and in lateral, y^d and $\dot{y}^d$, for each single support phase: If n is even number, the calculation of desired final position of CoM in sagittal is calculated from (1.11) and (1.13) as shown in (1.19). On the other hand, the calculation of desired final position of CoM in lateral is calculated from (1.12) and (1.15) as shown in (1.20). Furthermore, the desired final velocity in sagittal and lateral are calculated using (1.14) and (1.16), as shown in (1.21) and (1.22), correspondingly.

$$x^d = P_x^{(n)} + \bar{x}_{LP}^{(n)} \tag{1.19}$$

$$y^d = P_y^{(n)} + \bar{y}_{LP}^{(n)} \tag{1.20}$$

$$\dot{x}^d = \bar{v}_{x-LP}^{(n)} \tag{1.21}$$

$$\dot{y}^d = \bar{v}_{y-LP}^{(n)} \tag{1.22}$$

If n is odd number, the desired final position and desired final velocity of CoM for sagittal and lateral planes can be solved in the same way as (1.19)-(1.22) but with the respect to short pendulum.

Step 10) Calculation of foot landing modification: The foot landing modification in sagittal is calculated by using (1.23)[23].

$$\begin{aligned} p_x^* &= -\frac{a(C-1)}{D}(x^d - Cx_i^{(n)} - T_cS\dot{x}_i^{(n)}) \\ &- \frac{bS}{T_cD}(\dot{x}^d - \frac{S}{T_c}x_i^{(n)} - C\dot{x}_i^{(n)}) \end{aligned} \tag{1.23}$$

where $D = a(C-1)^2 + b(S/T_c)^2$.
a and b are the weight parameters in order to minimize the margin of error for position and velocity. Values of T_c, C, and S in (1.23) are the same values as in step 8. The foot landing modification in lateral can be solved in the same manner as in (1.23) but with all the values from the lateral plane.

Step 11) Go back to step 5: This step is repeated until all number of foot landing points, n are completed.

The details about application of DLLIPM in 2-D case is shown in Chapter 4. Furthermore, for the 3-D case is shown in Chapter 5.

1.4 Newton-Raphson and the Closed Form Solution

One of the objectives in this research is to obtain the appropriate walking parameters for walking along a step. In 2-D case, there are 4 walking parameters need to be obtained which are maximum stride of long pendulum phase, maximum stride of short pendulum phase, cycle time of long pendulum phase and cycle time of short pendulum phase. Furthermore, in 3-D case there are 6 parameters need to be obtained which are maximum stride of long pendulum phase in sagittal plane, maximum stride of short pendulum phase in sagittal plane, maximum stride of long pendulum phase in lateral plane, maximum stride of short pendulum phase in lateral plane, cycle time of long pendulum phase and cycle time of short pendulum phase. In both cases, 2-D and 3-D cases, the walking parameters are solved by using Newton-Raphson method which are explained in details in sub-section 4.2.3.2, 4.3.2 and 5.2.

It is general rule, that in order to find a solution to the set of equations, analytical solution is preferable. Analytical solution means the solution is done by using calculus, trigonometry, and or other math techniques to write down the solution. Sometimes, this is also referred as a closed form solution [24]. However, the analytical solution works only for the simple problem. In this research, especially for the 3-D case, the equations are non-linear and become extremely difficult to be solved analytically. Therefore, the Newton-Raphson method has been chosen to solve these complex equations numerically.

1.5 Research Objectives and Outline

In order to achieve a good research, the direction of the research must be clear. Therefore, a number of research objectives have been planned as the main goal to be realized. The main objectives are listed as below:

1. To design and develop the kinematics for MARI-3 biped robot. In this kinematics, orientation and position equations are included. The proposed kinematics calculations are then applied for walking on flat floor, slope and step surfaces.

2. To obtain appropriate walking parameters for walking along a step in 2-D case with DLLIPM approach. Stable walking, smooth and symmetry walking trajectories are intended to be achieved. The concept of DLLIPM is applied and treated seperately for sagittal or lateral for the 2-D case.

3. To obtain appropriate walking parameters for walking along a step in 3-D case with DLLIPM approach. Synchronization between sagittal and lateral planes is intended to be achieved for the 3-D case.

It is shown earlier in the first subsection of this chapter about the background and motivation of the research. Generally, the main concept of the proposed method and the whole structure of this thesis are presented in Chapter 1. In Chapter 2, the derivation of ZMP is shown systematically. Calculations of kinematics and applications to the biped robot platform are explained in Chapter 3. Concept and applications of DLLIPM in 2-D and 3-D cases are shown in Chapter 4 and 5, respectively. Finally, conclusion and future works are discussed in Chapter 6. The appendix sections contain of the mechanical specification of the biped robot, special research project and publications.

Chapter 2

ZMP Derivation

2.1 Definition

Zero moment point is a concept related with dynamics and control of legged locomotion, e.g., for humanoid robots. It specifies the point with respect to which dynamic reaction force at the contact of the foot with the ground does not produce any moment in the horizontal direction, i.e. the point where total of vertical inertia and gravity forces equals 0 (zero). The concept assumes the contact area is planar and has sufficiently high friction to keep the feet from sliding [27].

2.2 Derivation

The derivation of ZMP can be obtained from the concept of cart-table model [28].

2.2.1 Cart-table Model

The solution of a 2-D cart-table model can be solved by referring to Fig. 2.1 [29]. is shown as follows:

$$\begin{aligned} \tau_{zmp} &= F \times r \\ &= Mg(x-p) - M\ddot{x}z_h \\ &= 0 \end{aligned} \tag{2.1}$$

As defined in section 2.1, ZMP point, p is the point where total of vertical inertia and gravity forces equals 0 (zero) as shown by (2.1). (2.1) can be simplified further as follows:

$$Mg(x-p) = M\ddot{x}z_h$$

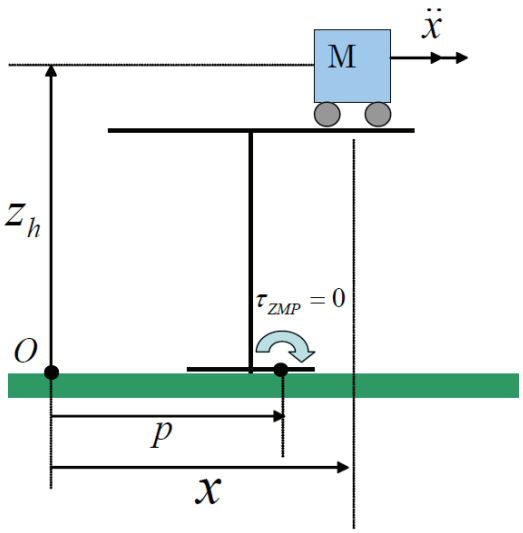

Figure 2.1: ZMP of the cart-table model

$$\begin{aligned} gx - \ddot{x}z_h &= gp \\ p &= x - \frac{\ddot{x}}{g}z_h \\ x_{zmp} &= x - \frac{\ddot{x}}{g}z_h \end{aligned} \tag{2.2}$$

The equation in (2.2) is for sagittal plane. As for the lateral plane, the equation is obtained identically as shown in (2.3).

$$y_{zmp} = y - \frac{\ddot{y}}{g}z_h \tag{2.3}$$

2.2.2 Analytical Solution

The (2.2) and (2.3) can be solved further analytically. The solution of (2.2) will be shown. As for the (2.3), it can be solved in the same manner.

As obtained above, the equation of ZMP in sagittal plane is given as follows:

$$x_{zmp} = x - \frac{\ddot{x}}{g}z \tag{2.4}$$

Then, (2.4) can be arranged as follows:

$$\begin{aligned} \frac{\ddot{x}}{g}z &= x - x_{zmp} \\ \ddot{x} &= (x - x_{zmp})\frac{g}{z} \end{aligned} \tag{2.5}$$

Let's now define ω as follows:

$$\begin{aligned} \omega &= \sqrt{\frac{g}{z}} \\ \omega^2 &= \frac{g}{z} \end{aligned} \tag{2.6}$$

By substituting (2.6) into (2.5), (2.7) is obtained as shown below.

$$\ddot{x} = (x - x_{zmp})\omega^2 \tag{2.7}$$

Then, MATLAB is used to expand (2.7) further. In the MATLAB environment, the 'Dsolve' function is used as shown in (2.8).

$$Dsolve('D2x = (x - x_{zmp}) * \omega * \omega)','Dx(0) = dx0','x(0) = x0') \tag{2.8}$$

By using (2.8), (2.7) is expanded as shown in (2.9).

$$x = -\frac{1}{2}e^{\omega t}\left(\frac{-dx0 - \omega x0 + \omega x_{zmp}}{\omega}\right) - \frac{1}{2}e^{-\omega t}\left(\frac{dx0 - \omega x0 + \omega x_{zmp}}{\omega}\right) + x_{zmp} \tag{2.9}$$

For easier understanding, (2.9) can be simplified as follows;

$$\begin{aligned} x &= -\frac{1}{2\omega}e^{\omega t}(-dx0) - \frac{1}{2\omega}e^{\omega t}(-\omega x0 + \omega x_{zmp}) \\ &- \frac{1}{2\omega}e^{-\omega t}(dx0) - \frac{1}{2\omega}e^{-\omega t}(-\omega x0 + \omega x_{zmp}) + x_{zmp} \end{aligned} \tag{2.10}$$

In order to simplify (2.10), hyperbolic functions must be taken into account as shown in (2.11).

$$\begin{aligned} cosh(x) &= \frac{1}{2}e^{x} + \frac{1}{2}e^{-x} \\ sinh(x) &= \frac{1}{2}e^{x} - \frac{1}{2}e^{-x} \end{aligned} \tag{2.11}$$

Before the hyperbolic functions can be implemented, (2.10) is rearranged as in (2.12).

$$\begin{aligned} x &= \frac{1}{2}e^{\omega t}\left(\frac{dx0 + \omega x0 - \omega x_{zmp}}{\omega}\right) + \frac{1}{2}e^{-\omega t}\left(\frac{-dx0 + \omega x0 - \omega x_{zmp}}{\omega}\right) + x_{zmp} \\ &= \frac{1}{2}e^{\omega t}\left(\frac{dx0}{\omega}\right) + \frac{1}{2}e^{\omega t}\left(\frac{\omega x0 - \omega x_{zmp}}{\omega}\right) \\ &+ \frac{1}{2}e^{-\omega t}\left(\frac{-dx0}{\omega}\right) + \frac{1}{2}e^{-\omega t}\left(\frac{\omega x0 - \omega x_{zmp}}{\omega}\right) + x_{zmp} \end{aligned} \tag{2.12}$$

By substituting (2.11) into (2.12), (2.13) is obtained as follows;

$$\begin{aligned} x &= \frac{dx0}{\omega}sinh(\omega t) + \left(\frac{\omega x0 - \omega x_{zmp}}{\omega}\right)cosh(\omega t) + x_{zmp} \\ &= (x_0 - x_{zmp})cosh\omega t + \frac{dx_0}{\omega}sinh\omega t + x_{zmp} \end{aligned} \tag{2.13}$$

Note that the terms of x_0 and dx_0 in (2.13) are referred to initial position and initial velocity, respectively. In this thesis, (2.13) will be used frequently for further derivations.

Chapter 3

Kinematics

In this chapter, the control method to plan for bipedal robot walking is explained. In this section forwad and inverse kinematics based on position and orientation will be explained [34]-[37].

3.1 Introduction

Humanoids are developed to perform some basic tasks that a normal human being can do for example walking, jumping and running. These basic tasks should be able to be performed in human environments such as stairs and inclined floor. Even though these tasks may seem easy for a human to perform it, many aspects must be taken carefully in bipedal robot case. A number of researchers have implemented control methods to solve biped walking problems on rough or uneven terrain [38]-[41]. Walking on inclined floor problems have been investigated [42, 43], but these methods need a special trajectory purposely for inclined floor. Feng and Sun [44] have developed a simple trajectory generation method for biped walking but the robot can walk only on flat floor using the off-line generated trajectory. It is intended in this paper to solve biped walking on inclined floor by simply modifying the IK (Inverse Kinematics) so that the same walking pattern on a flat floor can be applied on the inclined floor. This can be achieved by changing the orientation trajectory of pelvis. By doing this, the robot is able to walk on flat and inclined surface using the off-line generated trajectory.

Kim et al. [12] and Taskiran et al. [45] have proposed several control algorithms to achieve bipedal stable walking on inclined floor. One of the control algorithms is known as ankle torque control. This method has been validated successfully but it must be operated together with several more other control algorithms synchronously. However, it is afraid that by only consider the ankle joints for pose stabilization on inclined floor, the ankle joints may become saturate. Hence, if too much torque is applied, the ankle joints may damage. Of course, this situation must be avoided. Therefore, the authors' group have thought an idea to improve the situation and proposed a method which will distribute the angles caused by the inclined floors among the robot joints. It is believed that this is more efficient and can be done via modification of

IK algorithm.

Some researchers used pelvis and foot positions to solve the robot kinematics [46], while others may use CoM (Center of Mass) position. [47] implemented CoM and foot positions in his IK solution. Ugurlu and Kawamura [48] also proposed such IK which takes the position of CoM and foot, with zero orientation since they just consider walking on flat floor only. In this section, the approach in [48] is extended to consider the orientations for walking on inclined surface.

3.2 Forward Kinematics

FK equations are very essential to be determined, so that it can be inverted later for referential joint angle calculations. There are several possible FK equations that can be obtained from a bipedal robot such as CoM position, swing leg position and pelvis orientation.

The platform used in this section is MARI-3 biped robot. The purpose of FK is to determine an explicit IK solution of 12 joint angles variables in order to handle redundancy. Please note that the 13th yaw joint is not taken into account because it does not affect the CoM in the case of this section. For position vectors, CoM position and swing leg position are used. While for orientation, pelvis orientations with respect to the support foot is used.

3.2.1 CoM Position and Swing Foot Position

In the method of this section, right foot is used as reference. Therefore, the CoM position and the swing foot position are always referred to the right foot sole center as shown in Fig. 3.1. Some of biped researchers used pelvis as reference point and used it as input trajectory. This is because it is visible and easier to visualize compared to CoM point. However, it is believed that position of CoM is more accurate to be used as input trajectory since ZMP equations [8] are related to CoM point.

A position of robot during right foot's single support phase is shown in Fig. 3.1. From this figure, P_{CR} and P_{LR} are the position vectors from right foot to CoM, and right foot to left foot, respectively. ZMP equations are used to determine P_{CR}, while P_{LR} is generated from swing leg motion. From these 6 existing position vectors, the FK equations are determined. These functions contain the joint angles variables as shown in (3.1).

$$\begin{aligned} \vec{P_i} &= f_i(q_1, \ldots, q_{12}) \\ i &= 1, \ldots, 6 \end{aligned} \tag{3.1}$$

From the position vectors, there are 6 equations and 12 joint angles variables. In order to avoid redundancy, another 6 equations are needed. These additional equations are obtained

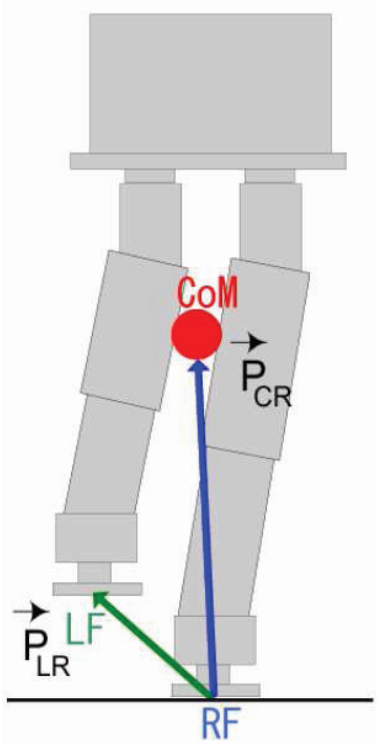

Figure 3.1: Single support phase.

from orientation which will be explained further in the next subsection. In (3.1) and other equations later, q symbolizes the joint angles. Please note that the left foot's single support phase case can be solved identically.

3.2.2 Pelvis Orientation

In this subsection, derivation of FK expressions for the pelvis orientation will be explained. Fig. 3.2 shows the pelvis orientation with respect to the right foot. θ_{x-RF}, θ_{y-RF} and θ_{z-RF} represents roll, pitch and yaw rotations with respect to the foot frame which is located in the middle of right foot sole.

In order to derive the expressions for the pelvis orientation, the basic rotation matrices around x, y and z axes must be determined. Multiplication all of the basic rotation matrices in x-y-z Euler sequence [49], gives a 3x3 matrix in functions of θ_{x-RF}, θ_{y-RF} and θ_{z-RF} as shown in equation (3.2). Please note that matrix element M_{21}, M_{22}, M_{31} and M_{32} are just ignored since they were not used to determine the orientation equations.

$$R_x \times R_y \times R_z = \begin{bmatrix} M_{11} & M_{12} & M_{13} \\ M_{21} & M_{22} & M_{23} \\ M_{31} & M_{32} & M_{33} \end{bmatrix} \tag{3.2}$$

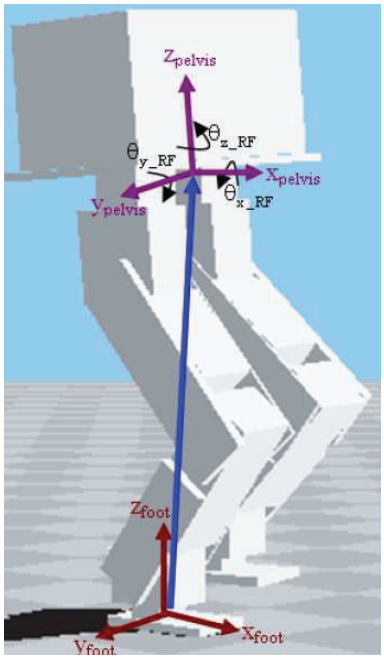

Figure 3.2: Pelvis orientation.

Where the value of each element in (3.2) is given below:

$$\begin{aligned} M_{11} &= cos(\theta_{y\_RF})cos(\theta_{z\_RF}) \\ M_{12} &= -cos(\theta_{y\_RF})sin(\theta_{z\_RF}) \\ M_{13} &= sin(\theta_{y\_RF}) \\ M_{23} &= -sin(\theta_{x\_RF})cos\theta_{y\_RF}) \\ M_{33} &= cos(\theta_{x\_RF})cos\theta_{y\_RF}) \end{aligned}$$

From the transformation matrix of the pelvis with respect to the right foot, the orientation in term of joint angle q_1 to q_6 is obtained as shown in (3.3). Value of 'a' in these equations is, $a = q_3 + q_4 + q_5$. Same as in (3.2), element N_{21}, N_{22}, N_{31} and N_{32} are ignored again because they were not utilized for orientation equations determination. Notice that only q_1 to q_6 are involved here since the joints angles involved are contributed from right leg only. On the other hand, for the left leg case, it can be solved in the same manner.

$$^{RightFoot}_{Pelvis}R = \begin{bmatrix} N_{11} & N_{12} & N_{13} \\ N_{21} & N_{22} & N_{23} \\ N_{31} & N_{32} & N_{33} \end{bmatrix} \tag{3.3}$$

Where the value of each element in (3.3) is given below:

$$
\begin{aligned}
N_{11} &= sin(a)sin(q_1)sin(q_2) + cos(a)cos(q_1) \\
N_{12} &= -sin(a)cos(q_1)sin(q_2) + cos(a)sin(q_1) \\
N_{13} &= sin(a)cos(q_2) \\
N_{23} &= sin(q_6)cos(a)cos(q_2) + sin(q_2)cos(q_6) \\
N_{33} &= cos(q_6)cos(a)cos(q_2) - sin(q_2)sin(q_6)
\end{aligned}
$$

Each element of matrix in (3.3) is then compared with each element of matrix in (3.2). By doing this, the equations are solved to obtain the FK orientation expressions for the pelvis with respect to right foot as shown in (3.4)-(3.6).

$$\theta_{x\_RF} = arctan\left[\frac{-sin(q_6)cos(a)cos(q_2) - sin(q_2)cos(q_6)}{cos(q_6)cos(a)cos(q_2) - sin(q_2)sin(q_6)}\right] \tag{3.4}$$

$$\theta_{y\_RF} = arcsin\left[sin(a)cos(q_2)\right] \tag{3.5}$$

$$\theta_{z\_RF} = arctan\left[\frac{sin(a)cos(q_1)sin(q_2) - cos(a)sin(q_1)}{sin(a)sin(q_1)sin(q_2) + cos(a)cos(q_1)}\right] \tag{3.6}$$

Where 'a' in (3.4)-(3.6) is the same as in (3.3). For the left leg case, the FK orientation equations, θ_{x-LF}, θ_{y-LF} and θ_{z-LF} are obtained in the same approach as (3.4)-(3.6).

3.3 Inverse Kinematics

In order to solve the IK, sufficient numbers of FK equations are needed. For position, it can be either selected CoM or foot position. Here, the approach is to use both CoM and foot positions as shown previously. CoM position is chosen as the input trajectory instead of pelvis joint for a more accurate dynamics representations. It is believed that by controlling the CoM in preference to pelvis joint, the robot will achieve a more natural and stable movement during walking. From position, there are 6 position equations and 12 joint angles variables as shown in (3.1) previously. Another 6 more equations are contributed from the orientation.

As for the orientation, the pelvis joint has been chosen for orientation. With 6 more equations from the orientation, now there are sufficient number of equations and solvable variables. One of the popular methods to solve the IK in robot study is by using a Jacobian based method. There are 12 joint angles variables from q_1 to q_{12}. Let's assigned the joint angles as in (3.7), while positions and orientations as in (3.8).

$$\vec{Q} = [q_1\ q_2\ q_3\ q_4\ q_5\ q_6\ q_7\ q_8\ q_9\ q_{10}\ q_{11}\ q_{12}]^T_{12\times1} \tag{3.7}$$

$$\vec{P} = [P_{CR}\ P_{LR}\ \theta_R\ \theta_L]^T_{12\times1} \tag{3.8}$$

Where the value of θ_R and θ_L in (3.8) are given as follows;

$$\theta_R = [\theta_{x\_RF}\ \theta_{y\_RF}\ \theta_{z\_RF}]^T_{3\times1}$$
$$\theta_L = [\theta_{x\_LF}\ \theta_{y\_LF}\ \theta_{z\_LF}]^T_{3\times1}$$

By having (3.7) and (3.8), a Jacobian matrix between these two equations can be defined as in (3.9).

$$\dot{\vec{P}} = J\dot{\vec{Q}} \tag{3.9}$$

Avoiding the singularities, (3.9) could be solved by using Newton-Raphson Method [50].

3.4 Application of IK for Straight Walking

In order to validate the proposed IK, several simulations have been done.

3.4.1 Walking Simulation on Flat Floor

A dynamically balanced bipedal walking pattern on flat floor has been developed first before simulations with the orientation IK method are done. CoM trajectories in x, y and z directions of the walking pattern are shown in Figs. 3.3 - 3.5.

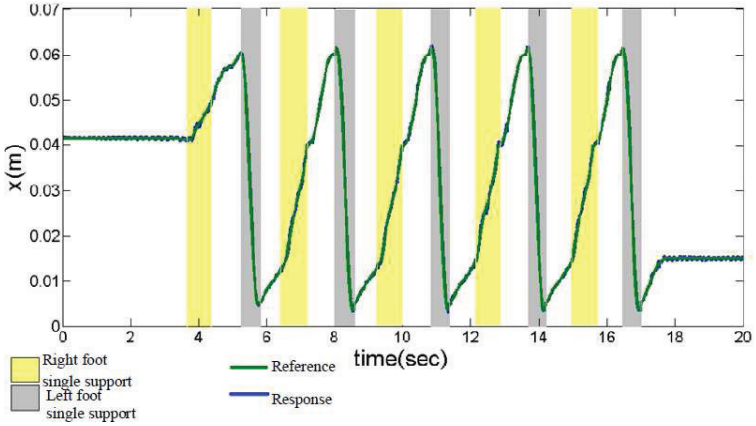

Figure 3.3: x-trajectory.

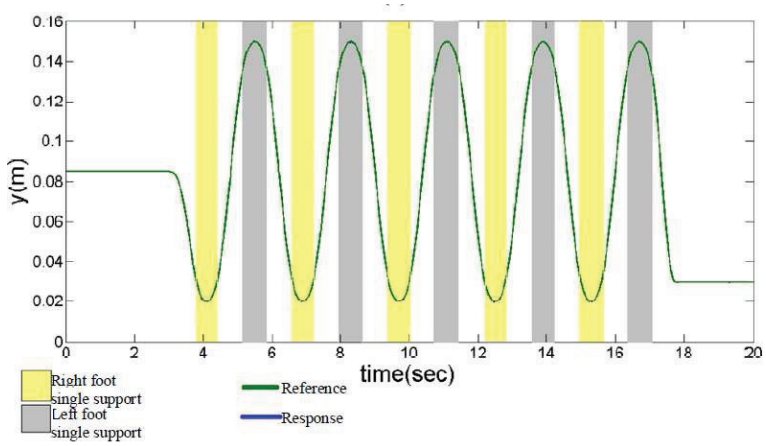

Figure 3.4: y-trajectory.

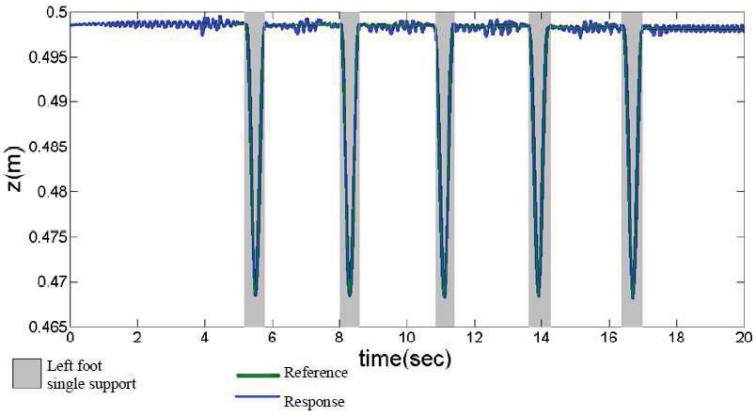

Figure 3.5: z-trajectory.

Please note that in Figs. 3.3 - 3.5, the CoM positions are referred to right foot of the biped robot. The notation of the axes is the same as used in Fig. 3.2 previously. The trajectories with respect to left foot are not shown. However, the regions of left foot single support and right foot single support is shown clearly in Figs. 3.3 - 3.5. The CoM trajectory in z direction is always constant at certain value with respect to the supporting leg. However, one might be confused with Fig. 3.5 since it does not look constant. During the grey region of Fig. 3.5, right foot is not in supporting mode anymore. During these times, left foot acts as supporting foot while right foot in swing phase.

3.4.2 Walking Simulation on 11^0 Inclined Floor without Orientation Included

From this simulation, it is noticed that when the floor is inclined to 11^0, the robot fell down after 2 steps if orientations are not included in IK. The snapshots of the biped robot walking

simulation for 11^0 inclined are shown in Fig. 3.6.

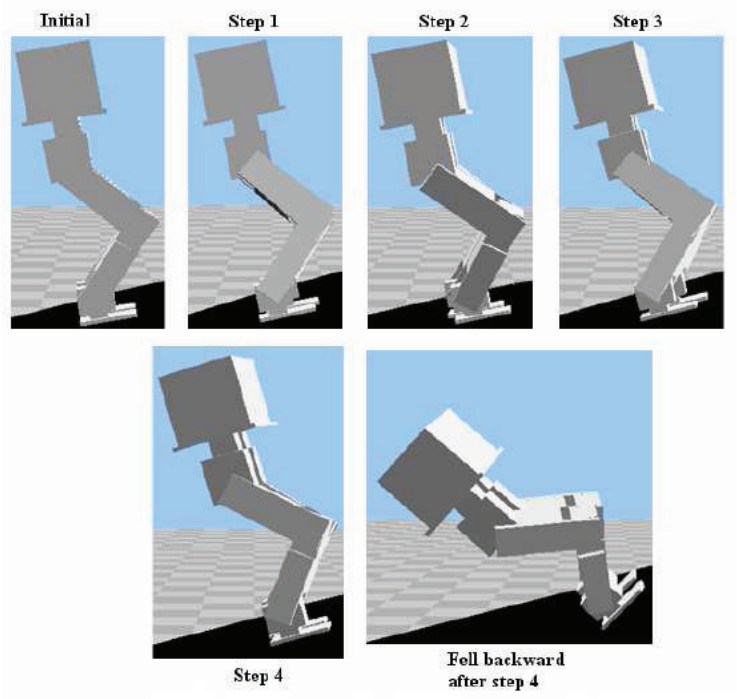

Figure 3.6: Snapshots of biped robot walking on 11^0 inclined floor without orientation included.

As shown in Fig. 3.6, the robot started with its initial standstill position on a 11^0 inclined floor. After 3s, the robot started to move by swinging out its left foot first. Continuously, right foot stepped out in step 2. Left and right foot stepped out repeatedly one after another for 10 steps. However, since the walking pattern is designed purposely for a flat floor, the robot fell down backward after step 4 because no pitch orientation is included in the trajectory planning. From the ZMP trajectrory, it can be seen in Fig. 3.7 that about 10s, ZMP in x direction already exceeded the foot boundary that caused the fell. For y direction, ZMP almost touched the boundary as shown in Fig. 3.8.

3.4.3 Walking Simulation on 11^0 Inclined Floor with Orientation Included

In order to achieve walking on the 11^0 inclined floor, orientations are included in the trajectory planning by using the method proposed in this section. Since the floor is inclined in pitch direction, all the related pitch axes are used, instead of only the ankle joints. The input angle orientation in pitch direction is set to 11^0 in order to compensate the 11^0 inclined floor. The robot is able to complete 10 steps walking on inclined floor successfully as shown in snapshots of Fig. 3.9.

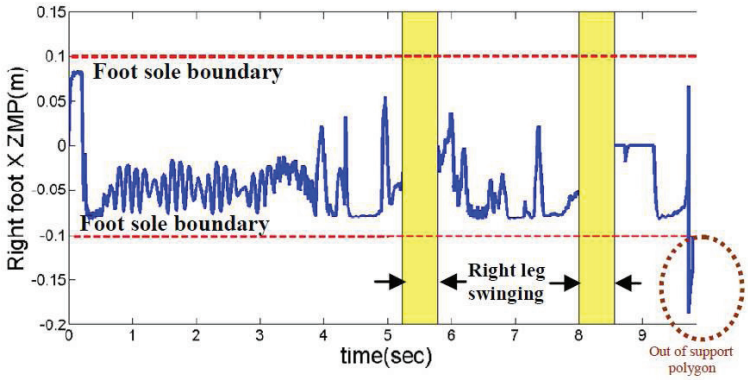

Figure 3.7: x-ZMP of biped robot walking on 11^0 inclined floor without orientation included.

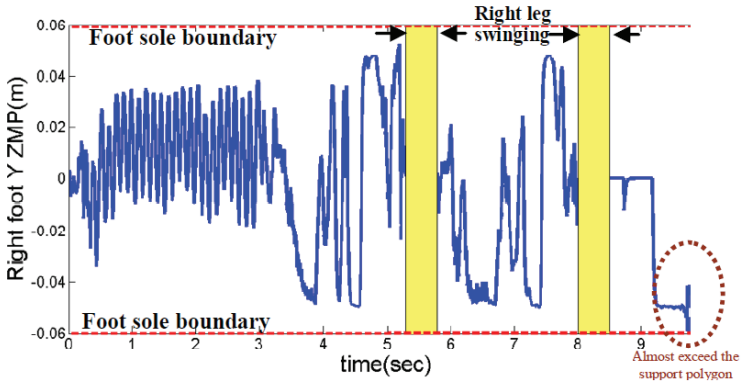

Figure 3.8: y-ZMP of biped robot walking on 11^0 inclined floor without orientation included.

ZMP trajectory is also plotted out as shown in Fig. 3.10 and Fig. 3.11. From the designed walking pattern, the robot will only started walking movements after 3s. It can be seen in Fig. 3.10 and Fig. 3.11 that at anytime, the trajectory of ZMP never crossed the foot boundary. This ensured the robot is in stable position until all 10 steps are completed. Please note that in Figs. 3.7, 3.8, 3.10 and 3.11, the foot sole boundary in x and y directions are drawn by red dotted lines.

3.4.4 Walking Simulations using Ankle Joints Modification only and with Orientation Included

For comparison, biped walking simulation on 11^0 inclined floor with modification at the ankle joints only has been done. In this simulation, it is found that the orientation of the robot feet after 10 steps walking are rotated about 20^0 to the right. The position and orientation of the robot at the beginning and after 10 steps walking are shown in Fig. 3.12.

Furthermore, simulation using proposed method to distribute angle caused by the inclined floor to all robot joints is done. On the same height inclined floor, the robot is able to maintain

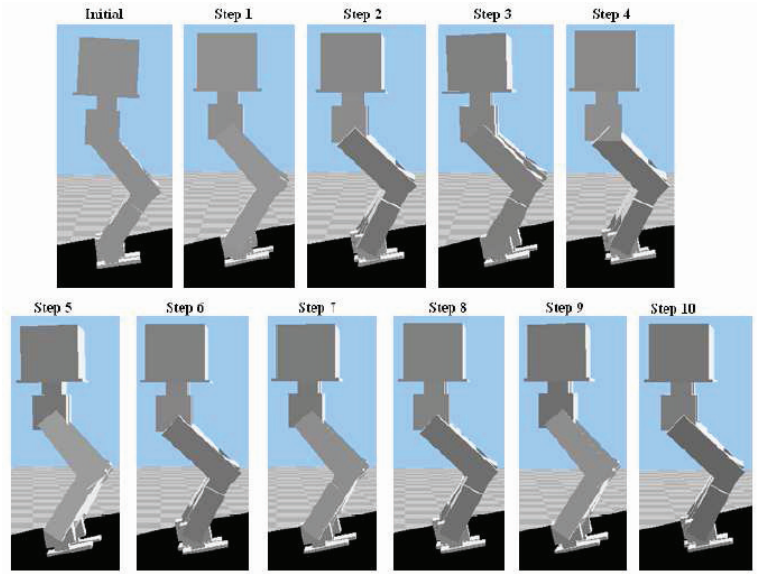

Figure 3.9: Snapshots of biped robot walking on 11^0 inclined floor with orientation included.

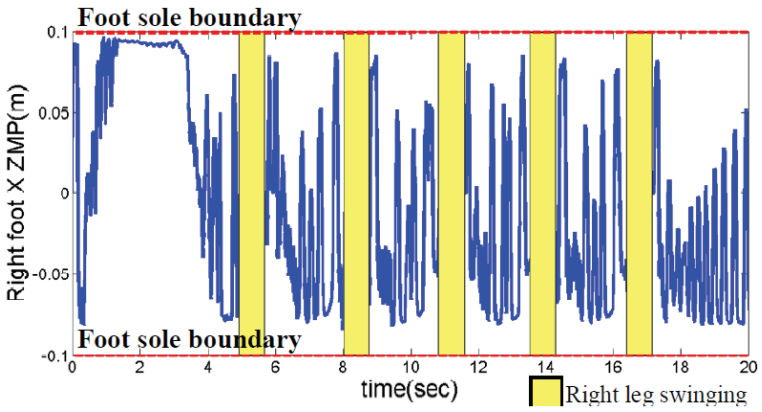

Figure 3.10: x-ZMP of biped robot walking on 11^0 inclined floor with orientation included.

the orientation of robot feet parallel to x-axis direction. Please note that the x-direction is the same as used in Fig. 3.2 which is the direction of forward movement. The position and orientation of the robot at the beginning and after 10 steps walking are shown in Fig. 3.13.

3.5 Application of IK for Diagonal Walking

In this section, the IK is applied for diagonal walking on slope [51]. Biped walking on slope has started as early as in 1990 by Zheng and Shen [31]. In [31], the researchers have proposed a motion scheme for slope walking that consisted of three major aspects. The major aspects are solutions related to inclination of landing foot and gradient of the slope, slope motion scheme and transitional walking. Kim et al. proposed many control schemes for biped walking on

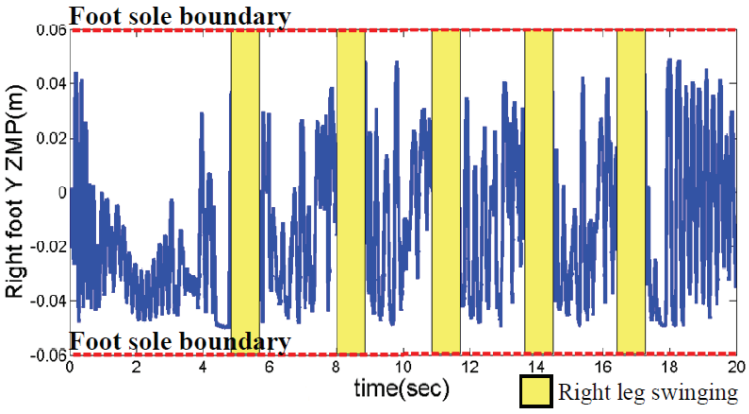

Figure 3.11: y-ZMP of biped robot walking on 11^0 inclined floor with orientation included.

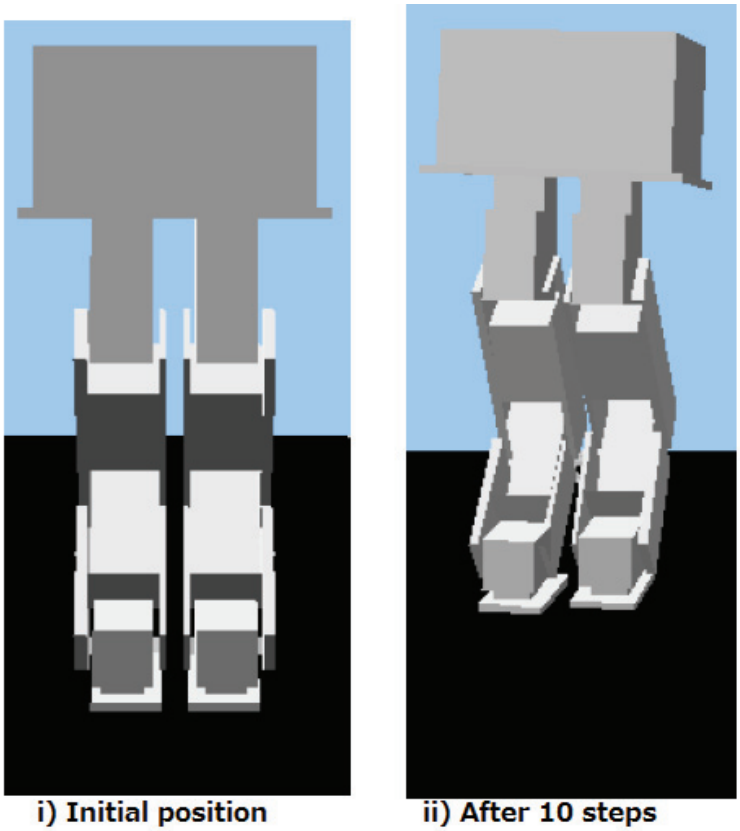

Figure 3.12: Biped walking with modifications at ankle joints only.

slope such as upright pose, landing angular momentum, landing shock absorber, landing timing and landing position controls [12]. Huang et al. [43] proposed a motion pattern generator for slope walking in 3-D dynamics by using preview control of ZMP. There are also researchers who implemented tactile sensing system to a humanoid robot for walking on the slopes [32]. The tactile sensors are installed on two robotic feet.

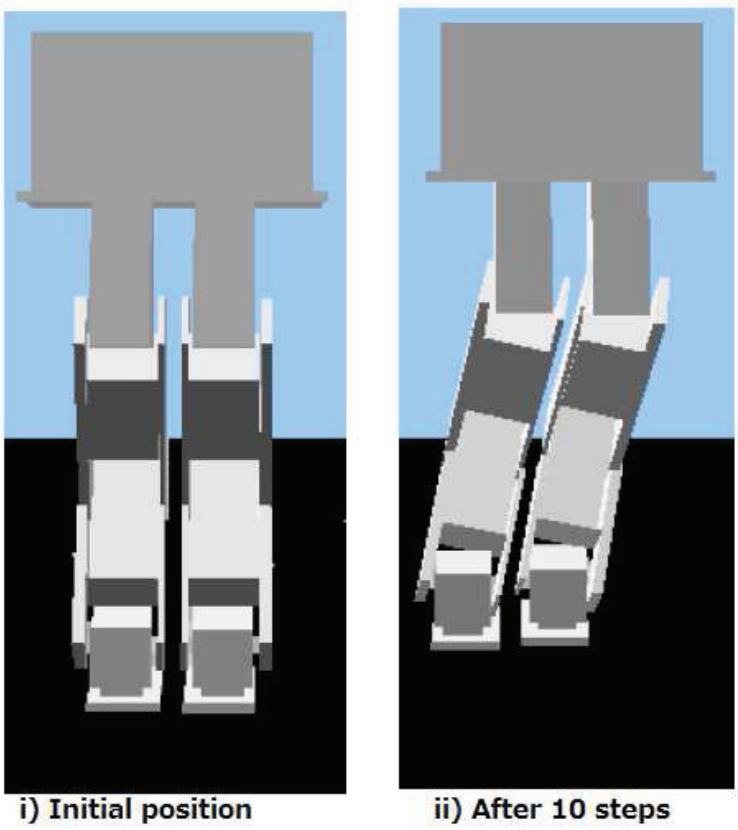

Figure 3.13: Biped walking with orientation included.

However, in all researches mentioned above, the walking is only done in straight direction on the inclined floor. The problems and difficulties of walking in diagonal walking on inclined floor are not considered in their papers. Therefore, in this section, diagonal walking method on inclined floor is proposed.

3.5.1 Trajectory Planning Procedure

The trajectory planning procedures for the diagonal walking are summarized into several steps. The procedures are categorized into two groups as follows:

- Calculation of the CoM Position Trajectory and the Foot Swing Position Trajectory
- Calculation of Roll and Pitch Joint Angles for Diagonal Walking on Inclined Floor

The details of the procedures above are explained as follows.

Calculation of the CoM Position Trajectory and the Foot Swing Position Trajectory

The CoM position is designed by using LIPM approach as explained in section 3.2.1. During the single support phase, equations 3.10 and 3.11 below are used in order to get the CoM-x and

CoM-y trajectories while maintaining the ZMP to be inside the support polygon. During the single support phase, the support polygon is bounded by the size of the support foot. When the CoM traveled in single support phase, foot swing will move to make a step. This swing foot is moved by using polynomial function.

$$x(t) = (x_0 - x_{zmp})cosh(\omega t) + \frac{\dot{x_0}}{\omega}sinh(\omega t) + x_{zmp} \tag{3.10}$$

$$y(t) = (y_0 - y_{zmp})cosh(\omega t) + \frac{\dot{y_0}}{\omega}sinh(\omega t) + y_{zmp} \tag{3.11}$$

where the value of ω in equations 3.10 and 3.11 is given as follows:

$$\omega = \sqrt{\frac{g}{z}} \tag{3.12}$$

Here, x_0 and y_0 denote the initial trajectory of CoM in x and y directions respectively.

In double support phase smooth connections between two phases are ensured by using a 5th polynomial function as given in (3.13) - (3.15). Position, velocity and acceleration are taken into account in order to get smooth movement or transition between phases.

$$p(t) = a_0 + a_1 t + a_2 t^2 + a_3 t^3 + a_4 t^4 + a_5 t^5 \tag{3.13}$$

$$v(t) = a_1 + 2a_2 t + 3a_3 t^2 + 4a_4 t^3 + 5a_5 t^4 \tag{3.14}$$

$$a(t) = 2a_2 + 6a_3 t + 12a_4 t^2 + 20a_5 t^3 \tag{3.15}$$

Here, p, v and a denote the position, velocity and acceleration respectively. a_0 to a_5 are determined with six constraints which are initial and ending of position, velocity and acceleration.

Calculation of Roll and Pitch Joint Angles for Diagonal Walking on Inclined Floor

Besides the positions, pelvis orientations must be designed according to the floor surface. If the floor is flat, all the orientation input trajectories, θ_{x_RF}, θ_{y_RF}, θ_{z_RF}, θ_{x_LF}, θ_{y_LF} and θ_{z_LF} are all zero. However, on the inclined floor these orientation input trajectories are not zero. θ_{x_RF} and θ_{x_LF} denote the roll orientation of the pelvis with respect to right foot and left foot respectively. θ_{y_RF} and θ_{y_LF} denote the pitch orientation of the pelvis with respect to right foot and left foot respectively. Furthermore, θ_{z_RF} and θ_{z_LF} denote the yaw orientation of the pelvis with respect to right foot and left foot respectively.

Diagonal walking is occurred when the biped robot rotated to right or left from the straight orientation on inclined floor as shown in Fig. 3.14. In this research, the inclined floor is assumed known. If the slope angle of the inclined floor is known, it is important to know the relationship

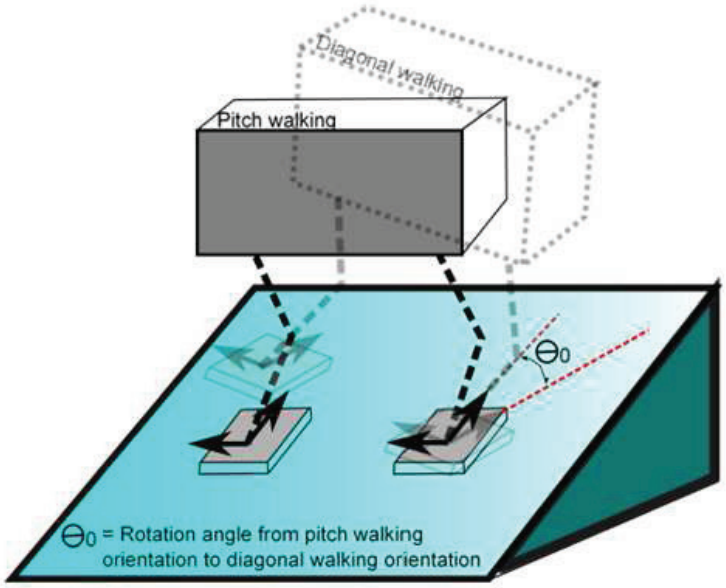

Figure 3.14: Diagonal walking on inclined floor.

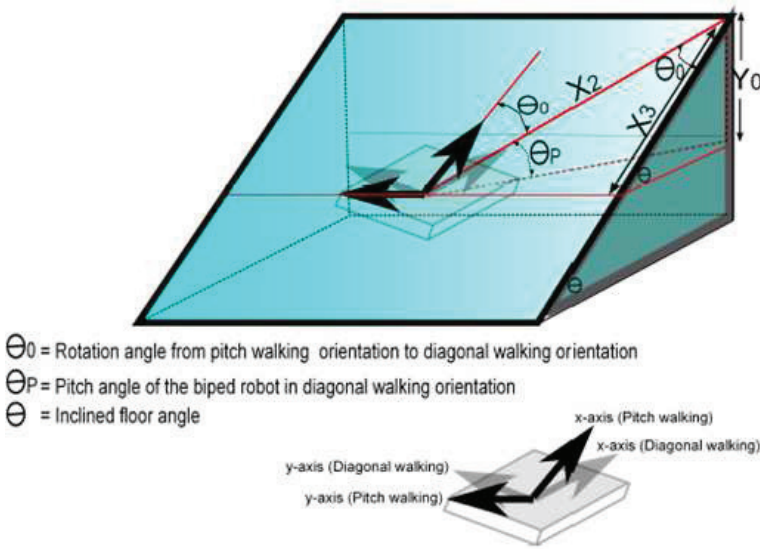

Figure 3.15: Relation between slope and pitch angles.

between the slope and the pitch angles. Later on, relationship between pitch and roll joints are determined.

The derivations of relation between slope and pitch angles can be obtained by using Fig. 3.15 as reference. θ_0 is the angle when the biped robot rotated to the right from its straight position to perform a diagonal walking position.

From Fig. 3.15, the equations are derived as follows:

$$Y_0 = sin(\theta_p) \times X_2 = sin(\theta) \times X_3 \tag{3.16}$$

$$sin(\theta_p) = sin(\theta) \times \frac{X_3}{X_2} \tag{3.17}$$

$$sin(\theta_p) = sin(\theta) \times cos(\theta_0) \tag{3.18}$$

It is shown in derivations above, the relationship between pitch and slope angles as shown in (3.18).

On the other hand, the derivations of relation between roll and pitch angles are obtained by using Fig. 3.16 as reference.

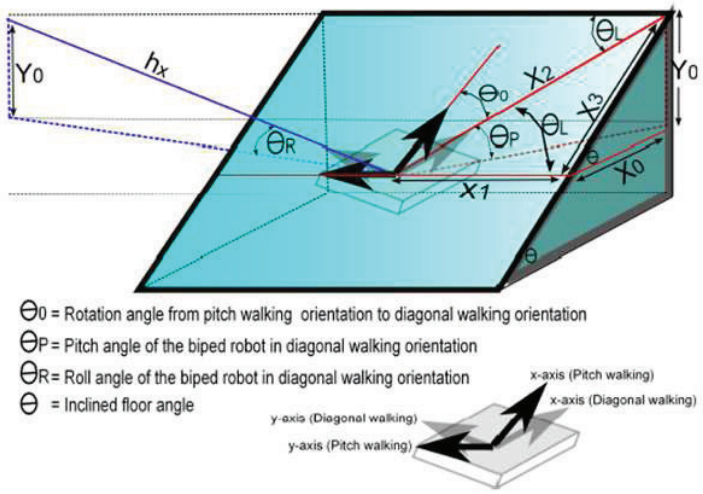

Figure 3.16: Relation between roll and pitch angles.

The derivations between roll and pitch angles are shown in (3.19) - (3.21).

$$X_3 = \frac{Y_0}{sin(\theta)} \tag{3.19}$$

$$X_2 = \sqrt{{X_1}^2 + (\frac{Y_0}{sin(\theta)})^2} \tag{3.20}$$

$$sin(\theta_p) = \frac{Y_0}{X_2} = \frac{Y_0}{\sqrt{{X_1}^2 + (\frac{Y_0}{sin(\theta)})^2}} \tag{3.21}$$

$$tan(\theta_p) = \frac{h_x}{X_2} \tag{3.22}$$

$$h_x = tan(\theta_L) \times \sqrt{{X_1}^2 + (\frac{Y_0}{sin(\theta)})^2} \tag{3.23}$$

Table 3.1: Simulation parameters

Maximum height of swing leg [m]	0.03
Forward foot stride [m]	0.07
Perpendicular of CoM height to slope surface [m]	0.4971
Single support time [s]	0.6
Double support time [s]	0.8
Inclined floor angle, θ [^{0}]	7.08
Roll orientation angle, θ_R [^{0}]	5
Pitch orientation angle, θ_p [^{0}]	5
Rotation from the straight, θ_0 [^{0}]	45

$$sin(\theta_R) = \frac{Y_0}{h_x} = \frac{Y_0}{tan(\theta_L) \times \sqrt{{X_1}^2 + (\frac{Y_0}{sin(\theta)})^2}} \tag{3.24}$$

Equs. (3.21), (3.22) and (3.24) are then compared. As the result, (3.25)-(3.26) are obtained as below.

$$sin(\theta_p) = sin(\theta_R) \times tan(\theta_L) \tag{3.25}$$

$$sin(\theta_p) = sin(\theta_R) \times tan(90^0 - \theta_0) \tag{3.26}$$

It is shown in the derivations above, the relationship between pitch and roll angles as shown in (3.26).

3.5.2 Simulation Results

The simulations are done by using ROCOS. The simulations setup parameters are shown in Table 3.1. In these simulations, the biped is walking on floor in diagonal direction.

As shown in the Table 3.1, the diagonal walking simulations are done for the inclined floor with slope angle of 7.08 degree. If the floor slope angle, θ and the rotation from straight, θ_0 are known, the roll and pitch joint angles can be calculated by using (3.18) and (3.26). It is also given that the θ_0 is 45 degree.

In this simulation, the biped robot performed a ten steps walking in diagonal direction on the inclined floor. The CoM trajectories in x, y and z directions are plotted and shown as in Figs. 3.17 and 3.18. The perpendicular distance of the CoM height in z direction between the CoM and the support foot is always constant at 0.4971m as shown in Fig. 3.18. It can be seen that smooth CoM trajectories are obtained by using the proposed method as confirmed in Figs. 3.17 and 3.18.

The value of θ_0 is 45 degree and the inclined floor slope angle is 7.08 degree. Using (3.18) the pitch orientation is obtained as (3.27).

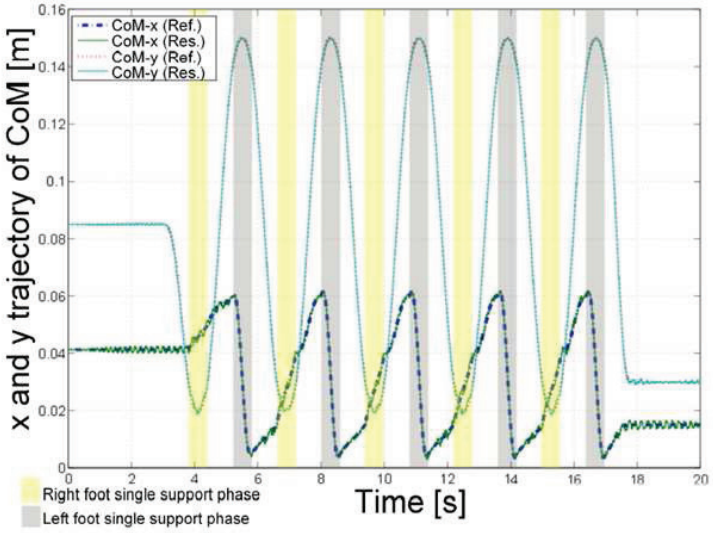

Figure 3.17: x and y trajectory of CoM.

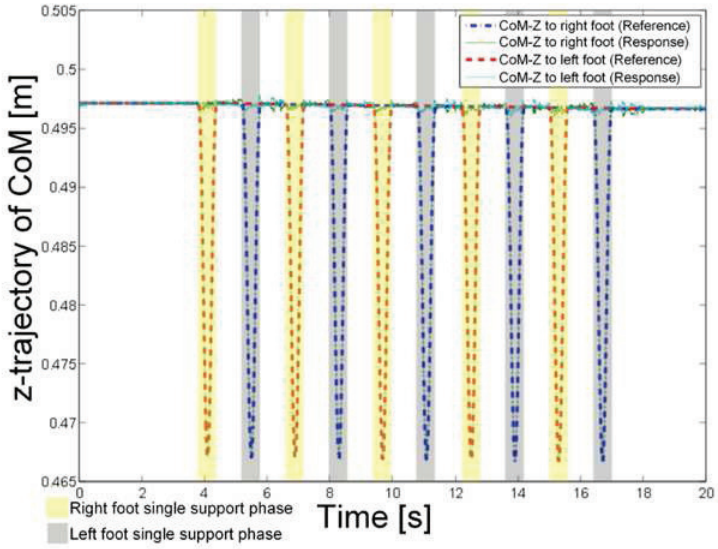

Figure 3.18: z trajectory of CoM.

$$\begin{aligned} sin(\theta_p) &= sin(\theta) \times cos(\theta_0) \\ sin(\theta_p) &= sin(7.08^0) \times cos(45^0) \\ \theta_p &= 5^0 \end{aligned} \tag{3.27}$$

Furthermore, the roll orientation is determined by using (3.26) as shown in (3.28).

$$sin(\theta_p) = sin(\theta_R) \times tan(90^0 - \theta_0)$$

$$
\begin{aligned}
sin(\theta_p) &= sin(\theta_R) \times tan(90^0 - 45^0) \\
\theta_R &= 5^0
\end{aligned}
\tag{3.28}
$$

The roll and pitch orientation of the pelvis with respect to the right foot is shown as in Fig. 3.19. With the proposed method, the positions and orientations are determined and the diagonal walking is achieved successfully.

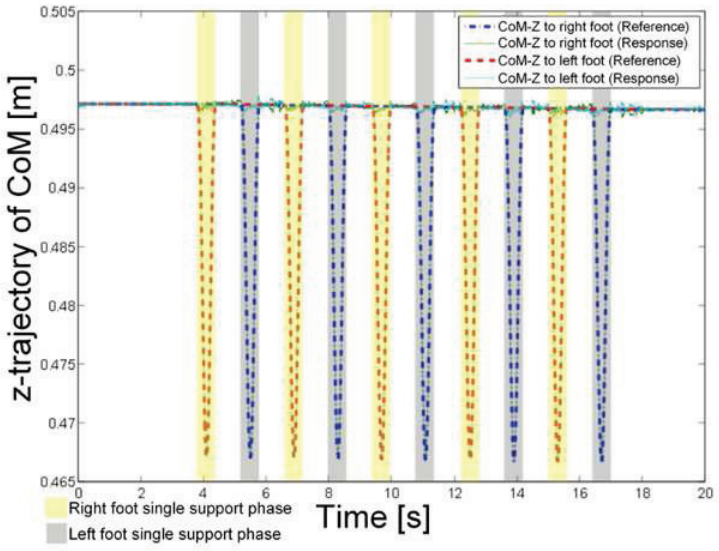

Figure 3.19: Pelvis orientation with respect to right foot.

Chapter 4

Biped Robot Walking along a Step in 2-D with DLLIPM

In this chapter the proposed method is explained for the 2-D of biped walking, in sagittal and lateral cases.

4.1 Introduction

This section is expanded from Sub-section 1.3. In the Sub-section 1.3, the concept of DLLIPM has been introduced. Now, the details of the derivations for 2-D cases, sagittal and lateral will be explained.

4.2 Sagittal

This sub-section will explain about the proposed method for walking along a step with consideration of sagittal plain only [30]. When different length of pendulum is used for representing RF and LF during the biped walking, there is possibility of unbalance shape of walking trajectory. Therefore, Newton-Raphson is used in order to obtain appropriate walking parameters. In this section, the proposed method is explained and derivations are done systematically.

4.2.1 Single Inverted Pendulum

In this sub-section, the equations of position, velocity and acceleration of a single inverted pendulum are derived [23]. The single inverted pendulum model is shown as in Fig. 4.1. In this figure, x_i,$\dot{x}_i$ and $\ddot{x}_i$ are the position, velocity and acceleration respectively at the beginning point. On the other hand, x_f,$\dot{x}_f$ and $\ddot{x}_f$ are the position, velocity and acceleration at the ending point. $x(t)$ and S denote the constantaneous value of CoM trajectory in x-direction and the stride of CoM, correspondingly. While g and Z_c denote the acceleration of gravity and the height of pendulum respectively.

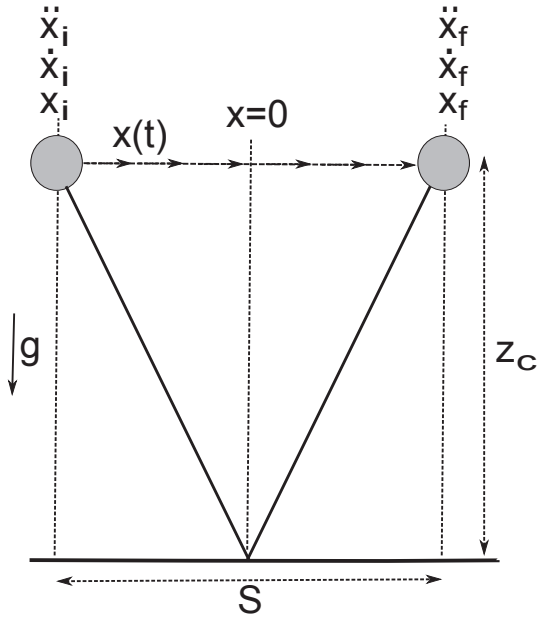

Figure 4.1: Single inverted pendulum model.

Position

In this sub-section, the derivations of equations which are related to position in single inverted pendulum model are shown. The equation of position is shown as in (4.1)

$$x(t) = x_i cosh(\frac{t}{T_c}) + T_c \dot{x}_i sinh(\frac{t}{T_c}) \tag{4.1}$$

The value of T_c in (4.1) is given as (4.2)

$$T_c = \sqrt{\frac{z_c}{g}} \tag{4.2}$$

In order to represent (4.1) in term of exponential function, (4.3) is derived.

$$x(t) = (\frac{x_i - T_c \dot{x}_i}{2}) e^{-\frac{t}{T_c}} + (\frac{x_i + T_c \dot{x}_i}{2}) e^{\frac{t}{T_c}} \tag{4.3}$$

Velocity

In this sub-section, the derivations of equations which are related to velocity in single inverted pendulum model are shown. Time derivative of (4.3), gives equation of velocity as shown in (4.4).

$$\dot{x}(t) = (\frac{\dot{x}_i - \frac{x_i}{T_c}}{2}) e^{-\frac{t}{T_c}} + (\frac{\dot{x}_i + \frac{x_i}{T_c}}{2}) e^{\frac{t}{T_c}} \tag{4.4}$$

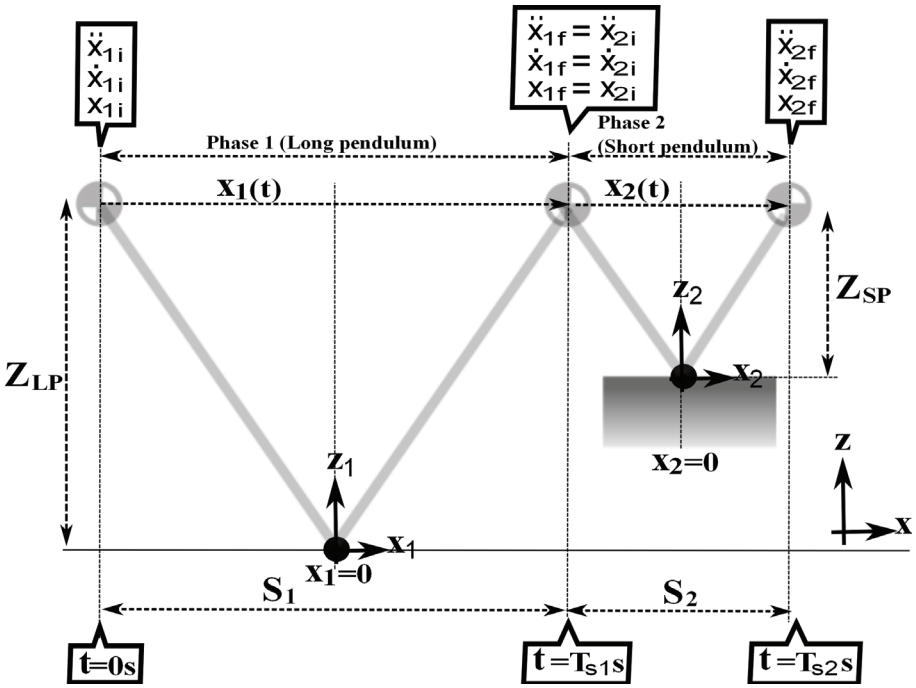

Figure 4.2: Dual length inverted pendulum model for parallel stair walking. In this figure, one leg is always lands on the higher ground and the other one always lands on the lower ground. These phases will be repeated for continuous walking.

Acceleration

In this sub-section, the derivations of equations which are related to acceleration in single inverted pendulum model are shown. Time derivative of (4.4) gives equation of acceleration as shown in (4.5).

$$\ddot{x}(t) = (\frac{\frac{x_i}{T_c^2} - \frac{\dot{x}_i}{T_c}}{2})e^{-\frac{t}{T_c}} + (\frac{\frac{x_i}{T_c^2} + \frac{\dot{x}_i}{T_c}}{2})e^{\frac{t}{T_c}} \tag{4.5}$$

(4.5) can be also rearranged as in (4.6)

$$\ddot{x}(t) = \frac{x_i}{T_c^2}(\frac{e^{\frac{t}{T_c}} + e^{-\frac{t}{T_c}}}{2}) + \frac{\dot{x}_i}{T_c}(\frac{e^{\frac{t}{T_c}} - e^{-\frac{t}{T_c}}}{2}) \tag{4.6}$$

4.2.2 Biped Walking Model by LIPM for Walking on a Step

Supposed that the long pendulum and short pendulum phases represent by phase 1 and phase 2 as shown in Fig. 4.2.

4.2.2.1 Definitions of Parameters

All parameters involved in Fig. 4.2 are explained and defined clearly as in Table 4.1.

Table 4.1: Definitions of parameters

Parameters	Definitions
Z_{LP}	CoM height of long pendulum
Z_{SP}	CoM height of short pendulum
S_1	CoM stride during phase 1
S_2	CoM stride during phase 2
$x_1(t)$	Instantaneous position during phase 1
$x_2(t)$	Instantaneous position during phase 2
x_{1i}	Initial position during phase 1
$\dot{x}_{1i}$	Initial velocity during phase 1
$\ddot{x}_{1i}$	Initial acceleration during phase 1
x_{1f}	Final position during phase 1
$\dot{x}_{1f}$	Final velocity during phase 1
$\ddot{x}_{1f}$	Final acceleration during phase 1
x_{2i}	Initial position during phase 2
$\dot{x}_{2i}$	Initial velocity during phase 2
$\ddot{x}_{2i}$	Initial acceleration during phase 2
x_{2f}	Final position during phase 2
$\dot{x}_{2f}$	Final velocity during phase 2
$\ddot{x}_{2f}$	Final acceleration during phase 2
T_{s1}	Instantaneous time at the end of phase 1
T_{s2}	Instantaneous time at the end of phase 2

4.2.2.2 Assumptions

All derivations shown later are based on five assumptions as following:

1. The initial position and initial velocity of phase 1 are known.
2. The height of the higher ground surface, h, which the robot will walk on is a known value.
3. The CoM height of long pendulum and short pendulum are known.
4. Both pendulums, the long and short pendulums are symmetrical. Reference of the position for each phase is the middle of each supporting foot.
5. There are four free parameters that need to be solved which are S_1, S_2, T_{s1} and T_{s2}.

4.2.2.3 Constraints

Based on assumptions designed in the previous sub-section, several constraints are enforced. In total, there are four constraints which resulted into four equations. The objectives of the constraints enforced are to ensure smooth motions between phases and also for reducing the force at the landing foot.

1. From the fourth assumption, the pendulums for phase 1 and 2 are made to be symmetrical by the following equations:

$$x_{1f} = +\frac{S_1}{2} \tag{4.7}$$

$$x_{2f} = +\frac{S_2}{2} \tag{4.8}$$

2. Velocity is continuous which means the end velocity of phase 1 has the same value with the initial velocity of phase 2. In the first constraint, all pendulums are made to be symmetrical. Therefore, to ensure the continuity of the velocity, the end velocity of phase 1 must be equal to the end velocity of phase 2 as shown by the following equation:

$$\dot{x}_{1f} = \dot{x}_{2f} \tag{4.9}$$

3. Acceleration is continuous which means the end acceleration of phase 1 has the same value with the absolute value of initial acceleration of phase 2. In the first constraint, all pendulums are made to be symmetrical. Therefore, to ensure the continuity of the acceleration, the end acceleration of phase 1 must be equal to the end acceleration of phase 2 as shown by the following equation:

$$\ddot{x}_{1f} = \ddot{x}_{2f} \tag{4.10}$$

Detailed Equations

In this part, the detailed equations are derived from the constraints mentioned in sub-section 3.2.3.

1. The previous constraint in (4.7) is realized using (4.3) as shown in (4.11).

$$\begin{aligned} x_{1f} &= \left(\frac{x_{1i} - T_{c1}\dot{x}_{1i}}{2} e^{-\frac{T_{s1}}{T_{c1}}}\right) \\ &+ \left(\frac{x_{1i} + T_{c1}\dot{x}_{1i}}{2} e^{\frac{T_{s1}}{T_{c1}}}\right) = \frac{S_1}{2} \end{aligned} \tag{4.11}$$

2. The previous constraint in (4.8) is also realized using (4.3) as shown in (4.12).

$$\begin{aligned} x_{2f} &= \left(\frac{x_{2i} - T_{c2}\dot{x}_{2i}}{2} e^{-\frac{T_{s2}}{T_{c2}}}\right) \\ &+ \left(\frac{x_{2i} + T_{c2}\dot{x}_{2i}}{2} e^{\frac{T_{s2}}{T_{c2}}}\right) = \frac{S_2}{2} \end{aligned} \tag{4.12}$$

3. The previous constraint in (4.9) is realized using (4.4) as shown in (4.13).

$$\begin{aligned}\left(\frac{\dot{x}_{1i}-\frac{x_{1i}}{T_{c1}}e^{-\frac{T_{s1}}{T_{c1}}}}{2}\right) &+ \left(\frac{\dot{x}_{1i}+\frac{x_{1i}}{T_{c1}}e^{\frac{T_{s1}}{T_{c1}}}}{2}\right)- \\ \left(\frac{\dot{x}_{2i}-\frac{x_{2i}}{T_{c2}}e^{-\frac{T_{s2}}{T_{c2}}}}{2}\right) &- \left(\frac{\dot{x}_{2i}+\frac{x_{2i}}{T_{c2}}e^{\frac{T_{s2}}{T_{c2}}}}{2}\right)=0\end{aligned} \tag{4.13}$$

4. The previous constraint in (4.10) is realized using (4.6) as shown in (4.14).

$$\begin{aligned}\left(\frac{x_{1i}}{T_{c1}^2}\frac{e^{\frac{T_{s1}}{T_{c1}}}+e^{-\frac{T_{s1}}{T_{c1}}}}{2}\right) &+ \left(\frac{\dot{x}_{1i}}{T_{c1}}\frac{e^{\frac{T_{s1}}{T_{c1}}}-e^{-\frac{T_{s1}}{T_{c1}}}}{2}\right)- \\ \left(\frac{x_{2i}}{T_{c2}^2}\frac{e^{\frac{T_{s2}}{T_{c2}}}+e^{-\frac{T_{s2}}{T_{c2}}}}{2}\right) &- \left(\frac{\dot{x}_{2i}}{T_{c2}}\frac{e^{\frac{T_{s2}}{T_{c2}}}-e^{-\frac{T_{s2}}{T_{c2}}}}{2}\right)=0\end{aligned} \tag{4.14}$$

4.2.3 Solution of S_1, S_2, T_{S1} and T_{S2} using Newton-Raphson Method

In order to find solution for S_1, S_2, T_{S1} and T_{S2}, a numerical method known as Newton-Raphson is chosen. There are several steps need to be taken.

4.2.3.1 Simplification of equations

Before Newton-Raphson method can be implemented, equations (4.15)-(4.20) are defined.

$$\alpha = e^{\frac{T_{s1}}{T_{c1}}} \tag{4.15}$$

$$\beta = e^{\frac{T_{s2}}{T_{c2}}} \tag{4.16}$$

$$A = \left(\frac{x_{1i}+T_{c1}\dot{x}_{1i}}{2}\right) \tag{4.17}$$

$$B = \left(\frac{x_{1i}-T_{c1}\dot{x}_{1i}}{2}\right) \tag{4.18}$$

$$C = \left(\frac{x_{2i}+T_{c2}\dot{x}_{2i}}{2}\right) \tag{4.19}$$

$$D = \left(\frac{x_{2i}-T_{c2}\dot{x}_{2i}}{2}\right) \tag{4.20}$$

By substituting (4.15), (4.17) and (4.18) into (4.11), equation (4.21) is obtained as following,

$$\left(B\alpha^{-1}\right)+(A\alpha)=\frac{S_1}{2} \tag{4.21}$$

By substituting (4.16), (4.19) and (4.20) into (4.12), equation (4.22) is obtained as following,

$$\left(D\beta^{-1}\right)+(C\beta)=\frac{S_2}{2} \tag{4.22}$$

By substituting (4.15) and (4.16) into (4.13), equation (4.23) is obtained,

$$\begin{aligned}\left(\frac{\dot{x}_{1i}-\frac{x_{1i}}{T_{c1}}\alpha^{-1}}{2}\right) &+ \left(\frac{\dot{x}_{1i}+\frac{x_{1i}}{T_{c1}}\alpha}{2}\right) - \\ \left(\frac{\dot{x}_{2i}-\frac{x_{2i}}{T_{c2}}\beta^{-1}}{2}\right) &- \left(\frac{\dot{x}_{2i}+\frac{x_{2i}}{T_{c2}}\beta}{2}\right) = 0\end{aligned} \tag{4.23}$$

Then, (4.23) is further simplified by substituting (4.17)-(4.20) into it as shown in (4.24).

$$\frac{1}{T_{c1}}\left(-B\alpha^{-1}+A\alpha\right)-\frac{1}{T_{c2}}\left(-D\beta^{-1}+C\beta\right) = 0 \tag{4.24}$$

By substituting (4.21) and (4.22) into (4.24), (4.25) is obtained as following;

$$\frac{1}{T_{c1}}\left(2A\alpha-\frac{S_1}{2}\right)-\frac{1}{T_{c2}}\left(2C\beta-\frac{S_2}{2}\right)=0 \tag{4.25}$$

By substituting (4.15) and (4.16) into (4.14), equation (4.26) is obtained,

$$\begin{aligned}\frac{1}{T_{c1}^2}\left(\frac{x_{1i}+T_{c1}\dot{x}_{1i}}{2}\alpha+\frac{x_{1i}-T_{c1}\dot{x}_{1i}}{2}\alpha^{-1}\right) &- \\ \frac{1}{T_{c2}^2}\left(\frac{x_{2i}+T_{c2}\dot{x}_{2i}}{2}\beta+\frac{x_{2i}-T_{c2}\dot{x}_{2i}}{2}\beta^{-1}\right) &= 0\end{aligned} \tag{4.26}$$

By substituting (4.21) and (4.22) into (4.26), (4.26) can be simplified as (4.27)

$$\frac{1}{T_{c1}^2}\frac{S_1}{2}-\frac{1}{T_{c2}^2}\frac{S_2}{2}=0 \tag{4.27}$$

From (4.21), (4.22), (4.25) and (4.27), the equations are defined as functions in (4.28)-(4.31)

$$f_1(x) = A\alpha^2-\frac{S_1}{2}\alpha+B \tag{4.28}$$

$$f_2(x) = C\beta^2-\frac{S_2}{2}\beta+D \tag{4.29}$$

$$f_3(x) = \frac{2A}{T_{c1}}\alpha-\frac{1}{2T_{c1}}S_1-\frac{2C}{T_{c2}}\beta+\frac{1}{2T_{c2}}S_2 \tag{4.30}$$

$$f_4(x) = \frac{1}{T_{c1}^2}S_1-\frac{1}{T_{c2}^2}S_2 \tag{4.31}$$

Then, (4.28)-(4.31) are rearranged as vectors shown in (4.32). In (4.32) the values of x are the variable or parameters that need to be solved as shown in (4.33).

$$\vec{f}(x) = [f_1(x)\ \ f_2(x)\ \ f_3(x)\ \ f_4(x)]^T \tag{4.32}$$

$$\vec{x} = [\alpha\ \ \beta\ \ S_1\ \ S_2]^T \tag{4.33}$$

4.2.3.2 Newton Raphson algorithm

Newton Raphson method is involving process of iterations. The objective is to obtain the roots from several complex functions. In this method, the roots are calculated using (4.34).

$$x_{n+1} = x_n - \frac{f(x_n)}{f'(x_n)} \tag{4.34}$$

$f'(x_n)$ in (4.34) are the derivative of functions which are obtained as follows;

$$f'(x_n) = \begin{bmatrix} \frac{\partial f_1}{\partial x_1} & \cdots & \frac{\partial f_1}{\partial x_4} \\ \vdots & \ddots & \vdots \\ \frac{\partial f_4}{\partial x_1} & \cdots & \frac{\partial f_4}{\partial x_4} \end{bmatrix}^{4\times4} \tag{4.35}$$

The value of each element in the matrix above is then obtained.

4.3 Lateral

This sub-section will explain about the proposed method for walking along a step with consideration of lateral plain only [33]. As for the lateral axis, it can be solved almost in the same manner as the sagittal but with slightly different constraints.

4.3.1 Biped Walking Model by DLLIPM for Walking along a Step in Lateral Plane

The long and the short pendulum phases are represented by phase 1 and 2 as shown in Fig. 4.3. In this figure, one leg lands on the higher ground and the other lands on the lower ground. These phases will be repeated for continuous walking. Phase 1 is defined as walking cycle of the biped robot when the robot is supporting by the foot on the lower ground which means the height of pendulum in this cycle is referred as long pendulum (LP). Whereas phase 2 is defined as walking cycle of the biped robot when the robot is supporting by the foot on the higher ground which means the height of pendulum in this cycle is referred as short pendulum (SP). The beginning point of the walking motion is started from the center of the RF sole.

Definitions of Parameters

All parameters involved in Fig. 4.3 are explained and defined in Table 4.2.

Assumptions

All derivations shown later are based on five assumptions as following:

- The initial position and initial velocity of phase 1 are known.

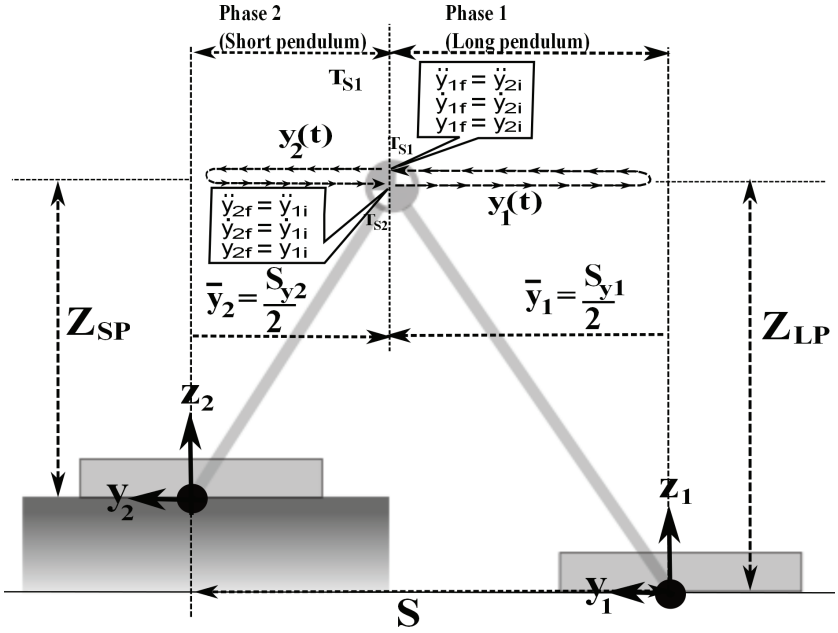

Figure 4.3: Dual length inverted pendulum model for walking along stair in lateral plane.

Table 4.2: Definitions of parameters (k is 1 or 2, which is referred to phase 1 or 2, respectively).

Parameters	Definitions
Z_{LP}	CoM height of long pendulum
Z_{SP}	CoM height of short pendulum
S_{yk}	Possible maximum stride during phase k
$y_k(t)$	Instantaneous position during phase k
y_{ki}	Initial position during phase k
$\dot{y}_{ki}$	Initial velocity during phase k
$\ddot{y}_{ki}$	Initial acceleration during phase k
$\bar{y}_k$=y_{kf}	Final position during phase k
$\dot{y}_{kf}$	Final velocity during phase k
$\ddot{y}_{kf}$	Final acceleration during phase k
T_{sk}	Instantaneous time at the end of phase k

- The height of the higher ground surface, h, which the robot will walk on is a known value.
- The CoM heights of long pendulum and short pendulum are known.
- Both pendulums, the long and the short pendulums are made to be symmetrical. Reference of the position for each phase is the middle of each supporting foot.
- There are four free parameters that need to be solved which are S_{y1}, S_{y2}, T_{s1} and T_{s2}. S_{y1}, S_{y2} are chosen because symmetrical pendulum motion can be determined when these parameters are made to be half as shown in the constraints sub-section later. Furthermore,

T_{s1} and T_{s2} are chosen since these parameters are also important in order to determine symmetrical pendulum motion when initial position and velocity have been decided.

Constraints

In order to ensure smooth motions and symmetrical pendulums, there are several constraints that must be enforced. In total, there are four constraints which resulted into four equations as shown by (4.36)-(4.39).

1. The pendulums for phase 1 and 2 are made to be symmetrical by the following equations:

$$y_{1f} = +\frac{S_{y1}}{2} \tag{4.36}$$

$$y_{2f} = -\frac{S_{y2}}{2} \tag{4.37}$$

2. In order to ensure a smooth and symmetrical trajectory of the velocity, the final velocity of phase 1 must be equal to the negative value of the final velocity of phase 2 as shown by the following equation:

$$\dot{y}_{1f} = -\dot{y}_{2f} \tag{4.38}$$

3. In order to ensure a smooth and symmetrical trajectory of the acceleration, the final acceleration of phase 1 must be equal to the negative value of the final acceleration of phase 2 as shown by the following equation:

$$\ddot{y}_{1f} = -\ddot{y}_{2f} \tag{4.39}$$

Detailed Equations of the Constraints

In this part, the detailed equations are derived from the constraints mentioned in sub-section 4.1.3.

1. The previous constraint in (4.36) is realized using (4.3) as shown in (4.40).

$$\begin{aligned} y_{1f} &= \left(\frac{y_{1i} - T_{c1}\dot{y}_{1i}}{2} e^{-\frac{T_{s1}}{T_{c1}}}\right) \\ &+ \left(\frac{y_{1i} + T_{c1}\dot{y}_{1i}}{2} e^{\frac{T_{s1}}{T_{c1}}}\right) = \frac{S_{y1}}{2} \end{aligned} \tag{4.40}$$

Where the value of T_{c1} above is given as in (4.41)

$$T_{c1} = \sqrt{\frac{Z_{LP}}{g}} \tag{4.41}$$

2. The previous constraint in (4.37) is also realized using (4.3) as shown in (4.42).

$$\begin{aligned} y_{2f} &= \left(\frac{y_{2i} - T_{c2}\dot{y}_{2i}}{2} e^{-\frac{T_{s2}}{T_{c2}}}\right) \\ &+ \left(\frac{y_{2i} + T_{c2}\dot{y}_{2i}}{2} e^{\frac{T_{s2}}{T_{c2}}}\right) = -\frac{S_{y2}}{2} \end{aligned} \tag{4.42}$$

Where the value of T_{c2} above is given as in (4.43)

$$T_{c2} = \sqrt{\frac{Z_{SP}}{g}} \tag{4.43}$$

3. The previous constraint in (4.38) is realized using (4.4) as shown in (4.44).

$$\begin{aligned} &\left(\frac{\dot{y}_{1i} - \frac{y_{1i}}{T_{c1}}}{2} e^{-\frac{T_{s1}}{T_{c1}}}\right) + \left(\frac{\dot{y}_{1i} + \frac{y_{1i}}{T_{c1}}}{2} e^{\frac{T_{s1}}{T_{c1}}}\right) + \\ &\left(\frac{\dot{y}_{2i} - \frac{y_{2i}}{T_{c2}}}{2} e^{-\frac{T_{s2}}{T_{c2}}}\right) + \left(\frac{\dot{y}_{2i} + \frac{y_{2i}}{T_{c2}}}{2} e^{\frac{T_{s2}}{T_{c2}}}\right) \\ &= 0 \end{aligned} \tag{4.44}$$

4. Time derivative of (4.4) results in equation of acceleration. This equation is then used in order to realize the previous constraint in (4.39) as shown in (4.45).

$$\begin{aligned} &\left(\frac{y_{1i}}{T_{c1}^2} \frac{e^{\frac{T_{s1}}{T_{c1}}} + e^{-\frac{T_{s1}}{T_{c1}}}}{2}\right) + \left(\frac{\dot{y}_{1i}}{T_{c1}} \frac{e^{\frac{T_{s1}}{T_{c1}}} - e^{-\frac{T_{s1}}{T_{c1}}}}{2}\right) + \\ &\left(\frac{y_{2i}}{T_{c2}^2} \frac{e^{\frac{T_{s2}}{T_{c2}}} + e^{-\frac{T_{s2}}{T_{c2}}}}{2}\right) + \left(\frac{\dot{y}_{2i}}{T_{c2}} \frac{e^{\frac{T_{s2}}{T_{c2}}} - e^{-\frac{T_{s2}}{T_{c2}}}}{2}\right) \\ &= 0 \end{aligned} \tag{4.45}$$

4.3.2 Solution of S_{y1}, S_{y2}, T_{S1} and T_{S2} using Newton-Raphson Method

In order to find solution for S_{y1}, S_{y2}, T_{S1} and T_{S2}, a numerical method known as Newton-Raphson is implemented. Newton-Raphson is a very popular iterative method to solve for long and complex equations. However, there are several steps need to be taken which will be discussed further in this section. Careful steps must be taken into account in order to ensure the convergence of equations.

Simplification of Equations

Before Newton-Raphson method can be implemented, long and complex equations must be simplified. Therefore, (4.46)-(4.51) are defined.

$$\alpha = e^{\frac{T_{s1}}{T_{c1}}} \tag{4.46}$$

$$\beta = e^{\frac{T_{s2}}{T_{c2}}} \tag{4.47}$$

$$A = \left(\frac{y_{1i} + T_{c1}\dot{y}_{1i}}{2}\right) \tag{4.48}$$

$$B = \left(\frac{y_{1i} - T_{c1}\dot{y}_{1i}}{2}\right) \tag{4.49}$$

$$C = \left(\frac{y_{2i} + T_{c2}\dot{y}_{2i}}{2}\right) \tag{4.50}$$

$$D = \left(\frac{y_{2i} - T_{c2}\dot{y}_{2i}}{2}\right) \tag{4.51}$$

As for the equation of position of phase 1, by substituting (4.46), (4.48) and (4.49) into (4.40), equation (4.52) is obtained as following,

$$\left(B\alpha^{-1}\right) + (A\alpha) = \frac{S_{y1}}{2}. \tag{4.52}$$

As for the equation of position of phase 2, by substituting (4.47), (4.50) and (4.51) into (4.42), equation (4.53) is obtained as following,

$$\left(D\beta^{-1}\right) + (C\beta) = -\frac{S_{y2}}{2}. \tag{4.53}$$

As for the equation of velocity, by substituting (4.46) and (4.47) into (4.44), equation (4.54) is obtained,

$$\begin{aligned} \left(\frac{\dot{y}_{1i} - \frac{y_{1i}}{T_{c1}}}{2}\alpha^{-1}\right) &+ \left(\frac{\dot{y}_{1i} + \frac{y_{1i}}{T_{c1}}}{2}\alpha\right) + \\ \left(\frac{\dot{y}_{2i} - \frac{y_{2i}}{T_{c2}}}{2}\beta^{-1}\right) &+ \left(\frac{\dot{y}_{2i} + \frac{y_{2i}}{T_{c2}}}{2}\beta\right) = 0 \end{aligned} \tag{4.54}$$

Then, (4.54) is further simplified by substituting (4.48)-(4.51) into it as shown in (4.55).

$$\frac{1}{T_{c1}}\left(-B\alpha^{-1} + A\alpha\right) + \frac{1}{T_{c2}}\left(-D\beta^{-1} + C\beta\right) = 0 \tag{4.55}$$

By substituting (4.52) and (4.53) into (4.55), (4.56) is obtained as following;

$$\frac{1}{T_{c1}}\left(2A\alpha - \frac{S_{y1}}{2}\right) + \frac{1}{T_{c2}}\left(2C\beta + \frac{S_{y2}}{2}\right) = 0 \tag{4.56}$$

As for the equation of acceleration, by substituting (4.46) and (4.47) into (4.45), equation (4.57) is obtained,

$$\begin{aligned}\frac{1}{T_{c1}^2}\left(\frac{y_{1i}+T_{c1}\dot{y}_{1i}}{2}\alpha+\frac{y_{1i}-T_{c1}\dot{y}_{1i}}{2}\alpha^{-1}\right) &+\\ \frac{1}{T_{c2}^2}\left(\frac{y_{2i}+T_{c2}\dot{y}_{2i}}{2}\beta+\frac{y_{2i}-T_{c2}\dot{y}_{2i}}{2}\beta^{-1}\right) &= 0\end{aligned} \tag{4.57}$$

(4.57) is then simplified as in (4.58) by substituting (4.52) and (4.53) into (4.57).

$$\frac{1}{T_{c1}^2}\frac{S_{y1}}{2}-\frac{1}{T_{c2}^2}\frac{S_{y2}}{2}=0 \tag{4.58}$$

From (4.52), (4.53), (4.56) and (4.58), the equations are defined as functions in (4.59)-(4.62).

$$f_1(y) = A\alpha^2-\frac{S_{y1}}{2}\alpha+B \tag{4.59}$$

$$f_2(y) = C\beta^2+\frac{S_{y2}}{2}\beta+D \tag{4.60}$$

$$f_3(y) = \frac{2A}{T_{c1}}\alpha-\frac{1}{2T_{c1}}S_{y1}+\frac{2C}{T_{c2}}\beta+\frac{1}{2T_{c2}}S_{y2} \tag{4.61}$$

$$f_4(y) = \frac{1}{T_{c1}^2}S_{y1}-\frac{1}{T_{c2}^2}S_{y2} \tag{4.62}$$

In the same manner as in the sagittal case, (4.59)-(4.62) are rearranged as vectors shown in (4.63). In (4.63) the values of y are the variables or parameters that need to be solved as shown in (4.64).

$$\vec{f}(y) = [f_1(y)\ \ f_2(y)\ \ f_3(y)\ \ f_4(y)]^T \tag{4.63}$$

$$\vec{y} = [\alpha\ \ \beta\ \ S_{y1}\ \ S_{y2}]^T \tag{4.64}$$

Newton Raphson Algorithm

Newton Raphson method involves the process of iterations. The objective is to obtain the roots from several complex functions. In this method, the roots are calculated using (4.65).

$$y_{n+1}=y_n-\frac{f(y_n)}{f'(y_n)} \tag{4.65}$$

$f'(y_n)$ in (4.65) is the derivative of functions which is obtained as in (4.66).

$$f'(y_n)=\begin{bmatrix}\frac{\partial f_1}{\partial y_1} & \cdots & \frac{\partial f_1}{\partial y_4}\\ \vdots & \ddots & \vdots\\ \frac{\partial f_4}{\partial y_1} & \cdots & \frac{\partial f_4}{\partial y_4}\end{bmatrix}^{4\times 4} \tag{4.66}$$

The value of each element in the matrix above is then obtained.

4.4 Concluding Remarks in 2-D DLLIPM

Application of DLLIPM in 2-D case is interesting. However, it is more practical to combine both sagittal and lateral in order to perform 3-D biped walking. The 3-D approach will be explained in Chapter 5. It is noted that the difference of constraints between sagittal and lateral are related with the velocity and acceleration equations. For the 2-D case, there are only 4 constraints involved. On the other hand, the 3-D case will have 6 constraints which are also related with position, velocity and acceleration equations.

Chapter 5

Biped Robot Walking along a Step in 3-D with DLLIPM

This chapter is expanded from Chapter 4. In this chapter, equations are derived to combine lateral and sagittal for 3-D biped walking along a step.

5.1 Constraints for 3-D DLLIPM

In order to ensure smooth motions and symmetrical pendulums, there are several constraints that must be enforced. In total, there are six constraints which resulted into six equations as shown by (5.1)-(5.6).

1. By using the position equations, the pendulums for phase 1 and 2 are made to be symmetrical by the following equations:

$$x_{1f} = +\frac{S_{x1}}{2} \tag{5.1}$$

$$x_{2f} = +\frac{S_{x2}}{2} \tag{5.2}$$

$$y_{1f} = +\frac{S_{y1}}{2} \tag{5.3}$$

$$y_{2f} = -\frac{S_{y2}}{2} \tag{5.4}$$

2. In order to ensure a smooth trajectory of the velocity and syncronization between sagittal and lateral, constraint as in (5.5) is enforced.

$$\dot{x}_{1f}^2 + \dot{y}_{1f}^2 = \dot{x}_{2f}^2 + (-\dot{y}_{2f})^2 \tag{5.5}$$

3. In order to ensure a smooth trajectory of the acceleration and syncronization between sagittal and lateral, constraint as in (5.6) is enforced.

$$\ddot{x}_{1f}^2 + \ddot{y}_{1f}^2 = \ddot{x}_{2f}^2 + (-\ddot{y}_{2f})^2 \tag{5.6}$$

5.2 Derivations of 3-D DLLIPM

In order to find solution for appropriate S_{x1}, S_{x2}, S_{y1}, S_{y2}, T_{S1} and T_{S2} parameters, a numerical method known as Newton-Raphson is chosen. There are several steps need to be taken which will be discussed further in this section.

Before Newton-Raphson method can be implemented, long and complex equations must be simplified. Therefore, (5.7)-(5.16) are defined. α and β are variables but A-H are constants. These constants are just defined as A-H equations in order to avoid long and repetitive equations in the derivations.

$$\alpha = e^{\frac{T_{s1}}{T_{c1}}} \tag{5.7}$$

$$\beta = e^{\frac{T_{s2}}{T_{c2}}} \tag{5.8}$$

$$A = \left(\frac{x_{1i} + T_{c1}\dot{x}_{1i}}{2}\right) \tag{5.9}$$

$$B = \left(\frac{x_{1i} - T_{c1}\dot{x}_{1i}}{2}\right) \tag{5.10}$$

$$C = \left(\frac{x_{2i} + T_{c2}\dot{x}_{2i}}{2}\right) \tag{5.11}$$

$$D = \left(\frac{x_{2i} - T_{c2}\dot{x}_{2i}}{2}\right) \tag{5.12}$$

$$E = \left(\frac{y_{1i} + T_{c1}\dot{y}_{1i}}{2}\right) \tag{5.13}$$

$$F = \left(\frac{y_{1i} - T_{c1}\dot{y}_{1i}}{2}\right) \tag{5.14}$$

$$G = \left(\frac{y_{2i} + T_{c2}\dot{y}_{2i}}{2}\right) \tag{5.15}$$

$$H = \left(\frac{y_{2i} - T_{c2}\dot{y}_{2i}}{2}\right) \tag{5.16}$$

The previous constraint which is stated earlier in (5.1) is realized by using the same position equation that used in Chapter 4, as shown in (5.17).

$$\begin{aligned} x_{1f} &= \left(\frac{x_{1i} - T_{c1}\dot{x}_{1i}}{2} e^{-\frac{T_{s1}}{T_{c1}}}\right) \\ &+ \left(\frac{x_{1i} + T_{c1}\dot{x}_{1i}}{2} e^{\frac{T_{s1}}{T_{c1}}}\right) = +\frac{S_{x1}}{2} \end{aligned} \tag{5.17}$$

By substituting (5.7), (5.9) and (5.10) into (5.17), $f_1(q)$ is defined as following,

$$f_1(q) = A\alpha^2 - \frac{S_{x1}}{2}\alpha + B \tag{5.18}$$

The previous constraint in (5.2) is realized as shown in (5.19).

$$\begin{aligned} x_{2f} &= \left(\frac{x_{2i} - T_{c2}\dot{x}_{2i}}{2} e^{-\frac{T_{s2}}{T_{c2}}}\right) \\ &+ \left(\frac{x_{2i} + T_{c2}\dot{x}_{2i}}{2} e^{\frac{T_{s2}}{T_{c2}}}\right) = +\frac{S_{x2}}{2} \end{aligned} \tag{5.19}$$

By substituting (5.8), (5.11) and (5.12) into (5.19), $f_2(q)$ is obtained as following,

$$f_2(q) = C\beta^2 - \frac{S_{x2}}{2}\beta + D \tag{5.20}$$

The previous constraint in (5.3) is realized as shown in (5.21).

$$\begin{aligned} y_{1f} &= \left(\frac{y_{1i} - T_{c1}\dot{y}_{1i}}{2} e^{-\frac{T_{s1}}{T_{c1}}}\right) \\ &+ \left(\frac{y_{1i} + T_{c1}\dot{y}_{1i}}{2} e^{\frac{T_{s1}}{T_{c1}}}\right) = +\frac{S_{y1}}{2} \end{aligned} \tag{5.21}$$

By substituting (5.7), (5.13) and (5.14) into (5.21), $f_3(q)$ is defined as following,

$$f_3(q) = E\alpha^2 - \frac{S_{y1}}{2}\alpha + F \tag{5.22}$$

The previous constraint in (5.4) is realized as shown in (5.23).

$$\begin{aligned} y_{2f} = &\left(\frac{y_{2i} - T_{c2}\dot{y}_{2i}}{2} e^{-\frac{T_{s2}}{T_{c2}}}\right) + \\ &\left(\frac{y_{2i} + T_{c2}\dot{y}_{2i}}{2} e^{\frac{T_{s2}}{T_{c2}}}\right) = -\frac{S_{y2}}{2} \end{aligned} \tag{5.23}$$

By substituting (5.8), (5.15) and (5.16) into (5.23), $f_4(q)$ is defined as following,

$$f_4(q) = G\beta^2 + \frac{S_{y2}}{2}\beta + H \tag{5.24}$$

The previous constraint in (5.5) is realized using (4.4), (5.7)-(5.16) as shown in (5.25).

$$\begin{aligned} &\left(\frac{1}{T_{c1}}\left(2A\alpha - \frac{S_{x1}}{2}\right)\right)^2 + \left(\frac{1}{T_{c1}}\left(2E\alpha - \frac{S_{y1}}{2}\right)\right)^2 = \\ &\left(\frac{1}{T_{c2}}\left(2C\beta - \frac{S_{x2}}{2}\right)\right)^2 + \left(\frac{-1}{T_{c2}}\left(2G\beta + \frac{S_{y2}}{2}\right)\right)^2 \end{aligned} \tag{5.25}$$

Then, $f_5(q)$ is expanded as following:

$$\begin{aligned} f_5(q) = &\frac{4A^2\alpha^2}{{T_{c1}}^2} - \frac{2A\alpha S_{x1}}{{T_{c1}}^2} + \frac{{S_{x1}}^2}{4{T_{c1}}^2} + \\ &\frac{4E^2\alpha^2}{{T_{c1}}^2} - \frac{2E\alpha S_{y1}}{{T_{c1}}^2} + \frac{{S_{y1}}^2}{4{T_{c1}}^2} - \\ &\frac{4C^2\beta^2}{{T_{c2}}^2} + \frac{2C\beta S_{x2}}{{T_{c2}}^2} - \frac{{S_{x2}}^2}{4{T_{c2}}^2} - \\ &\frac{4G^2\beta^2}{{T_{c2}}^2} - \frac{2G\beta S_{y2}}{{T_{c2}}^2} - \frac{{S_{y2}}^2}{4{T_{c2}}^2} \end{aligned} \tag{5.26}$$

The previous constraint in (5.6) is realized using time derivative of (4.4), (5.7)-(5.16) as simplified in (5.27).

$$\begin{aligned} &\left(\frac{S_{x1}}{2{T_{c1}}^2}\right)^2 + \left(\frac{S_{y1}}{2{T_{c1}}^2}\right)^2 = \\ &\left(\frac{S_{x2}}{2{T_{c2}}^2}\right)^2 + \left(\frac{S_{y2}}{2{T_{c2}}^2}\right)^2 \end{aligned} \tag{5.27}$$

Then, $f_6(q)$ is defined by expanding (5.27) as following:

$$f_6(q) = \frac{{S_{x1}}^2}{{T_{c1}}^4} + \frac{{S_{y1}}^2}{{T_{c1}}^4} - \frac{{S_{x2}}^2}{{T_{c2}}^4} - \frac{{S_{y2}}^2}{{T_{c2}}^4} \tag{5.28}$$

All the functions are arranged as in (5.29). In (5.29) the values of q are the variables or parameters that need to be solved as shown in (5.30).

$$\vec{f}(q) = [f_1(q)\ f_2(q)\ f_3(q)\ f_4(q)\ f_5(q)\ f_6(q)]^T \tag{5.29}$$

$$\vec{q} = [\alpha\ \ \beta\ \ S_{x1}\ \ S_{x2}\ \ S_{y1}\ \ S_{y2}]^T \tag{5.30}$$

At the moment only six equations as in (5.29) with six variables as in (5.30) are optimized. Other parameters are able to be optimized but left for future works. The six variables are chosen because they are among important parameters that will determine the walking features of biped robot. α and β determine the walking cycle of phase 1 (long pendulum) and phase 2 (short pendulum). S_{x1} and S_{x2} determine the stride length of phase 1 and 2 in sagittal plane, respectively. S_{y1} and S_{y2} determine the stride length of phase 1 and 2 in lateral plane, respectively.

Newton Raphson algorithm

Newton Raphson method is involving process of iterations. The objective is to obtain the roots from several complex functions. In this method, the roots are calculated using (5.31) [25].

$$q_{n+1} = q_n - \frac{f(q_n)}{f'(q_n)} \tag{5.31}$$

$f'(q_n)$ in (5.31) is the derivative of functions which is obtained as in (5.32).

$$f'(q_n) = \begin{bmatrix} \frac{\partial f_1}{\partial q_1} & \cdots & \frac{\partial f_1}{\partial q_6} \\ \vdots & \ddots & \vdots \\ \frac{\partial f_6}{\partial q_1} & \cdots & \frac{\partial f_6}{\partial q_6} \end{bmatrix}^{6\times 6} \tag{5.32}$$

The value of each element in the matrix above is then obtained.

5.3 Simulation Results

5.3.1 The Predetermined and Initial Guess Values for Newton Raphson Calculations

In the Newton Raphson method there are initial guess values for iterations that must be given. These parameters are shown as in Table 5.1. The meaning of each parameters in Table 5.1 can be determined from Table 4.1. There are also predetermined values which means the values are decided before the Newton Raphson Calculations are done.

Table 5.1: Parameters for Newton Raphson calculations

Parameters	Values	Note
Z_{LP}	0.5376m	Predetermined value
Z_{SP}	0.4376m	Predetermined value
x_{1i}	-0.164m	Predetermined value
$\dot{x}_{1i}$	0.7887 m/s	Predetermined value
x_{2i}	-0.10265m	Predetermined value
$\dot{x}_{2i}$	0.7887 m/s	Predetermined value
y_{1i}	0.1027m	Predetermined value
$\dot{y}_{1i}$	-0.33 m/s	Predetermined value
y_{2i}	-0.0808m	Predetermined value
$\dot{y}_{2i}$	0.33 m/s	Predetermined value
T_{c1}	$\sqrt{\frac{Z_{LP}}{g}} = \sqrt{\frac{0.5376}{9.80665}}$	Predetermined value
T_{c2}	$\sqrt{\frac{Z_{SP}}{g}} = \sqrt{\frac{0.4376}{9.80665}}$	Predetermined value
T_{s1}	0.9s	For calculation of α_0
T_{s2}	0.6s	For calculation of β_0
α_0	$e^{\frac{T_{s1}}{T_{c1}}} = e^{\frac{0.9}{0.2341}}$	Initial guess
β_0	$e^{\frac{T_{s2}}{T_{c2}}} = e^{\frac{0.6}{0.2112}}$	Initial guess
S_{x10}	0.3280m	Initial guess
S_{x20}	0.2800m	Initial guess
S_{y10}	0.2053m	Initial guess
S_{y20}	0.1616m	Initial guess

Table 5.2: Range of initial guess values

Initial values of parameters	Minimum	Maximum
α_0	$e^{\frac{0.6}{0.2341}}$	$e^{\frac{1.0}{0.2341}}$
β_0	$e^{\frac{0.37}{0.2112}}$	$e^{\frac{1.0}{0.2112}}$
S_{x10}	0.3m	0.34m
S_{x20}	0.1m	0.30m
S_{y10}	0.16m	1.0m
S_{y20}	0.14m	0.19m

In the proposed method, the constrained equations can be achieved with certain limitation of the initial settings as shown in Table 5.2. If the initial guess values are chosen outside of these limitations, the convergence may not be achieved. Furthermore, all the obtained parameters from the Newton Raphson method must be positive values since it is related with time and length of CoM trajectory motions. All values in Table 5.2 are limited to the physical structure of the robot.

Table 5.3: Strides table

n	1	2	3	4	5	6	7	8	9	10
$s_y^{(n)}$	0.2	0.2	0.2	0.2	0.2	0.2	0.2	0.2	0.2	0.2
$s_x^{(n)}$	0.3	0.3	0.3	0.3	0.3	0.3	0.3	0.3	0.3	0.3

5.3.2 Results of the iterations with the Newton Raphson method

From the values used in sub-section 5.3.1, iterations are done by using (5.31). The results are shown in Fig. 5.1 and Fig. 5.2. α is obtained as 10.5198 at 5^{th} iteration and β is obtained as 10.2831 at 4^{th} iteration. Furthermore, S_{x1}, S_{x2}, S_{y1} and S_{y2} are obtained as 0.1842, 0.2438, 0.2841 and 0.1287, correspondingly. During the iterations process of the Newton Raphson method, different initial settings may give negative values of the parameters or may not converge. If it is not converge or negative values of parameters are obtained, different initial settings must be selected again. The initial settings are chosen by trial and error. All the parameters, α, β, S_{x1}, S_{x2}, S_{y1} and S_{y2} must be always positive. It should not be negative because α and β represent the time which is impossible to be negative sign. On the other hand, the S_{x1}, S_{x2}, S_{y1} and S_{y2} are the distance of the center of mass maximum trajectory which should also be always positive in sign.

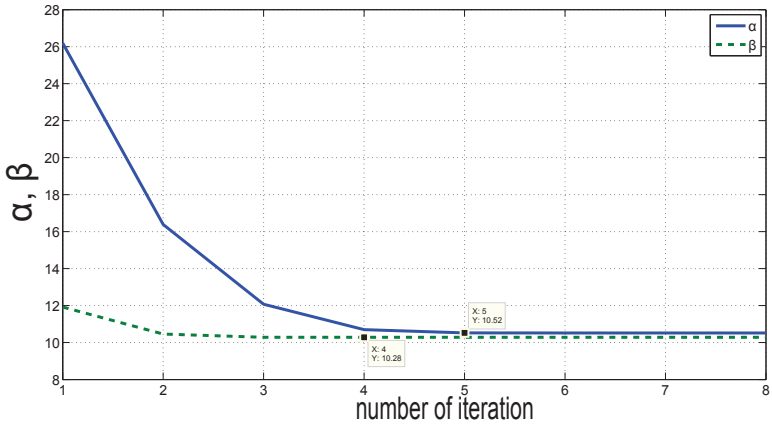

Figure 5.1: Results of α and β after several iterations by using Newton Raphson algorithm.

In order to verify all the functions from the Newton Raphson solutions, Fig. 5.3 is plotted. In this figure, all functions are obtained as '0' values after all the parameters are converged. This validated that all the constraints have been fulfilled.

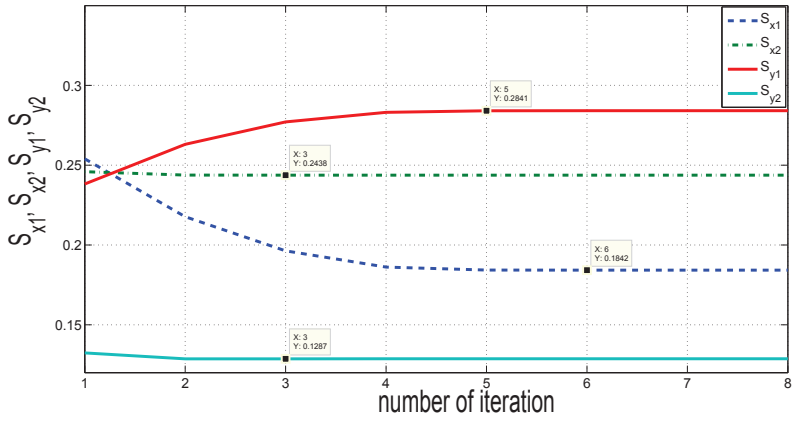

Figure 5.2: Results of S_{x1}, S_{x2}, S_{y1} and S_{y2} after several iterations by using Newton Raphson algorithm.

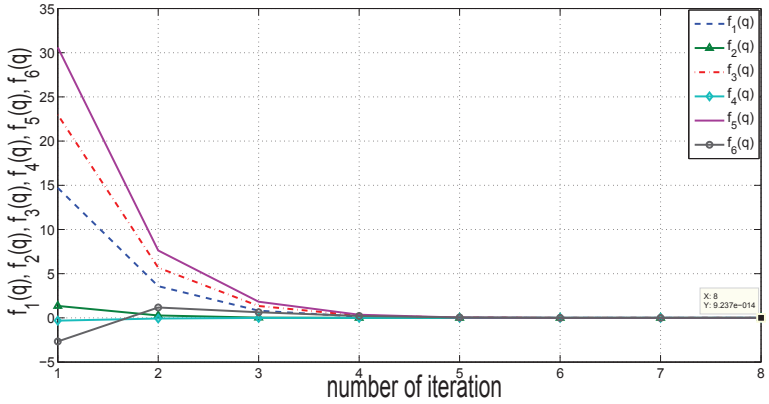

Figure 5.3: Results of all functions from $f_1(q)$ to $f_6(q)$ by using Newton Rahpson algorithm.

5.3.3 Simulation of 3D Walking Pattern with DLLIPM (without Newton Raphson)

In this sub-section, simulation of biped robot walking along a step with the height of 0.1 [m] is presented. The strides are decided to be as in Table 5.3. The Z_{LP}, Δt_{-LP} and Δt_{-SP} are decided to be 0.5376 [m], 0.9 [s] and 0.6 [s] correspondingly. Here, the parameter settings are just chosen intuitively without the Newton Raphson method. With these settings, the trajectory planning method in sub-section 1.3.2 is used. The result for sagittal plane is obtained as in Fig. 5.4. On the other hand, the result for lateral plane is shown as in Fig. 5.5.

As for the sagittal plane, it is noticed from Fig. 5.4 that the CoM position trajectory shown by the blue line is accelerated and deaccelerated repeatedly. Thus, the impact force may increase. It is also noticed that the there are multiple levels of maximum and minimum velocity for long pendulum and short pendulum cycles. These multiple level of velocity will

create unsmooth motion during the walking. As for the lateral plane, it is observered from Fig. 5.5 that the CoM position trajectory becomes deviated from its initial straight position. The deviated problem is more critical during the first few steps. It is also observed in this figure that the shape of velocity trajectory, shown by the red line is not symmetry.

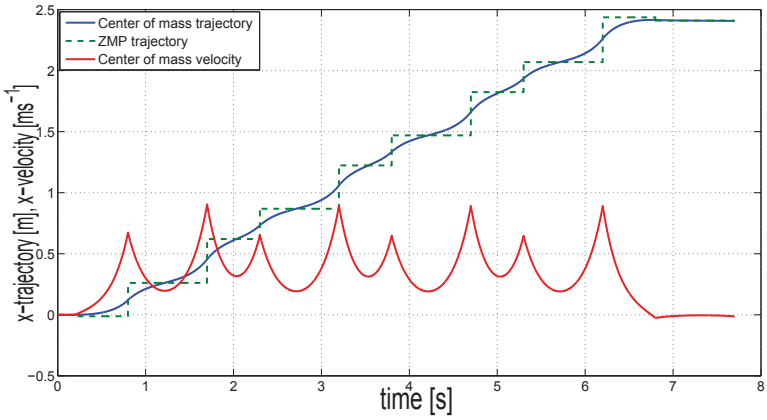

Figure 5.4: Walking pattern of 10 steps in sagittal plane (without proposed method).

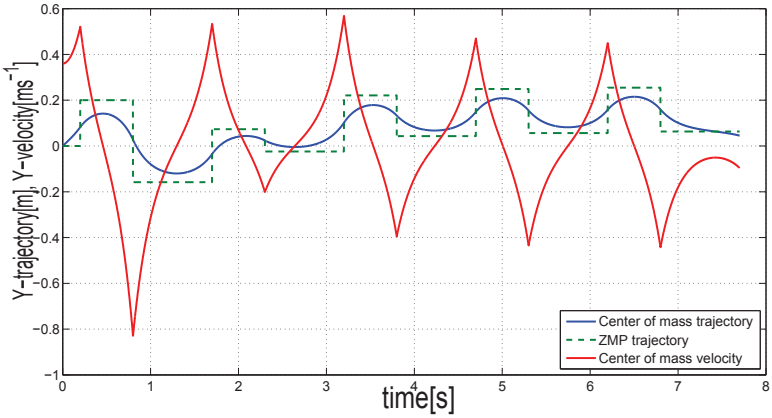

Figure 5.5: Walking pattern of 10 steps in lateral plane (without proposed method).

5.3.4 Simulation of 3D Walking Pattern with Improved DLLIPM (with Newton Raphson)

By using DLLIPM algorithm shown earlier in sub-section 1.3.2, the walking pattern for the environment or situation in sub-section 5.3.3 is simulated again with the new walking parameters obtained from sub-section 5.3.2. The result for sagittal plane is obtained as in Fig. 5.6. On the other hand, the result for lateral plane is shown as in 5.7.

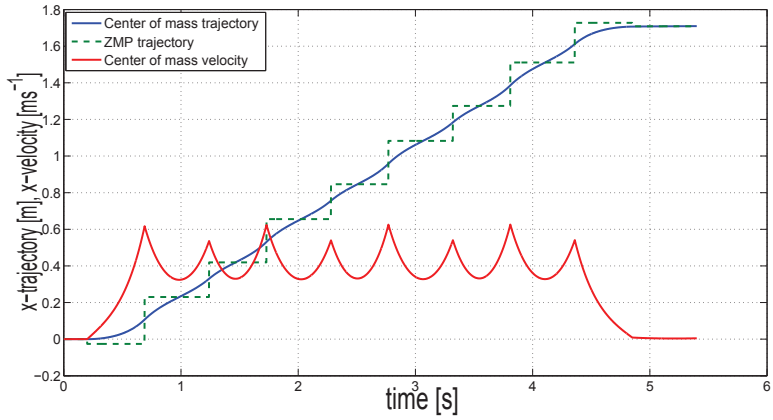

Figure 5.6: Walking pattern of 10 steps in sagittal plane (with proposed method).

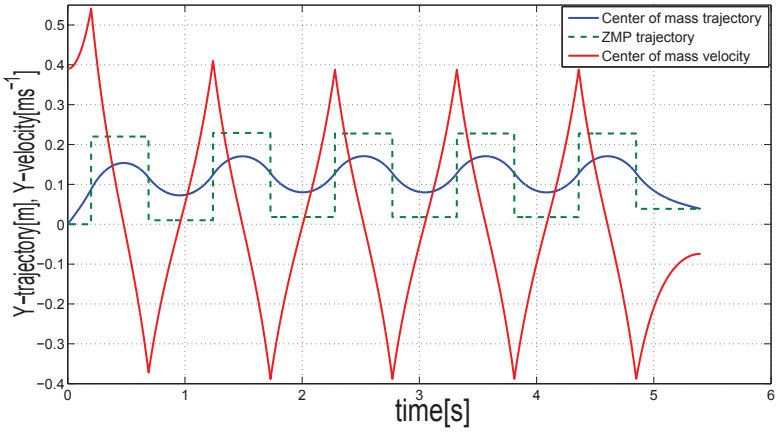

Figure 5.7: Walking pattern of 10 steps in lateral plane (with proposed method).

As for the sagittal plane, it is noticed in the Fig. 5.6 that the trajectory of CoM does not accelerated and deaccelerated repeatedly as much as the previous situation, shown in the Fig. 5.4. Thus, the impact force may reduce. Besides that, it is noticed that the minimum velocity for long pendulum and short pendulum cycles is now at the same value which results smoother walking motion. As for the lateral plane, it is observed that the motion of the CoM is not deviated from its intial straight position as shown in the Fig. 5.7. Furthermore, it is also noticed from this figure that the problem of unsymmetrical shape of velocity trajectory has been solved. Smooth trajectories will help a bipedal robot to achieve safer and more stable walking. From all the shown results, it is verified that with the proposed method, the biped walking pattern for walking along a step have been improved. In orders to validate the velocity and acceleration constraints suggested in sub-section 5.1, Figs. 5.8, 5.9, 5.10 and 5.11 are plotted. In Figs. 5.8 and 5.9, the differences between the peak values are larger in comparison to the

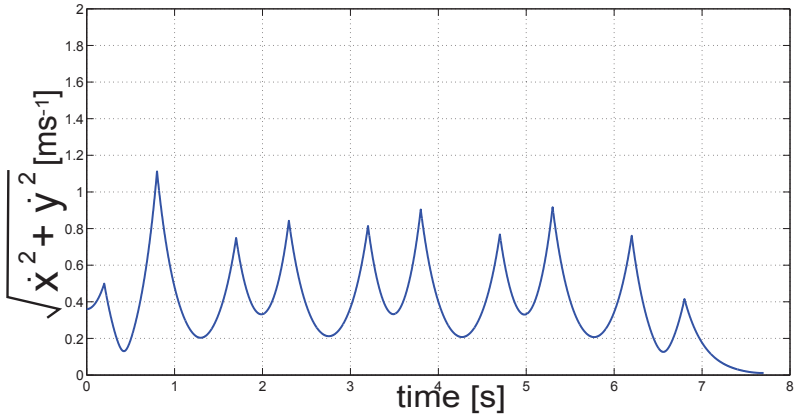

Figure 5.8: Combination of velocity vectors, sagittal and lateral (without proposed method).

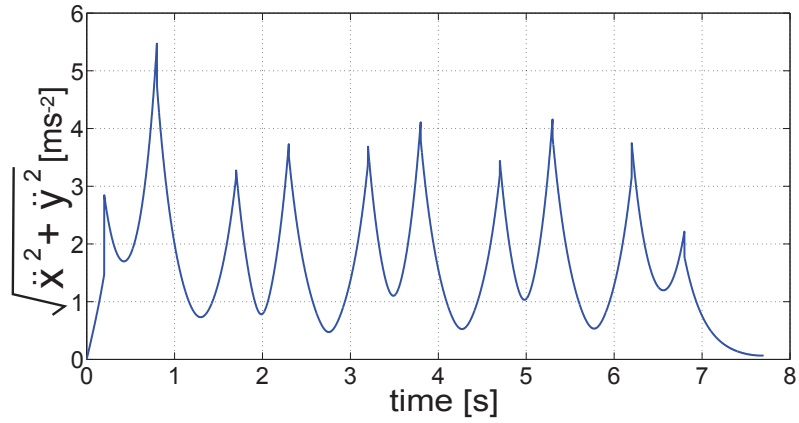

Figure 5.9: Combination of acceleration vectors, sagittal and lateral (without proposed method).

situations in Figs. 5.10 and 5.11. Here, there are still some small differences because of the foot landing modification used in trajectory planning. However, the proposed method which are shown in Figs. 5.10 and 5.11 have about the same minimum values of velocity and acceleration in comparison to Figs. 5.8 and 5.9. This will ensure a smooth and better motion of the proposed method.

5.3.5 Walking Stability

It is intended to observe the stability of the proposed method in comparison without the proposed method. In order to analyse the stability of the biped robot walking with and without the proposed method, the observation in lateral plane will be considered. It is easier to see the advantage of the proposed method over without the proposed method by referring to Figs. 5.5 and 5.7.

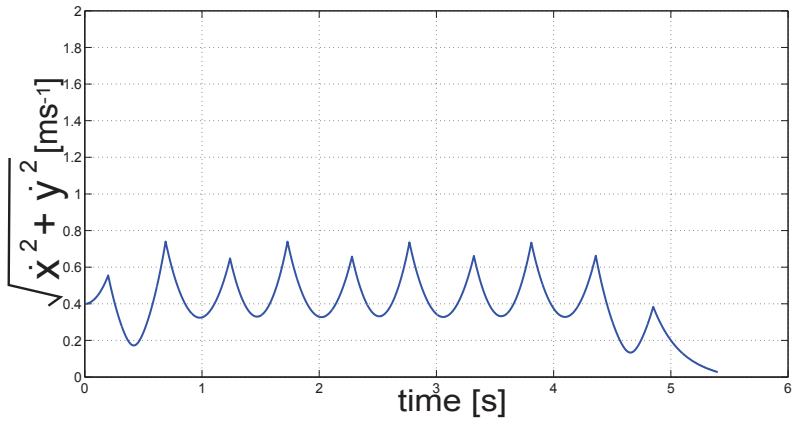

Figure 5.10: Combination of velocity vectors, sagittal and lateral (with proposed method).

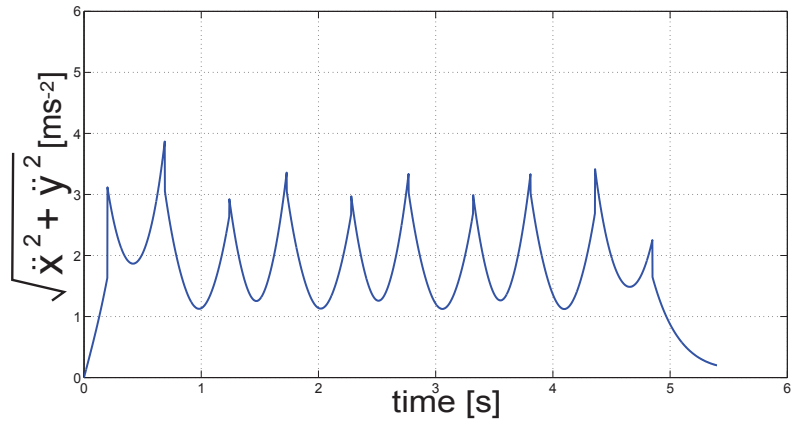

Figure 5.11: Combination of acceleration vectors, sagittal and lateral (with proposed method).

In order to realized the biped walking without fall down, the right foot (RF) and left foot (LF) must be landed at the point of ZMP trajectory. In other words, the ZMP trajectory which is shown by the green dashed line must be within the foot sole as shown in Figs. 5.12 and 5.13. As shown in Table 5.3, the walking pattern is designed for a biped robot that has distance between RF and LF as 0.2[m]. However, without the proposed method, the robot must do the side step about 0.35[m] at the beginning as shown in Fig. 5.12. If the side step is too big, beyond the limitation of the physical structure, the ZMP trajectory will be outside of the foot sole boundary and the robot will fall down. This problem is solved by using the proposed method where the side step is always about 0.2[m] as shown in Fig. 5.13.

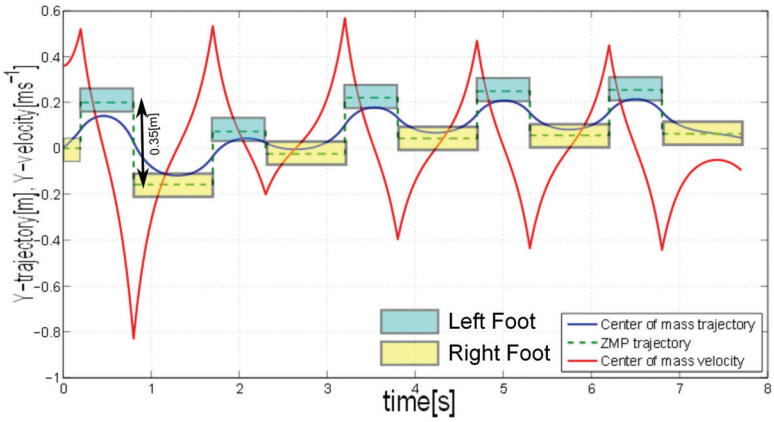

Figure 5.12: Walking pattern of 10 steps in lateral plane (without proposed method).

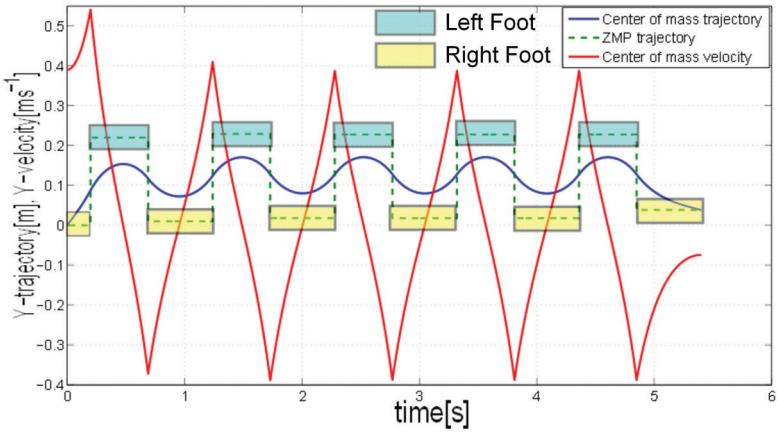

Figure 5.13: Walking pattern of 10 steps in lateral plane (with proposed method).

5.3.6 Simulation Results of LIPM and DLLIPM

Simulations of biped robot walking with LIPM and DLLIPM methods are conducted by using ROCOS. In ROCOS, the real environment of bipedal robot can be simulated and the results are almost similar to the real experiment surroundings. The simulations are conducted for walking with two different concepts as shown in Figs. 1.4 a) and b) earlier in this thesis. RF always lands on the lower step. Whereas LF always lands on the higher step of the stairs during the walking. The GRF during these walking simulations are measured with the force sensors located at the RF and LF of the biped robot. The heights of the step in the simulations are 0.1[m] and the sampling time is 1[ms] or 1[kHz].

The results are shown in Figs. 5.14 for LIPM and 5.15 for DLLIPM. In these figures, the regions of left foot single support phase (LFSS) and right foot single support phase (RFSS) are shown by the yellow and grey area, correspondingly. The maximum impact forces during

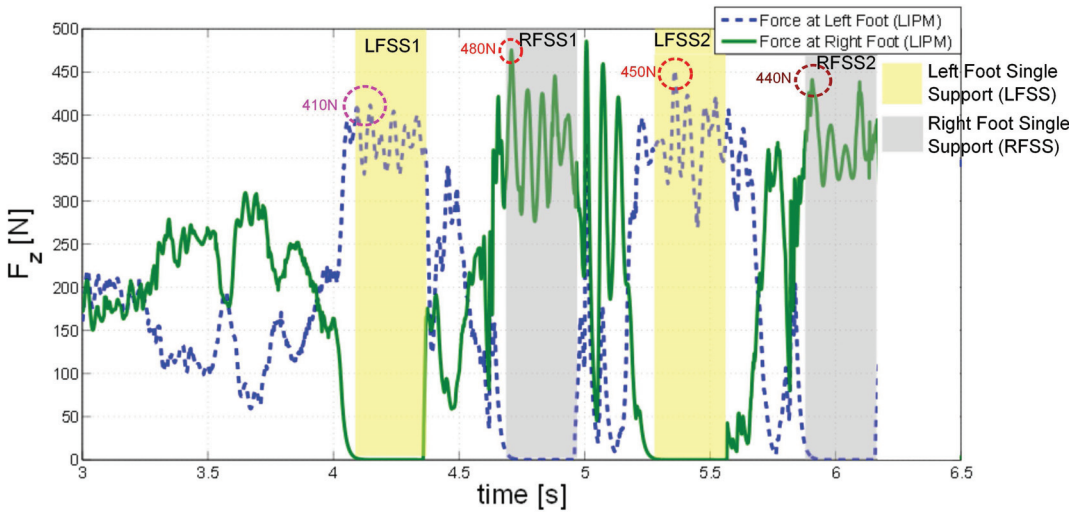

Figure 5.14: GRF data measured from force sensors during walking simulation (LIPM).

LFSS1 in LIPM and DLLIPM simulations are similar which are 410 [N] as shown by the purple dashed circles in Fig. 5.14 for LIPM and Fig. 5.15 for DLLIPM. There is a small reduction of maximum impact forces during RFSS2 which is from 440 [N] to 430 [N] as shown by the brown dashed circles in Fig. 5.14 for LIPM and Fig. 5.15 for DLLIPM.

Moreover, bigger differences occurred during the RFSS1 and LFSS2. In LIPM simulation, the maximum impact forces during RFSS1 and LFSS2 are 480 [N] and 450 [N], respectively as shown by the red dashed circles in Fig. 5.14. These impact forces are reduced with the proposed method where maximum impact forces during RFSS1 and LFSS2 are 370 [N] and 430 [N], respectively as shown by the red dashed circles in Fig. 5.15. The motion of up and down of CoM during walking along stair in LIPM simulation contributed in the higher impact forces shown by the data of GRF sensors. On the other hand, the proposed method maintained the CoM height horizontally to reduce the impact forces. These facts demonstrated the effectiveness of the proposed method in order to reduce the GRF.

As for statistical validation, the walking with DLLIPM approach is repeated for the slightly different environment and longer foot steps (10 steps). This time, the height of the environment is the same but now, RF always lands on the lower step and LF always lands on the higher step of the stairs during the walking. The results are shown in Figs. 5.16 for LIPM and 5.17 for DLLIPM. It is proofed that the maximum impact forces with DLLIPM concept in Fig. 5.17 are lower than the maximum impact forces with LIPM concept in Fig. 5.16.

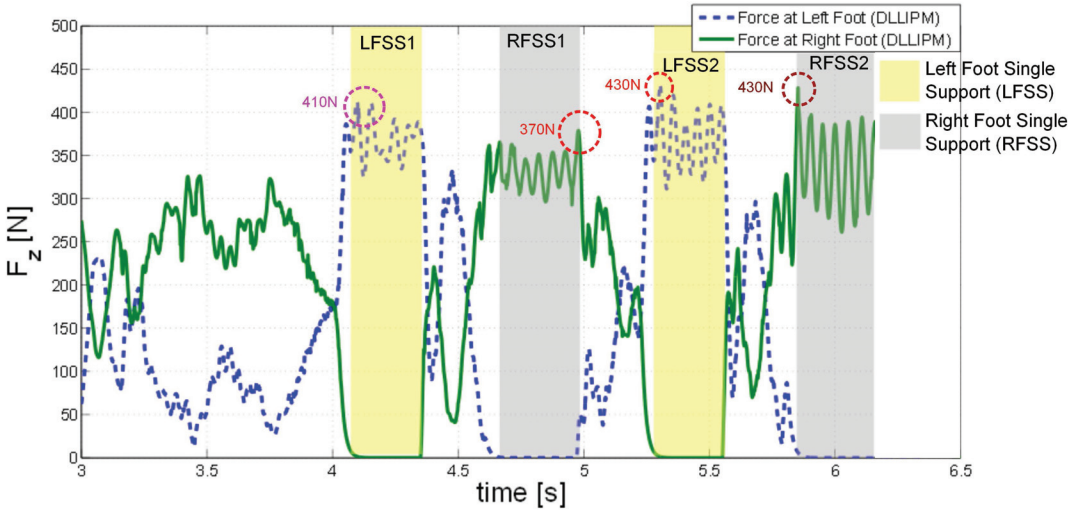

Figure 5.15: GRF data measured from force sensors during walking simulation (DLLIPM).

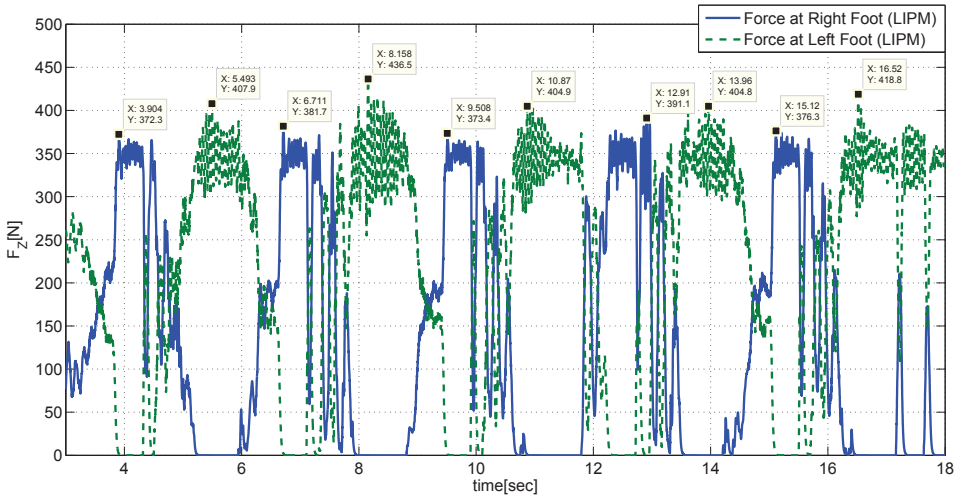

Figure 5.16: GRF data measured from force sensors during 10 steps walking simulation (LIPM).

5.4 Experiment Results

Experiments of biped robot walking with consideration of lateral plane are conducted for walking on a step by using MARI-3 biped robot. The experiments are done as shown by the snapshots in Fig. 5.18. In these experiments, only lateral walking is taken into account which means the robot walked without moving forward. Emphasis is given to the lateral plane since the stair is elevated in this direction. The walking cycles of each experiment consists of two steps of right foot single support (RFSS), two steps of left foot single support (LFSS) and double support phases. The experiments are conducted for walking with two different concepts as shown in Figs. 1.4 a) and 1.4 b) which have been shown earlier in this paper. In the experiments,

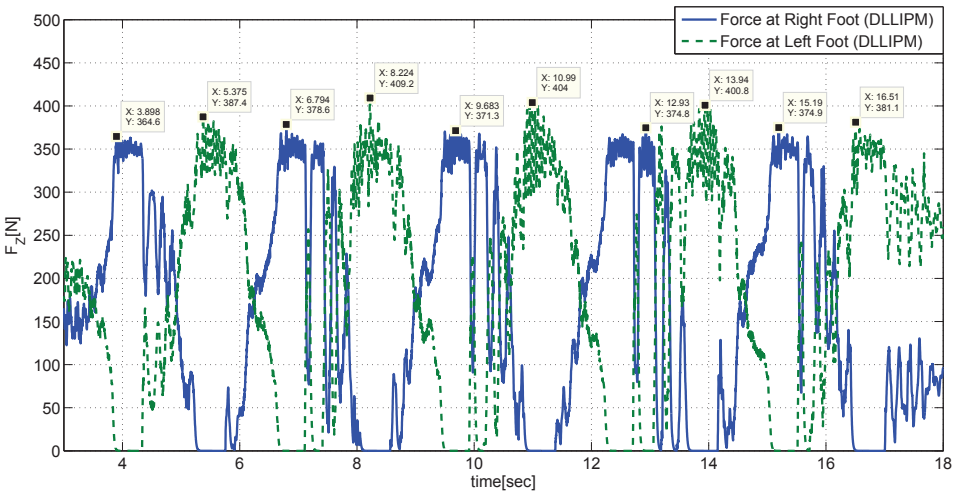

Figure 5.17: GRF data measured from force sensors during 10 steps walking simulation (DLLIPM).

RF always lands on the lower step. Whereas LF always lands on the higher step of the stair during the walking. The ground reaction forces (GRF) during these walking experiments are measured with the force sensors located at the RF and LF of the biped robot. The heights of the step in the experiments are 0.05 [m] and the sampling time is 0.001 [s] (1kHz). Each joint angle is processed in a servo block in which position control, velocity control and disturbance observer is applied [26]. These servo blocks output the torque references for the actuators and the robot moves. The foot swing trajectories are generated by using polynomial function [11] and the height of each swing is 30 [cm]. As for the LIPM experiment, (5.33) is used to generate the CoM trajectory of z-axis [23]. k is obtained by dividing the stair height with the distance between the robot's feet. As for the experiment of DLLIPM, the CoM trajectories are simulated by using DLLIPM scheme as explained in section 1.3.2. The results are shown in Figs. 5.19 and 5.20.

$$CoM_z = CoM_y \times k + Z_c \tag{5.33}$$

The solid lines in the Figs. 5.19 and 5.20 represent forces measured at the RF of the biped robot. Furthermore, the dashed lines in the Figs. 5.19 and 5.20 are the forces measured at the LF of the biped robot. In these figures, the regions of right foot single support phase (RFSS) and left foot single support phase (LFSS) are shown. In the experiment with LIPM, maximum impact forces during RFSS1, LFSS1, RFSS2 and LFSS2 are 359.5 [N], 328.2 [N], 473.6 [N] and 401 [N], respectively as shown by the horizontal dashed lines in Fig. 5.19. These impact forces are reduced with the proposed method where the maximum impact forces during RFSS1, LFSS1, RFSS2 and LFSS2 are 354.1 [N], 303 [N], 398.3 [N] and 366 [N], respectively as shown

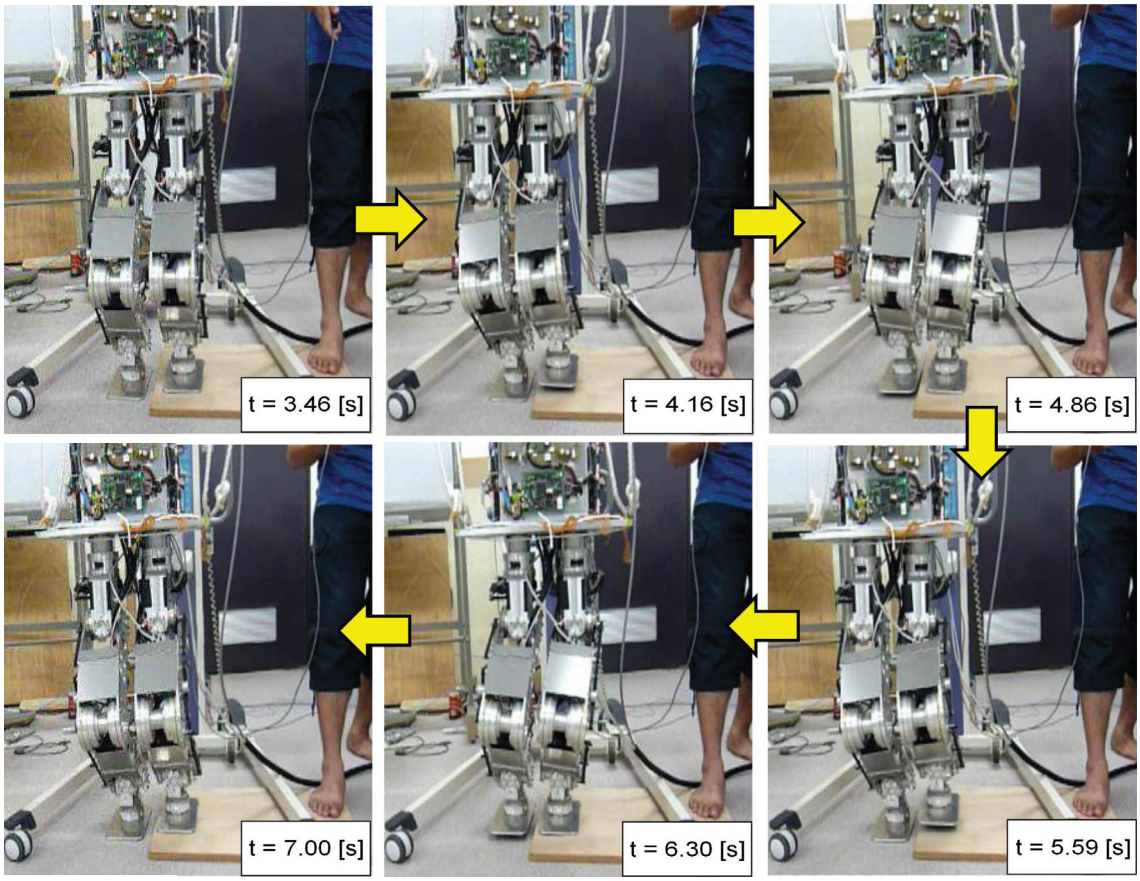

Figure 5.18: MARI-3 walking in the experiment with the proposed method.

by the horizontal dashed lines in Fig. 5.20. These facts demonstrated the effectiveness of the proposed method in order to reduce the maximum impact forces of the GRF.

5.5 Derivations of 3-D DLLIPM with Other Constraints

The main objective of this sub-section is to derive equations of 3-D DLLIPM with other constraints. This time, the constraints are related to position and velocity equations only. The acceleration equation will be not considered.

First, let's refresh about the previous constraints. Previously, the constrainst with consideration of position, velocity and acceleration equations are given as follows:

1. As for the position equations, the pendulums for phase 1 and 2 are made to be symmetrical by the following equations:

$$x_{1f} = +\frac{S_{x1}}{2} \tag{5.34}$$

$$x_{2f} = +\frac{S_{x2}}{2} \tag{5.35}$$

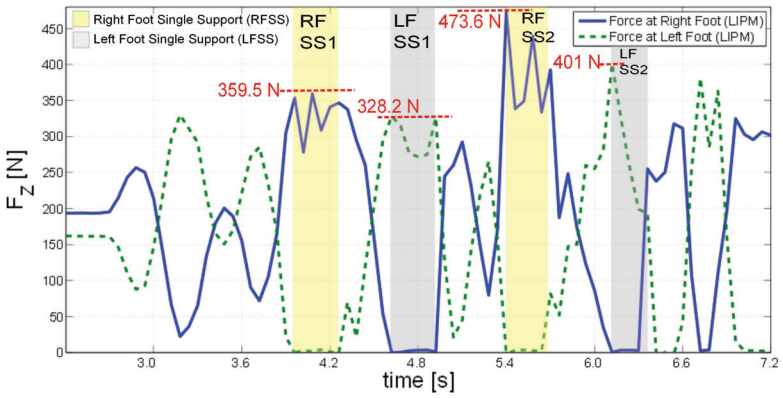

Figure 5.19: Ground reaction force data measured from force sensors during walking experiment (LIPM).

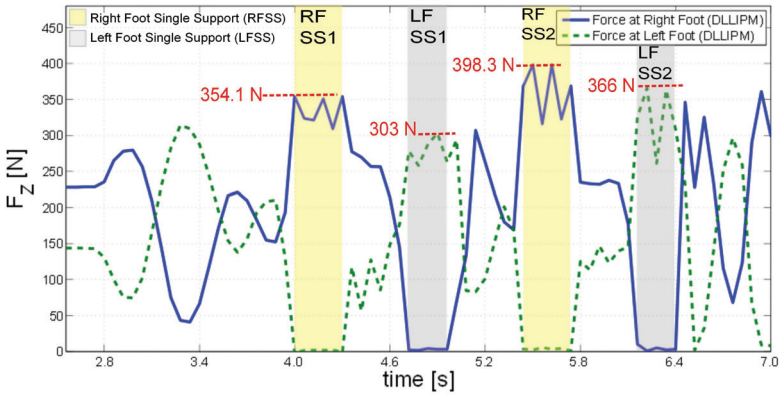

Figure 5.20: Ground reaction force data measured from force sensors during walking experiment (DLLIPM).

$$y_{1f} = +\frac{S_{y1}}{2} \tag{5.36}$$

$$y_{2f} = -\frac{S_{y2}}{2} \tag{5.37}$$

2. In order to ensure a smooth trajectory of the velocity and syncronization between sagittal and lateral, constraint as in (5.38) is enforced.

$$\dot{x}_{1f}^2 + \dot{y}_{1f}^2 = \dot{x}_{2f}^2 + (-\dot{y}_{2f})^2 \tag{5.38}$$

3. In order to ensure a smooth trajectory of the acceleration and syncronization between sagittal and lateral, constraint as in (5.39) is enforced.

$$\ddot{x}_{1f}^2 + \ddot{y}_{1f}^2 = \ddot{x}_{2f}^2 + (-\ddot{y}_{2f})^2 \tag{5.39}$$

It is intended to re-derive equations above with new constraints. In the new constraints, (5.38) and (5.39) are modified. Now, the 6 constraints are defined as follows:

1. The position equations are maintained as in the previous:

$$x_{1f} = +\frac{S_{x1}}{2} \tag{5.40}$$
$$x_{2f} = +\frac{S_{x2}}{2} \tag{5.41}$$
$$y_{1f} = +\frac{S_{y1}}{2} \tag{5.42}$$
$$y_{2f} = -\frac{S_{y2}}{2} \tag{5.43}$$

2. As for the sagittal velocity:

$$\dot{x}_{1f} = \dot{x}_{2f} \tag{5.44}$$

3. As for the lateral velocity:

$$\dot{y}_{1f} = -\dot{y}_{2f} \tag{5.45}$$

In the same manner as previous derivation, labels are defined as follows:

$$\alpha = e^{\frac{T_{s1}}{T_{c1}}} \tag{5.46}$$
$$\beta = e^{\frac{T_{s2}}{T_{c2}}} \tag{5.47}$$
$$A = \left(\frac{x_{1i} + T_{c1}\dot{x}_{1i}}{2}\right) \tag{5.48}$$
$$B = \left(\frac{x_{1i} - T_{c1}\dot{x}_{1i}}{2}\right) \tag{5.49}$$
$$C = \left(\frac{x_{2i} + T_{c2}\dot{x}_{2i}}{2}\right) \tag{5.50}$$
$$D = \left(\frac{x_{2i} - T_{c2}\dot{x}_{2i}}{2}\right) \tag{5.51}$$
$$E = \left(\frac{y_{1i} + T_{c1}\dot{y}_{1i}}{2}\right) \tag{5.52}$$
$$F = \left(\frac{y_{1i} - T_{c1}\dot{y}_{1i}}{2}\right) \tag{5.53}$$
$$G = \left(\frac{y_{2i} + T_{c2}\dot{y}_{2i}}{2}\right) \tag{5.54}$$
$$H = \left(\frac{y_{2i} - T_{c2}\dot{y}_{2i}}{2}\right) \tag{5.55}$$

As shown in (5.18), (5.20), (5.22) and (5.24) previously, the contraints of position equations are defined as follows:

$$f_1(q) = A\alpha^2 - \frac{S_{x1}}{2}\alpha + B \tag{5.56}$$

$$f_2(q) = C\beta^2 - \frac{S_{x2}}{2}\beta + D \tag{5.57}$$

$$f_3(q) = E\alpha^2 - \frac{S_{y1}}{2}\alpha + F \tag{5.58}$$

$$f_4(q) = G\beta^2 + \frac{S_{y2}}{2}\beta + H \tag{5.59}$$

From modification of (5.25), the new constraints for velocity are shown as below. Note that the previous equation of acceleration are omitted.

$$f_5(q) = \frac{1}{T_{c1}}\left(2A\alpha - \frac{S_{x1}}{2}\right) - \frac{1}{T_{c2}}\left(2C\beta - \frac{S_{x2}}{2}\right) \tag{5.60}$$

$$f_6(q) = \frac{1}{T_{c1}}\left(2E\alpha - \frac{S_{y1}}{2}\right) + \frac{1}{T_{c2}}\left(2G\beta + \frac{S_{y2}}{2}\right) \tag{5.61}$$

Furthermore, (5.60) and (5.61) are expanded as follows:

$$f_5(q) = \frac{2A\alpha}{T_{c1}} - \frac{S_{x1}}{2T_{c1}} - \frac{2C\beta}{T_{c2}} + \frac{S_{x2}}{2T_{c2}} \tag{5.62}$$

$$f_6(q) = \frac{2E\alpha}{T_{c1}} - \frac{S_{y1}}{2T_{c1}} + \frac{2G\beta}{T_{c2}} + \frac{S_{y2}}{2T_{c2}} \tag{5.63}$$

Next, all the functions that shown in (5.56), (5.57), (5.58), (5.59), (5.62) and (5.63) can be solved by using Newton-Raphson method.

Chapter 6

Generalized Conclusions

In this section, the conclusions for each chapter, from chapter 1-5 will be explained. In total, this thesis is divided into 6 chapters including this chapter, the generalized conclusions. A the end of this thesis, there are appendix sections that included the MARI-3's mechanical specification, special research report and publications.

In chapter 1, background and motivation of this research is discussed. Previous research studies that related to biped walking on slope and stairs are cited properly. The motivation of this research is that walking along a step has not investigated yet by other researchers yet. Most of them investigated for walking directions of up and down only. Research objectives are also statetd at the end of chapter 1. There are three research objectives to be achieved which are to design and develop the kinematics for MARI-3 biped robot, to obtain appropriate walking parameters for walking along a step in 2-D case with DLLIPM approach and to obtain appropriate walking parameters for walking along a step in 3-D case with DLLIPM approach.

ZMP derivation by using cart-table model is shown in chapter 2. Furthermore, the analytical solution of ZMP is also shown. The general ZMP equation which is shown as in (2.13) is used repeatedly in many derivations in this thesis.

In chapter 3, the kinematics calculations that included orientation and position equations are shown. The proposed kinematics are applied at MARI-3 biped robot for walking on flat floor, slope and diagonal walking. ROCOS has been used as simulator to proof the applications of the proposed kinematics. By using ROCOS, the x, y and z-trajectory of CoM are obtained for the walking on the various floor surfaces. The proposed kinematics is validated successfully since the responses of the trajectory are obtained similarly as the references of the trajectory.

Biped robot walking along a step in 2-D with DLLIPM is discussed in chapter 4. In this chapter, the derivations of the proposed method are done seperately for sagittal and lateral cases. There are 4 variables to obtain which are S_{x1}, S_{x2}, T_{s1} and T_{s2} for sagittal case. On the other hand, there are also 4 variables to obtain for lateral case which are S_{y1}, S_{y2}, T_{s1} and T_{s2}. In both cases, there are 4 constraints used which are related to position equations in phase 1

and phase 2, velocity and acceleration equations.

In chapter 5, biped robot Walking along a step in 3-D with DLLIPM is discussed. In this chapter, the derivations are done in order to synchronous between sagittal and lateral planes. There are 6 variables to obtain which are S_{x1}, S_{x2}, S_{y1}, S_{y2}, T_{s1} and T_{s2}. Furthermore, there are 6 constraints used which are related to position equations in phase 1 and phase 2 for sagittal and lateral planes, velocity and acceleration equations. Simulations are done with ROCOS simulator in order to realized the biped robot walking with LIPM and DLLIPM methods. Experiments are also done by using MARI-3 biped robot. In simulations and experiments, findings are found that the maximum impact forces are reduced by using DLLIPM method, in comparison to LIPM method.

6.1 Summary of Results

There are some important merits from the proposed method, DLLIPM for biped walking along a step:

- Synchronization between sagittal and lateral in order to perform 3-D biped robot walking. In chapter 5, the derivations included 6 constraints which synchronized between sagittal and lateral planes.

- Minimization of maximum impact forces. It is found that, by using DLLIPM method in biped walking along a step, the CoM is always maintained horizontally which contributed in minimization of maximum impact forces. In LIPM method, CoM is brought up and down repeatedly and this contributed to higher maximum impact forces.

- Walking stability from the observation of the ZMP trajectory. It is discussed in sub-section 5.3.5 that with the proposed method, a more stable walking is achieved.

6.2 Future Research

There are several future works which can be considered and have not done yet because of time limitation. The topics that could be explored and will be the near future research topics are listed as below.

- Simulation and experiment by using other constraints. It is just noticed recently that there are other options in determination of the constraints. In this research, position, velocity and acceleration equations have been used for the constraints. It is intended to continue the simulation and experiment by using position and velocity equations only as suggested in sub-section 5.5.

- Optimization of other walking parameters. In this research, only 6 walking parameters have been chosen for optimization as shown in Table 5.1. The rest are pre-determined values and able to be optimized in the future.
- As the limitation of time, experiments in this thesis are done only for the lateral plane. In the future, it is intended to do experiment of forward walking along the step too.
- It is intended to expand the concept of DLLIPM for biped diagonal walking on stairs.
- It is also intended to expand the concept of DLLIPM for a more challenging motion which is biped robot turning on stairs.

Bibliography

[1] T. Saitoh, N. Tada, and R. Konishi, "Indoor mobile robot navigation by central following based on monocular vision," *IEEJ Trans. on Electronics, Information and Systems*, Vol.129, No.8, pp. 1576-1584, 2009.

[2] T. Yoshioka, T. Takubo, T. Arai, and K. Inoue, "Hybrid locomotion of leg-wheel ASTERISK H," *J. of Robotics and Mechatronics*, Vol.20, No.3, pp. 403-412, 2008.

[3] A. Irawan and K. Nonami, "Compliant walking control for hydraulic driven hexapod robot on rough terrain," *J. of Robotics and Mechatronics*, Vol.23, No.1, pp. 149-162, 2011.

[4] H. Igarashi and M. Kakikura, "Adaptive gait control for a quadruped robot on 3D path planning," *IEEJ Trans. on Electronics, Information and Systems*, Vol.123, No.10, pp. 1813-1821, 2003.

[5] Y. Asano and A. Kawamura, "Proposal and verification of visual walk aiming at the rotation target object based on feature value caused by biped walking motion," *IEEJ Trans. on Industry Applications*, Vol.128, No.8, pp. 1020-1028, 2008.

[6] M. Ito and N. Oda, "Motion stabilization by using laser distance sensor for biped walking robot with flexible ankle joints," *IEEJ Trans. on Industry Applications*, Vol.130, No.3, pp. 368-374, 2010.

[7] K. Erbatur and O. Kurt, "Natural ZMP trajectories for biped robot reference generation ", *IEEE Trans. on Industrial Electronics*, Vol.56, No.3, pp. 835-845, 2009.

[8] M.Vukabrotovic and B.Borovac, "Zero-moment point - thirty five years of its life", *Int. Journal of Humanoid Robotics*, Vol. 1, No.1, pp. 157-173, 2004.

[9] T. Tsuji and K. Ohnishi, "A global step planning method for biped robot considering obstacles", *IEEJ Trans. on Industry Applications*, Vol.124, No.6, pp. 549-555, 2004.

[10] S. Kajita, F. Kanehiro, K. Kaneko, K. Fujiwara, K. Yokoi and H. Hirukawa, "Biped walking pattern generation by a simple three-dimensional inverted pendulum model", *Advanced Robotics*, Vol. 17, No.2, pp. 131-147, 2003.

[11] N. Motoi, T. Suzuki, and K. Ohnishi, "A bipedal locomotion planning based on virtual linear inverted pendulum mode," *IEEE Transactions on Industrial Electronics*, Vol. 56, No.1, pp. 54-61, 2009.

[12] J.-Y. Kim, I.-W. Park and J.-H. Oh, "Walking control algorithm of biped humanoid robot on uneven and inclined floor," *Journal of Intelligent and Robotic Systems*, vol. 48, pp. 457-484, 2007.

[13] T. Sato, S. Sakaino, E. Ohashi and K. Ohnishi, "Walking trajectory planning on stairs using virtual slope for biped robots," *IEEE Transactions on Industrial Electronics*, Vol. 58, No.4, pp. 1385-1392, 2011.

[14] C. Fu and K. Chen, "Gait synthesis and sensory control of stair climbing for a humanoid robot," *IEEE Transactions on Industrial Electronics*, Vol. 55, No.5, pp. 2111-2120, 2008.

[15] Y. Hu, G. Yan, and Z. Lin, "Feedback control of planar biped robot with regulable step length and walking speed," *IEEE Transactions on Robotics*, Vol. 27, No.1, pp. 162-169, 2011.

[16] M. J. Powell, H. Zhao, and A. D. Ames, "Motion primitives for human-inspired bipedal robotic locomotion: walking and stair climbing," in *Proc. IEEE International Conference on Robotics and Automation*, pp. 543-549, May 2012.

[17] S. Park, E. Seo, D. Kim, B. You, and S. Oh, "Stair boundary extraction using the 2D laser scanner," in *Proc. IEEE International Conference on Mechatronics and Automation*, pp. 1538-1543, August 2011.

[18] J. Chestnutt, Y. Takaoka, K. Suga, K. Nishiwaki, J. Kuffner, and S. Kagami, "Biped navigation in rough environments using on-board sensing," in *Proc. IEEE/RSJ International Conference on Intelligent Robots and Systems*, pp. 3543-3548, October 2009.

[19] C. Guodong, M. Xie, Z. Xia, L. Sun, J. Ji, Z. Du, and W. Lei, "Fast and accurate humanoid robot navigation guided by stereovision," in *Proc. IEEE International Conference on Mechatronics and Automation*, pp. 1910-1915, August 2009.

[20] A. Kawamura, and C. Zhu, "The development of biped robot MARI-3 for fast walking and running," *Proc. IEEE Conference Intelligent Systems and Robots*, pp. 599-604, 2006.

[21] Y. Fujimoto, and A. Kawamura, "Simulation of an autonomous biped walking robot including environmental force interaction," *IEEE Robotics and Automation Magazine*, Vol. 5, No. 2, pp. 33-42, 1998.

[22] F. Ali, B. Ugurlu, and A. Kawamura, "Center of mass based inverse kinematics algorithm for bipedal robot motion on inclined surfaces," in *Proc. IEEE International Workshop on Advanced Motion Control*, pp. 396-401, March 2010.

[23] Kajita: Humanoid Robot (Japanese) book, Ohmsha (2005).

[24] http://www.myphysicslab.com/numerical_vs_analytic.html.

[25] Venkataraman: Applied Optimization With Matlab Programming book, John Wiley & Sons (2009).

[26] B. Ugurlu and A. Kawamura, "Online running trajectory planning for bipedal robots based on ZMP and Euler's equation," *JSME Technical Journal*, Vol.3, No.1, pp. 1-12, 2009.

[27] http://en.wikipedia.org/wiki/Zero_moment_point.

[28] S. Kajita, F. Kanehiro, K. Kaneko, K. Fujiwara, K. Harada, K. Yokoi, and H. Hirukawa, "Biped Walking Pattern Generation by using Preview Control of Zero-Moment Point", in *Proc. IEEE International Conference on Robotics and Automation*, pp. 16201626, 2003.

[29] S. Kajita, "Overview of ZMP-based Biped Walking", Keynote Presentation in *DynamicWalking2008*, Delft, Netherlands, 2008.

[30] F. Ali, N. Motoi, and A. Kawamura, "A new pattern generation of biped walking along a step", in *IEEJ Technical Meeting on Industrial Instrumentation and Control*, IIC-12-121, pp. 67-72, 2012.

[31] Y. F. Zheng and J. Shen, "Gait synthesis for the SD-2 biped robot to climb sloping surface", in *IEEE Trans. On Robotics and Automation*, vol. 6, no. 1, pp. 86-96, 1990.

[32] K. Suwanratchatamanee, M. Matsumoto and S. Hashimoto "Walking on the slopes with tactile sensing system for humanoid robot", in *Int. Conf. on Control, Automation and Systems*, pp. 350-355, 2010.

[33] F. Ali, N. Motoi, and A. Kawamura, "An improved trajectory of biped robot for walking along slope", in *Humanoid 2012*, will be published.

[34] F. Ali, B. Ugurlu, and A. Kawamura, "Center of mass based inverse kinematics algorithm for bipedal robot motion on inclined surfaces," in *Proc. IEEE International Workshop on Advanced Motion Control*, pp. 396-401, 2010.

[35] F. Ali, A. Che Amran, and A. Kawamura, "Position and orientation based inverse kinematics algorithm for bipedal robot walking on inclined floor," in *Proc. International Conference on Advanced Mechatronics*,pg. 141-146, 2010.

[36] F. Ali, A. Che Amran, and A. Kawamura, "Bipedal Robot Walking Strategy on Inclined Surfaces using Position and Orientation based Inverse Kinematics Algorithm," in *Proc. International Conference on Control, Automation, Robotics and Vision*,pg. 181-186, 2010.

[37] F. Ali, A. Che Amran, and A. Kawamura, "Slope-Walking of a Biped Robot with Position and Orientation based Inverse Kinematics Method," in *Proc. International Conference on Control, Automation and Systems*,pg. 1724-1728, 2010.

[38] S. Kajita et al., "Biped walking pattern generator allowing auxiliary ZMP control," in *Proc. International Conference on Intelligent Robots and Systems*, pp. 2993-2999, 2006.

[39] H. Hirukawa et al., "A pattern generator of humanoid robots walking on a rough terrain," in *Proc. International Conference on Robotics and Automation*, pp. 2181-2187, 2007.

[40] M. Ogino, H. Toyama and M. Asada, "Stabilizing biped walking on rough terrain based on the compliance control," in *Proc. International Conference on Robotics and Automation*, pp. 4047-4052, 2007.

[41] T. Erez and W.D. Smart, "Bipedal walking on rough terrain using manifold control," in *Proc. International Conference on Intelligent Robots and Systems*, pp. 1539-1544, 2007.

[42] C. Zhou, P.K. Yue, J. Ni and S.-B. Chan, "Dynamically stable gait planning for a humanoid robot to climb sloping surface," in *Proc. IEEE Conference on Robotics, Automation and Mechatronics*, pp. 341-346, 2004.

[43] W. Huang, C.-M. Chew, Y. Zheng and G.-S. Hong, "Pattern generation for bipedal walking on slopes and stairs," in *Proc. International Conference on Humanoid Robots*, pp. 205-210, 2008.

[44] S. Feng and Z. Sun, "A simple trajectory generation method for biped walking," in *Proc. International Conference on Control, Automation, Robotics and Vision*, pp. 2078-2082, 2008.

[45] E. Taskiran, U. Seven, O. Koca, M. Yilmaz and K. Erbatur, "Walking control of a biped robot on an inclined plane," in *Proc. International Conference on Intelligent Control Systems and Signal Processing*, 2009.

[46] C. Zhu, M. Okamura, A.Kawamura and Y. Tomizawa, "Experimental approach for high speed walking of biped robot MARI-1," in *Proc. International Advanced Motion Control*, pp. 427-432, 2004.

[47] T. Sugihara, "Boundary condition relaxation method for stepwise pedipulation planning of biped robots," in *IEEE Transactions on Robotics*, vol. 25, pp. 658-669, June 2009.

[48] B. Ugurlu and A. Kawamura, "Eulerian ZMP resolution based bipedal walking: discussions on the intrinsic angular momentum rate change about center of mass," in *Proc. IEEE Int. Conf. on Robotics and Automation*, pp. 4218-4223, 2010.

[49] J.J. Craig, Introductions to Robotics: Mechanics and Control 3nd Edition, Prentice Hall, 2004.

[50] W.H. Press, S. A. Teukolsky, W.T. Vatterling, and B.P. Flannery Numerical Recipes in c: The Art of Scientific Computing 2nd Edition, Cambridge University Press, 1992.

[51] Fariz Ali and Atsuo Kawamura, "Diagonal Walking Strategy on Inclined Floor with Orientation Based Inverse Kinematics for Biped Robot," *International Journal of Mechanical & Mechatronics Engineering*, Vol.11, No.4, pp. 38-44, 2011.

[52] K. Suzuki, "Basic study on realizing biped running", in *Master Thesis Dissertation*, Yokohama National University, Yokohama, Japan, 2006, (in Japanese).

[53] M.W. Spong, S. Hutchinson and M. Vidyasagar, Robot Dynamics and Control, 2004.

[54] C.H. An, C.G. Atkeson, J.D. Griffiths and J.M. Hollerbach, "Experiment evaluation of feedforward and computed toque control," IEEE transactions on robotics and automotion, Vol.5, No.3, June 1989.

[55] T. Murakami, F. Yu and K. Ohnishi, "Torque sensorless control in multidegree-of-freedom manipulator ," IEEE transactions on industrial electronics, Vol.40, No.2, April 1993.

[56] T. Sato, "Advanced motion control of biped robot," Ph.D. thesis, 2010.

Appendix A

MARI-3's Mechanical Specifications

A.1 Link Wise Specs

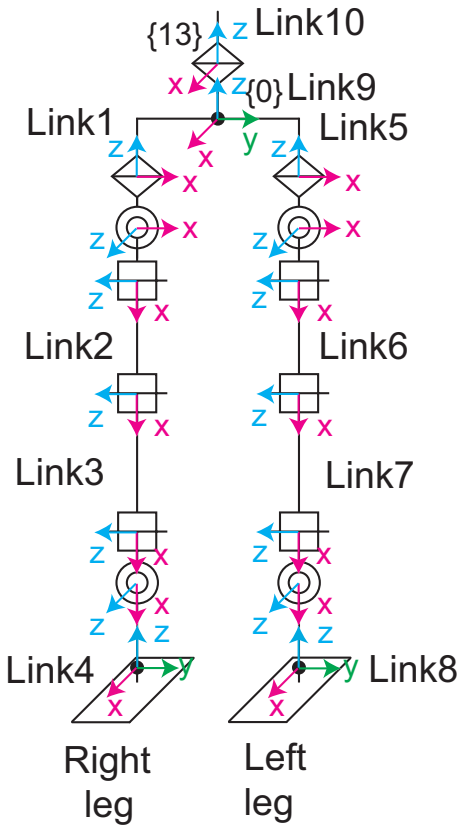

Figure A.1: Numbered Links on MARI-3

Below, MARI-3's link parameters are given in a link-wise manner[52]. m symbolizes mass, d indicates the CoM position with respect to corresponding joint position. Please refer to Fig.

A.1. The data are used in the kinematics calculations.

Link 1

$$m_1 = 3.641\ [kg] \tag{A.1}$$
$$d_1 = \begin{bmatrix} 0.02716 & 0.00942 & -0.06381 \end{bmatrix}^T\ [m] \tag{A.2}$$

Link 2

$$m_2 = 4.212\ [kg] \tag{A.3}$$
$$d_2 = \begin{bmatrix} -0.01634 & 0.01494 & -0.13399 \end{bmatrix}^T\ [m] \tag{A.4}$$

Link 3

$$m_3 = 3.101\ [kg] \tag{A.5}$$
$$d_3 = \begin{bmatrix} -0.00283 & 0.00893 & -0.18926 \end{bmatrix}^T\ [m] \tag{A.6}$$

Link 4

$$m_4 = 3.253\ [kg] \tag{A.7}$$
$$d_4 = \begin{bmatrix} -0.01359 & 0.00163 & -0.08821 \end{bmatrix}^T\ [m] \tag{A.8}$$

Link 5

$$m_5 = 3.641\ [kg] \tag{A.9}$$
$$d_5 = \begin{bmatrix} 0.02716 & -0.00942 & -0.06381 \end{bmatrix}^T\ [m] \tag{A.10}$$

Link 6

$$m_6 = 4.212\ [kg] \tag{A.11}$$
$$d_6 = \begin{bmatrix} -0.01635 & -0.01494 & -0.13399 \end{bmatrix}^T\ [m] \tag{A.12}$$

Link 7

$$m_7 = 3.101\ [kg] \tag{A.13}$$
$$d_7 = \begin{bmatrix} -0.00283 & -0.00893 & -0.18926 \end{bmatrix}^T\ [m] \tag{A.14}$$

Link 8

$$m_8 = 3.253\ [kg] \tag{A.15}$$
$$d_8 = \begin{bmatrix} 0.01359 & -0.00215 & -0.08821 \end{bmatrix}^T\ [m] \tag{A.16}$$

Link 9

$$m_9 = 3.731\ [kg] \tag{A.17}$$
$$d_9 = \begin{bmatrix} 0.0 & 0.0 & -0.01138 \end{bmatrix}^T\ [m]\ \ (\textit{with respect to pelvis}) \tag{A.18}$$

Link 10

Note that CoM position of link 10 is exactly on the z-axis. The corresponding joint, q_{13}, only rotates about yaw axis. Therefore, q_{13} has no influence neither on the upper body CoM nor on the overall CoM position.

$$m_{10} = 5.87\ [kg] \tag{A.19}$$
$$d_{10} = \begin{bmatrix} 0.0 & 0.0 & 0.0862 \end{bmatrix}^T\ [m] \tag{A.20}$$

Transformation Matrix from Right Ankle Roll Joint to Right Foot Sole Center

$$T_{6\to RF} = \begin{bmatrix} 0.0 & 0 & -1.0 & 0.11 \\ 0.0 & 1.0 & 0.0 & 0.0 \\ 1.0 & 0.0 & 0.0 & 0.0 \\ 0 & 0.0 & 0.0 & 1.0 \end{bmatrix} \tag{A.21}$$

Transformation Matrix from Left Ankle Roll Joint to Left Foot Sole Center

$$T_{12\to LF} = \begin{bmatrix} 0.0 & 0 & -1.0 & 0.11 \\ 0.0 & 1.0 & 0.0 & 0.0 \\ 1.0 & 0.0 & 0.0 & 0.0 \\ 0 & 0.0 & 0.0 & 1.0 \end{bmatrix} \tag{A.22}$$

Appendix B

Stability observation of a 2-link robot manipulator with disturbance observer and computed torque control (Mass fluctuation consideration)

B.1 Introduction

Robot manipulator is a very non-linear system. In practical, the manipulator is exposed to some kinds of disturbances such as joint frictions and end-effectors payloads. If these disturbances are ignored, some problems like poor tracking performance and unstable system will be appeared. Therefore, controllers are crucial and must be implemented in order to have a good manipulator system.

This report is prepared for a special research subject (Subject code: SD10039). The objective of this research is to observe stability of a 2-link planar manipulator on mass fluctuations. In the observations, two type of control methods are used which are computed torque control (CTC) and disturbance observer (DOB). Furthermore, this report presents some results of simulations. Simulation tool used is MATLAB. In the simulations, the mass fluctuations are created by using two methods which are explained more detail in section B.4.

This section is organized as following; section B.1 is explaining about the whole idea of this report, section B.2 explains the forward kinematics of the 2-link planar manipulator, section B.3 explains on the dynamics equations of the manipulator and how they are derived, section B.4 explains about the definitions of the mass fluctuations, section B.5 is the main content which is the control section. Section B.6 is the discussions on the simulation results obtained in section B.5. Finally, section B.7 concludes the findings or observations obtained from this special research project.

B.2 Kinematics

Kinematics is the analysis of motion without consideration of torque or forces produced the motion. The structure of the 2-link planar robot for kinematics calculations is shown as in Fig.B.1. The structure consists of 2 links, l_1 and l_2. The movement of link 1 and link 2 produce angles denote by θ_1 and θ_2. x_0 and y_0 is the position of the end effector in the Cartesian plane. It is noticeable from Fig.B.1 that the movement of link 1 affects the link 2; whereas movement of link 2 will not effects the link 1.

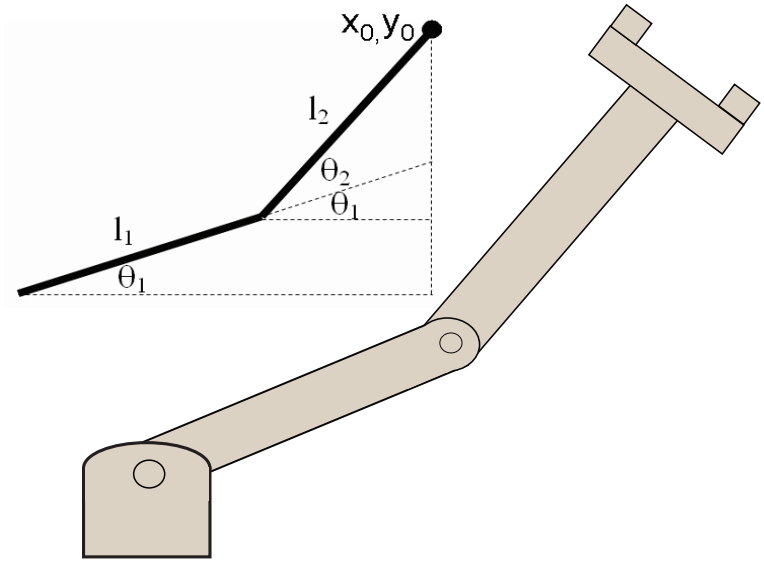

Figure B.1: 2-link planar manipulator

B.3 Dynamics

The derivations of the dynamics equations in this report are developed by using Euler Lagrange motion of equations[53]. The equation is shown as in (B.1).

$$D(\theta)\ddot{\theta} + C(\theta, \ddot{\theta})\ddot{\theta} + g(\theta) = \tau \tag{B.1}$$

D, C and g are known as inertia/mass, centrifugal/coriolis and gravity matrices respectively which are essential to produce torque.

B.4 Mass Fluctuations

As mentioned earlier, the main objective of this project is to observe the stability of a 2-link planar with consideration of mass fluctuations. There are two options to create the mass

fluctuations which are shown in B.4.1 and B.4.2 sub-sections below;

B.4.1 Definition 1

In definition 1, the mass fluctuations are created by changes of mass matrix as in (B.2).

$$D_n = (10 \sim 100\%) \times D \tag{B.2}$$

B.4.2 Definition 2

In definition 2, the mass fluctuations are created by changes of the mass itself as shown in (B.3).

$$m_{new} = (10 \sim 100\%) \times m_{original} \tag{B.3}$$

B.5 Control

This is the main section of this report. Here, two types of controllers will be explained which are computed torque control (CTC) and disturbance observer (DOB).

B.5.1 Part A: Computed Torque Control (CTC)

The computed torque control equations are shown as in (B.5)[54].

$$D\ddot{\theta} + C\dot{\theta} + g = \tau \tag{B.4}$$

$$D\ddot{\theta} + C\dot{\theta} + g = D_n U + C_n\dot{\theta} + g_n \tag{B.5}$$

where U in (B.5) is given as follows;

$$U = \ddot{\theta}_{ref} + K_p(\theta_{ref} - \theta_{res}) + K_d(\dot{\theta}_{ref} - \dot{\theta}_{res})$$

The blockdiagram of CTC is shown as in Fig.B.2. The term $\ddot{\theta}_{ref}$ in Fig.B.2 is known as feed-forward acceleration reference [56].

CTC simulations

The simulations setting and physical parameters are shown in Table B.1 and Table B.2 respectively.

The results of the simulations with step input and sine input are given as in Fig.B.3 and Fig.B.4 respectively.

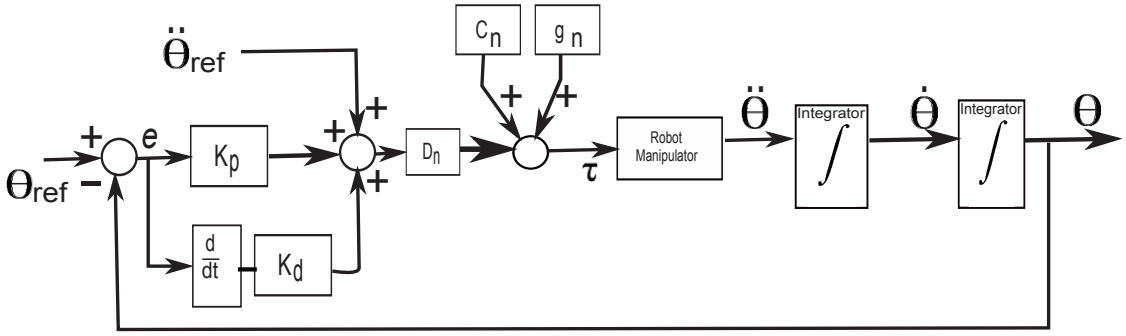

Figure B.2: Computed torque control block diagram

Table B.1: CTC simulation setting

Items	Info
Controller	CTC, Kp1=100, Kp2=150, Kd1=30, Kd2=60
Mass fluctuations	Dn=10%D, Dn=30%D, Dn=50%D, Dn=70%D, Dn=100%D
References	θ_{1ref}=θ_{2ref}=50xπ/180 (Step), θ_{1ref}=θ_{2ref}=0.87sin(2πt) (Sine)

Table B.2: Physical structure setting

Items	Sspecifications
$l_1 = l_2$	0.5[m]
$S_1 = S_2$	0.25[m]
$m_1 = m_2$	5[kg]
inertia link 1 =inertia link 2	0.42[kgm^2]
g	9.81[m/s^2]

B.5.2 Part B: Disturbance Observer (DOB)

The disturbance observer equations are shown as in (B.6)-(B.7)[55].

$$\tau = \ddot{\theta}_{ref} + K_p(\theta_{ref} - \theta_{res}) + K_d(\dot{\theta}_{ref} - \dot{\theta}_{res}) + \hat{dis} \tag{B.6}$$

where $\hat{dis}$ in (B.6) is given as follows;

$$\hat{dis} = \frac{g_{dob}}{s + g_{dob}}(\tau + g_{dob}D_n) - g_{dob}D_n \tag{B.7}$$

The blockdiagram of DOB is shown as in Fig.B.5.

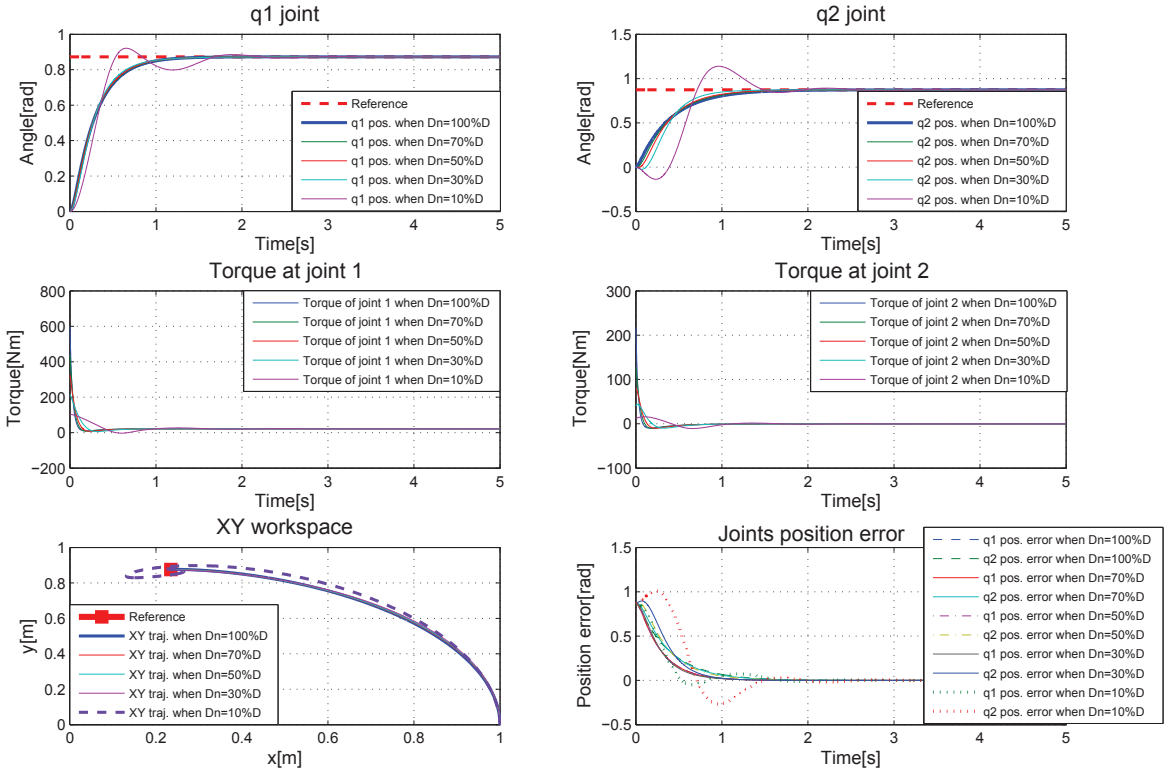

Figure B.3: CTC with step input

DOB simulations

The simulations setting is shown in Table B.3. Actually only g_{dob} parameters are added into Table B.3, whereas other settings are still similiar as in Table B.1. The physical parameters are the same as previous CTC simulations as shown in Table B.2.

Table B.3: DOB simulation setting

Items	Info
Controller	CTC, Kp1=100, Kp2=150, Kd1=30, Kd2=60 g_{dob1}=300, g_{dob2}=300
Mass fluctuations	Dn=10%D, Dn=30%D, Dn=50%D, Dn=70%D, Dn=100%D
References	θ_{1ref}=θ_{2ref}=50xπ/180 (Step), θ_{1ref}=θ_{2ref}=0.87sin(2πt) (Sine)

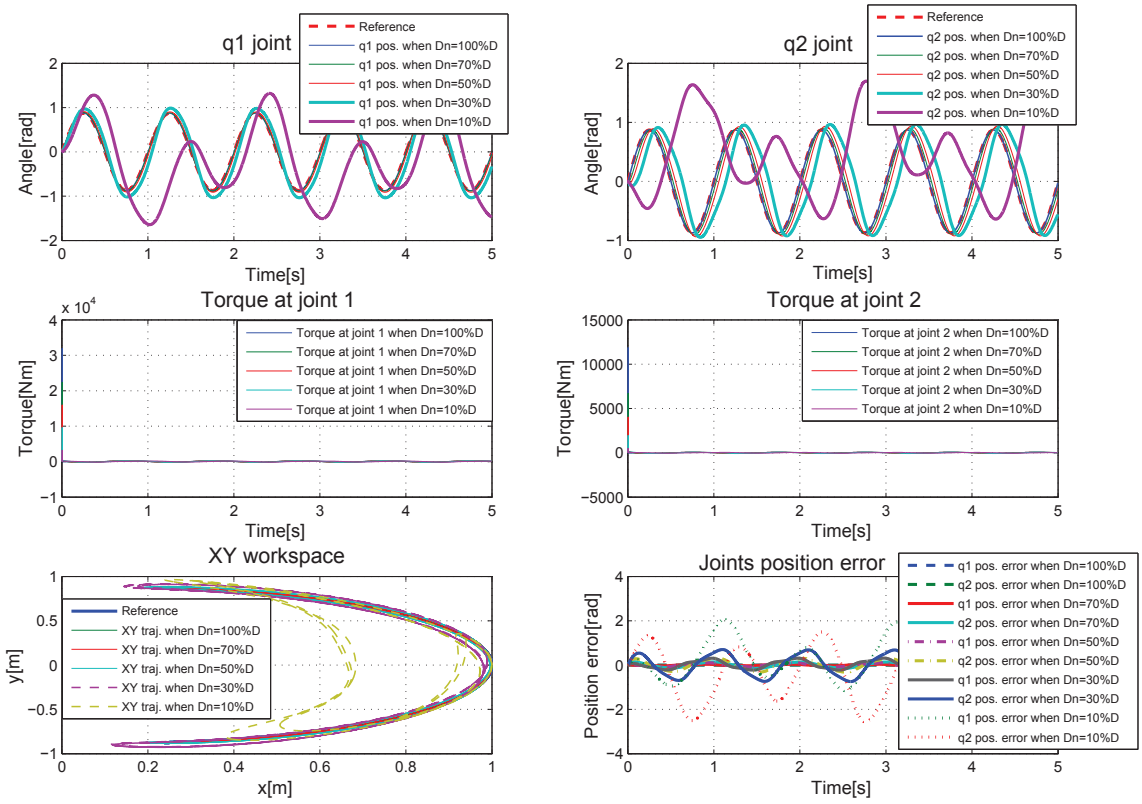

Figure B.4: CTC with sine input

The results of the DOB simulations with step input and sine input are given as in Fig.B.6 and Fig.B.7 respectively.

B.5.3 CTC and DOB simulations by using definition 2

In this section, results of simulations by using definition 2 as explained earlier in sub-section B.4.2 are shown.

The CTC simulations with step and sine inputs are shown as in Fig.B.8 and Fig.B.9 correspondingly.

The DOB simulations with step and sine inputs are shown as in Fig.B.10 and Fig.B.11 correspondingly.

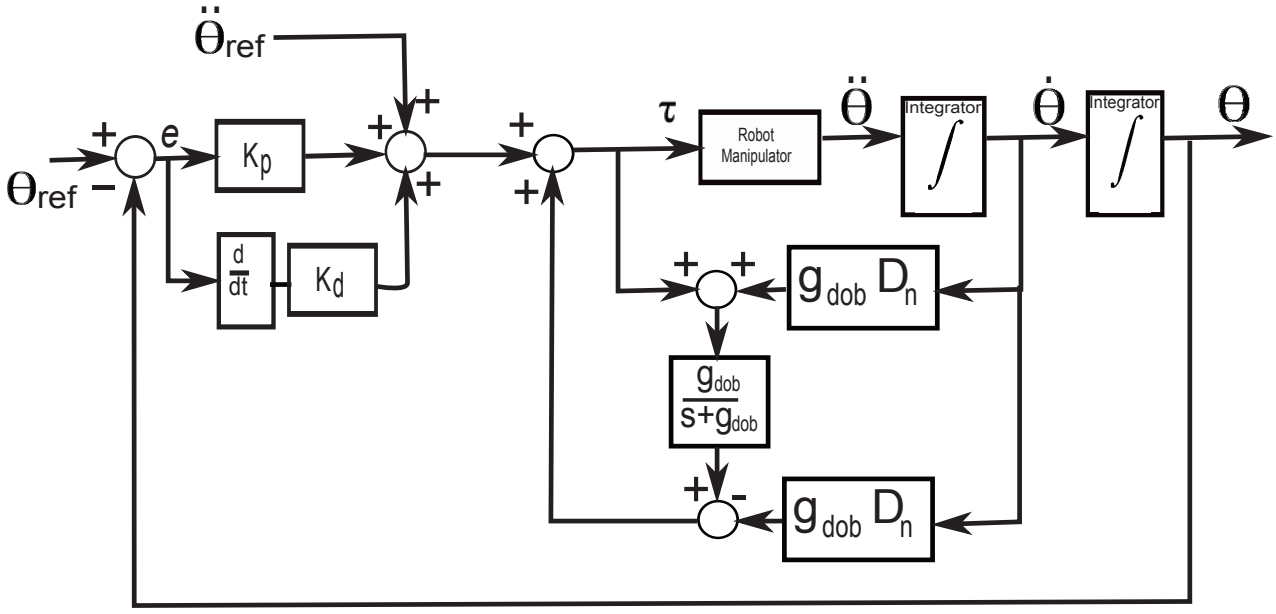

Figure B.5: Disturbance observer block diagram

B.6 Discussion

B.6.1 Tracking performance of q_1 and q_2 responses

The CTC simulations with step and sine inputs are shown as in Fig.B.3 and Fig.B.4. In these figures, it is noticed that when the value of D_n is smaller than D, the tracking performance becomes poor. At $D_n = 10\%D$, the q_1 and q_2 responses produced oscillation and overshoot. By using definition 2 as mass fluctuations, the tracking performance becomes worse as shown in Fig.B.8 and Fig.B.9.

On the other hand, DOB simulations are shown in Fig.B.6, Fig.B.7, Fig.B.10 and Fig.B.11. In all of these simulations, the tracking performance is quite good and the responses are within acceptable range from the input references.

B.6.2 XY trajectory of responses in Cartesian plane

The XY trajectory of responses by using CTC deviated from its reference trajectory during mass fluctuations as clearly seen in Fig.B.3 and Fig.B.8.

Conversely, DOB produced a better and more accurate XY trajectory during mass fluctuations as shown in Fig.B.6 and Fig.B.10.

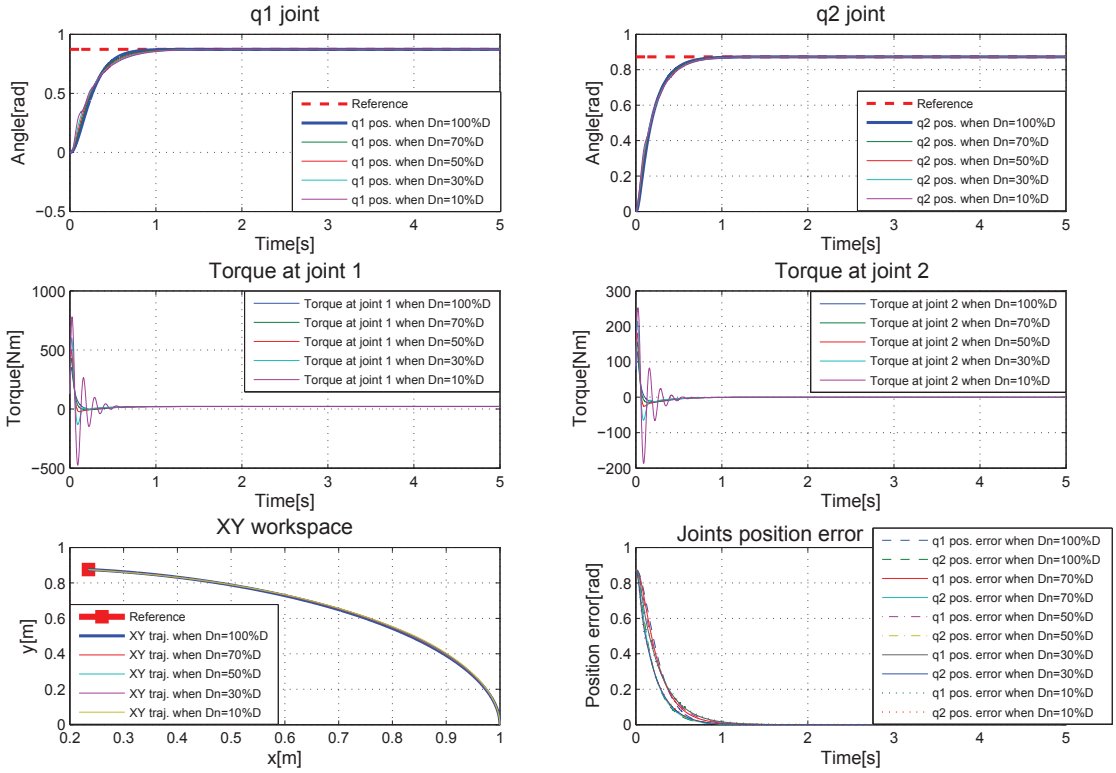

Figure B.6: DOB with step input

B.6.3 Joint position error

After observation on all simulations of CTC and DOB, it is found that in CTC simulations, the maximum joint position error is about 2.5 [rad] and the minimum is about -2.5 [rad] as shown in Fig.B.4. While, in DOB simulations, the errors are 10 times lower which are between -0.25 [rad] to 0.25 [rad] Fig.B.7.

B.7 Conclusion

In this research, stability observations of a 2-link planar manipulator with computed torque control (CTC) and disturbance observer (DOB) have been investigated. Mass flactuations consideration is taken into account in this investigation. It is noted from the simulations that CTC is only performed well with small modeling errors. However, when mass fluctuates, modeling errors become big and this affected the CTC system. It have been proofed via simulations, that the CTC results are not very good especially when $D_n = 10\%D$ in all CTC simulations, either

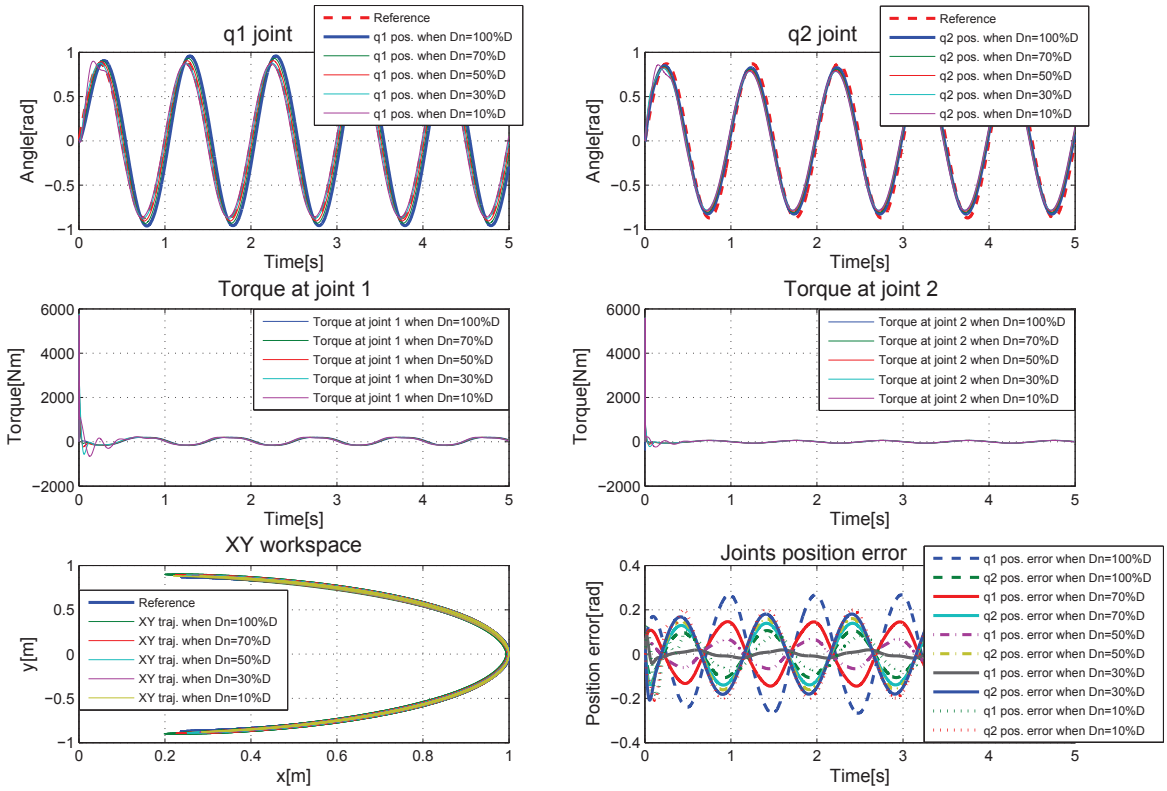

Figure B.7: DOB with sine input

using sine or step input, using definition 1 or 2.

However, in DOB control system, the disturbances are observed and even though the mass fluctuates, DOB has overcome this fluctuation by swapped back the observed disturbances back into the system. Finally, it is concluded that CTC is not very robust to mass fluctuations whereas DOB is robust.

Acknowledgements

This chapter reports the special research activities that are carried under the supervision of Assoc. Prof. Dr. Yasutaka Fujimoto. The author would like to thank Dr. Yasutaka Fujimoto his support.

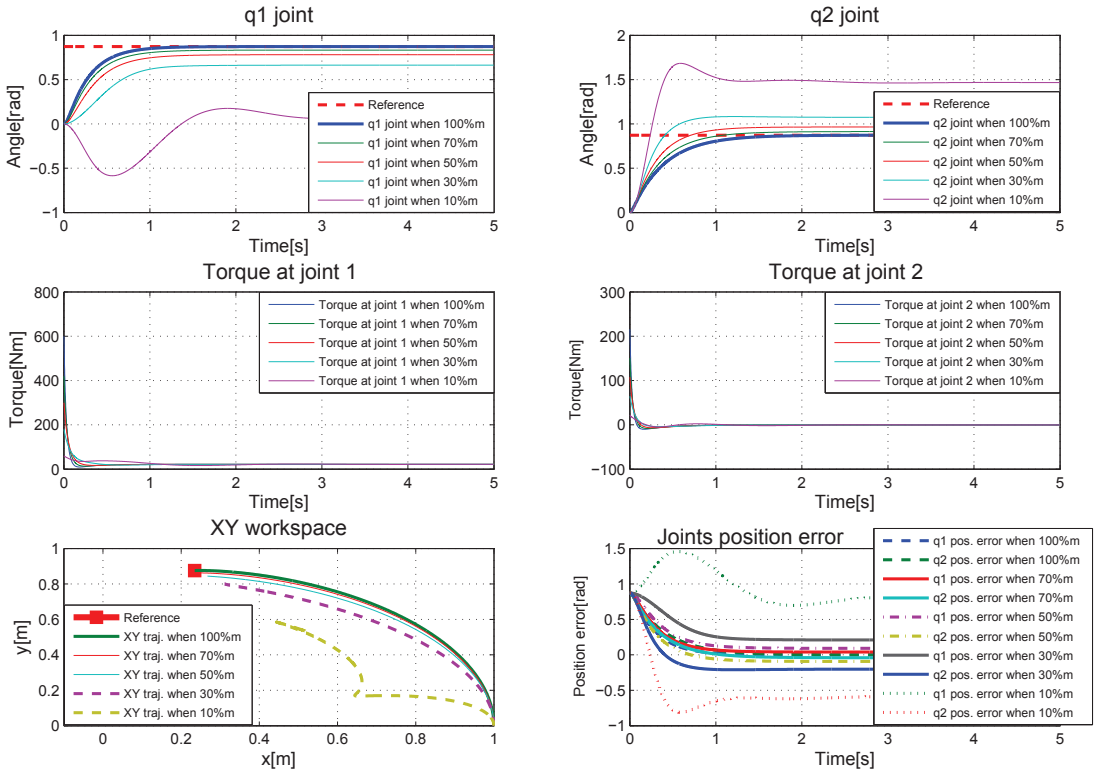

Figure B.8: CTC with step input using definition 2

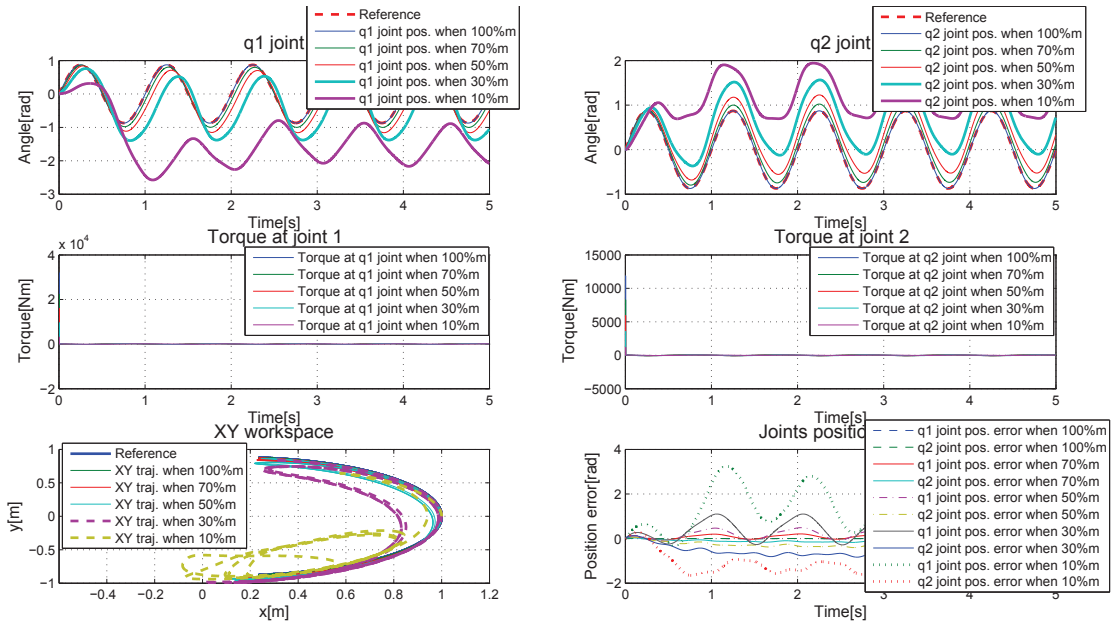

Figure B.9: CTC with sine input using definition 2

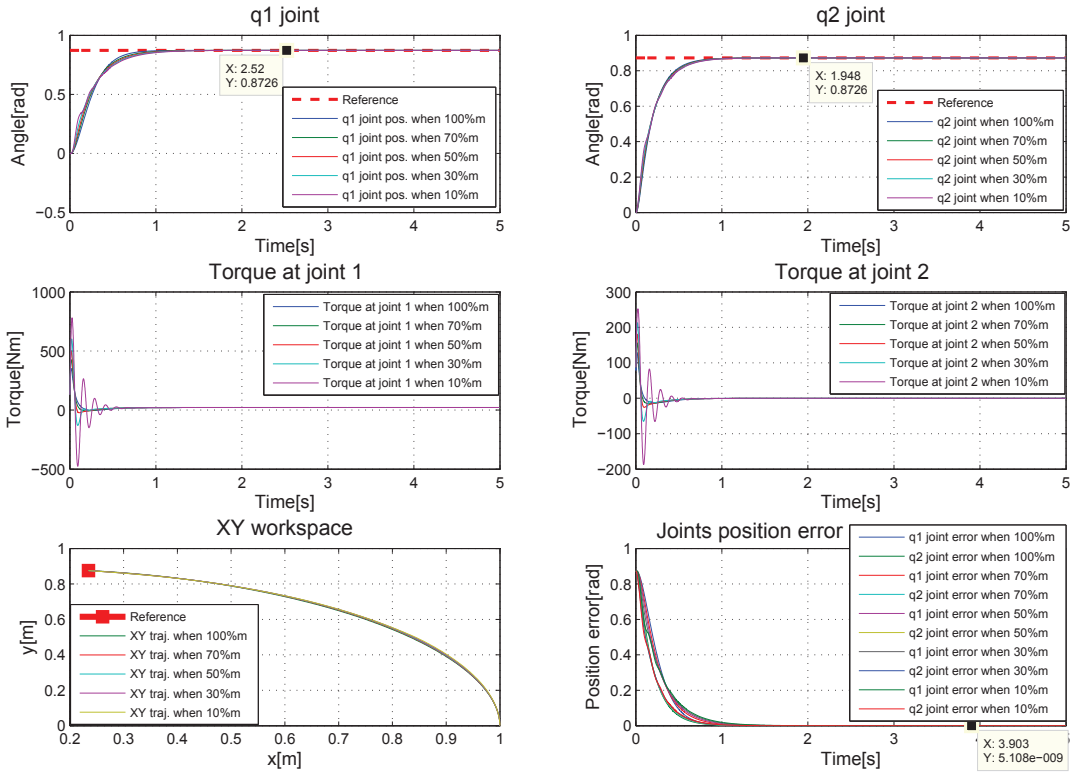

Figure B.10: DOB with step input using definition 2

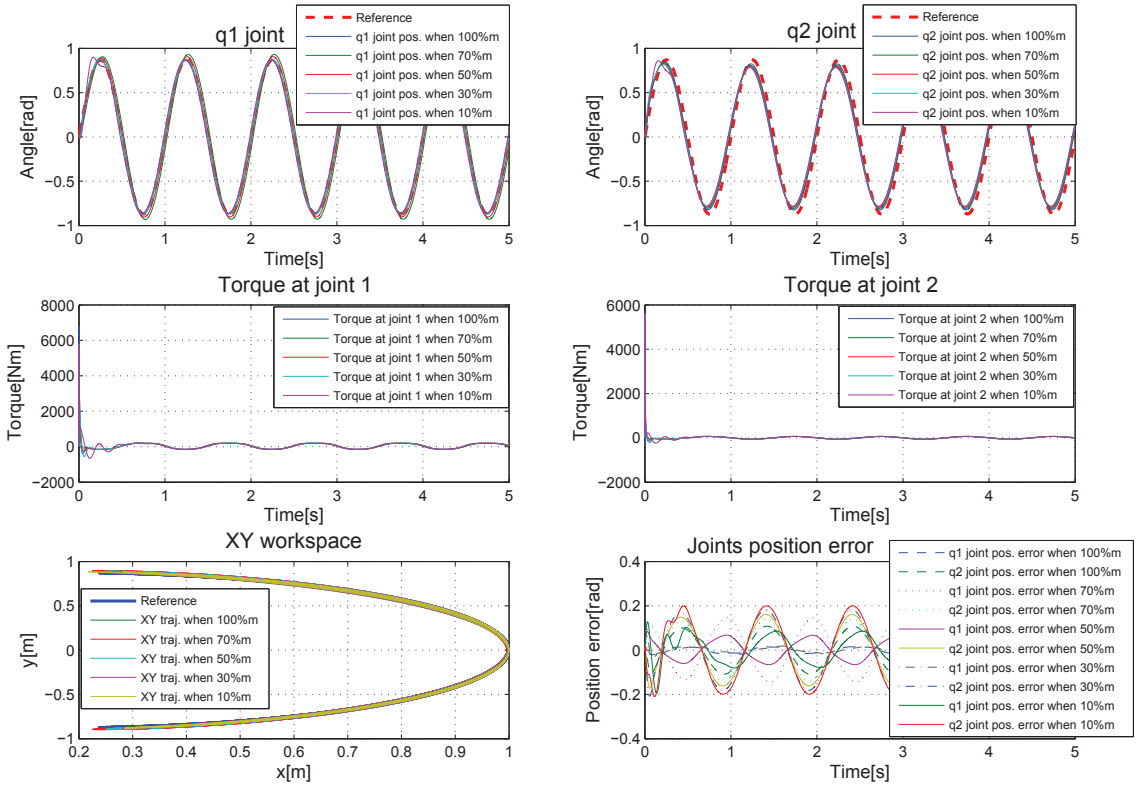

Figure B.11: DOB with sine input using definition 2

Appendix C

Publications

C.1 Journal Papers

Fariz Ali, Naoki Motoi, and Atsuo Kawamura, "An Improved Trajectory of Bipedal Robot Walking along a Step with Dual Length Linear Inverted Pendulum Method", IEEJ Transactions on Industry Applications, vol.2, no.2 , 2013 (will be published).

Fariz Ali, Naoki Motoi, Kirill Van Herdeen, and Atsuo Kawamura, "Ground Reaction Force Reduction of Biped Robot for Walking along a Step with Dual Length Linear Inverted Pendulum Method", Journal of Robotics and Mechatronics, vol.25, no. 1, 2013 (will be published).

Fariz Ali and Atsuo Kawamura, "Diagonal Walking Strategy on Inclined Floor with Orientation Based Inverse Kinematics for Biped Robot", International Journal of Mechanical & Mechatronics Engineering IJMME-IJENS, vol.11, no. 4, pp. 38-44, 2011.

C.2 International Conferences

F. Ali, B. Ugurlu, and A. Kawamura, "Center of mass based inverse kinematics algorithm for bipedal robot motion on inclined surfaces," in *Proc. IEEE International Workshop on Advanced Motion Control*, pp. 396-401, 2010.

F. Ali, A. Che Amran, and A. Kawamura, "Position and orientation based inverse kinematics algorithm for bipedal robot walking on inclined floor," in *Proc. International Conference on Advanced Mechatronics*, pg. 141-146, 2010.

F. Ali, A. Che Amran, and A. Kawamura, "Slope-Walking of a Biped Robot with Position and Orientation based Inverse Kinematics Method," in *Proc. International Conference on Control, Automation and Systems*, pg. 1724-1728, 2010.

F. Ali, A. Che Amran, and A. Kawamura, "Bipedal Robot Walking Strategy on Inclined Surfaces using Position and Orientation based Inverse Kinematics Algorithm," in *Proc. International Conference on Control, Automation, Robotics and Vision*, pg. 181-186, 2010.

F. Ali, N. Motoi, and A. Kawamura, "An improved trajectory of biped robot for walking along slope," in *Proc. Humanoids 2012*, November 2012 (will be published).

C.3 Domestic Conferences

F. Ali, N. Motoi, and A. Kawamura, "A new pattern generation of biped walking along a step", in *IEEJ Technical Meeting on Industrial Instrumentation and Control*, IIC-12-121, pp. 67-72, 2012.